UNIVERSIDADE FEDERAL DE PERNAMBUCO
CENTRO DE TECNOLOGIA E GEOCIÊNCIAS
Programa de Pós-Graduação em Engenharia Mecânica

VIVIANNE MARIE BRUÈRE DE CARVALHO PAIVA

A MULTIPHYSICS NUMERICAL SIMULATION OF THE CURING PROCESS OF A THERMOSETTING POLYMER RESIN

RECIFE
2018

VIVIANNE MARIE BRUÈRE DE CARVALHO PAIVA

A MULTIPHYSICS NUMERICAL SIMULATION OF THE CURING PROCESS OF A THERMOSETTING POLYMER RESIN

Dissertação apresentada junto à Universidade Federal de Pernambuco, como parte dos requisitos para obtenção do grau de Mestra em Engenharia Mecânica pelo Programa de Pós-Graduação em Engenharia Mecânica / CTG / EEP / UFPE.

Área de Concentração: Projetos.

Orientadora: Nadège Sophie Bouchonneau da Silva, D. Sc[1].

Coorientador: Christian Jochum, Dr.-Ing. Habil[2].

[1] Departamento de Engenharia Mecânica, Universidade Federal de Pernambuco, Recife, Brasil;

[2] Laboratoire Brestois de Mécanique et des Systèmes (LBMS), ENSTA Bretagne, Brest, França.

RECIFE

2018

Catalogação na fonte
Bibliotecária: Neide Mesquita Gonçalves Luz / CRB4-1361 (BCTG)

P149m Paiva, Vivianne Marie Bruère de Carvalho.
A multiphysics numerical simulation of the curing process of a thermosetting polymer resin / Vivianne Marie Bruère de Carvalho Paiva . – Recife, 2018.
149f., il., figs., gráfs., tabs.

Orientadora: Nadège Sophie Bouchonneau da Silva, D.Sc
Coorientador: Christian Jochum, Dr.-Ing. Habil.
Dissertação (Mestrado) – Universidade Federal de Pernambuco. CTG. Programa de Pós-Graduação em Engenharia Mecânica, 2018.
Inclui Referências, Apêndices e Anexos.

1. Engenharia Mecânica. 2. Cura. 3. Método dos Elementos Finitos. 4. Sistema epóxi LY 556. 5. Simulação multifísica. I. Silva, Nadège Sophie Bouchonneau da (Orientadora). II. Jochum, Christian (Coorientador). III. Título.

621 CDD (22.ed) UFPE/BCTG-2018/ 214

28 de Fevereiro de 2018

"A MULTIPHYSICS NUMERICAL SIMULATION OF THE CURING PROCESS OF A THERMOSETTING POLYMER RESIN"

VIVIANNE MARIE BRUÈRE DE CARVALHO PAIVA

ESTA DISSERTAÇÃO FOI JULGADA ADEQUADA PARA OBTENÇÃO DO TÍTULO DE MESTRE EM ENGENHARIA MECÂNICA

ÁREA DE CONCENTRAÇÃO: PROJETOS

APROVADA EM SUA FORMA FINAL PELO
PROGRAMA DE PÓS-GRADUAÇÃO EM ENGENHARIA MECÂNICA/CTG/EEP/UFPE

_____

Profª Drª NADÈGE SOPHIE BOUCHONNEAU DA SILVA
ORIENTADORA/PRESIDENTE

_____

Prof. Dr. CHRISTIAN JOCHUM
COORIENTADOR

_____

Prof. Dr. CEZAR HENRIQUE GONZALEZ
COORDENADOR DO PROGRAMA

BANCA EXAMINADORA:

_____

Profª Drª NADÈGE SOPHIE BOUCHONNEAU DA SILVA (UFPE)

_____

Prof. Dr. CHRISTIAN JOCHUM (ENSTA BRETAGNE)

_____

Prof. Dr. PAULO ROBERTO MACIEL LYRA (UFPE)

_____

Prof. Dr. RAMIRO BRITO WILLMERSDORF (UFPE)

À minha família.

Amo vocês até a lua…ida e volta!

ACKNOWLEDGEMENTS

Once again, thank you, God, for every grace that you've given me along this path. Two more years of hard work and silent nights in Your company led to another great achievement in my life. One of many still to come.

This couldn't be done, however, without the contribution of important people. I am particularly grateful to my supervisor and friend Nadège Bouchonneau, for her guidance and companionship. Thank you for helping me shape the professional I am and for reasserting my desire for an academic life. Bientôt on aura un autre Paris Brest sur place!

I would also like to express my deepest appreciation to my co-supervisor Christian Jochum for allowing me to take a part in his research. I couldn't feel more welcome at Brest and learn as much as I did, and for that, danke!

My special thanks are extended to the staff of ENSTA Bretagne, including all professors and technicians who were directly or indirectly involved in the research. Their help and consideration were truly remarkable and are mostly valued. My fellow colleagues and dear friends represented as well an important part during this working period. Many thanks in particular to Marinna and Marcia, for their understanding and marvellous de-stressing moments.

Last, but not least, I couldn't leave out my family and foundation, for supporting me every step of the way and always cheering on my victories, even the small ones. My most profound thanks to my great newly PhD mother and my highly enthusiastic father, my dear sister and brother-in-law and my loving grandmothers (by blood and by heart). Este trabalho é por vocês e para vocês!

“All our dreams can come true, if we have the courage to pursue them.”

(Walt Disney)

ABSTRACT

Quality issues represent a great deal of interest in the field of fibre-reinforced composites with thermosetting polymer matrix, where such concerns are derived from matrix heterogeneity, defects (bubbles and cracks, for instance) and fibre microbuckling. These group of composite materials undergoes a complex coupled thermal, chemical and mechanical phenomenon during curing of the polymer, enhanced by the exothermal behaviour of the thermosetting chemical reaction, which can lead to important gradients of degree of cure and change of properties in the materials, more specifically in thick composites. Numerical simulations were carried out on the commercial software COMSOL Multiphysics®, based on the Finite Element Method, for the investigation of the curing process of a thick LY 556 epoxy system by considering the chemical, thermal and mechanical couplings. The curing parameters and material properties, which evolve with the curing, were thus evaluated. Experimental tests were also performed in order to obtain epoxies with different levels and degree of cure gradients, by varying the temperature and the curing time for each sample. Agreements between numerical predictions, experimental data and previous numerical results reinforce the presented model and the promising capacity of the multiphysics simulation of the epoxies curing process.

KEYWORDS: Curing. Finite Element Method. LY 556 epoxy system. Multiphysics simulation.

RESUMO

As questões de qualidade representam um grande interesse no campo dos compósitos de matriz polimérica termoendurecível reforçados com fibras, onde tais preocupações são derivadas da heterogeneidade da matriz, defeitos (bolhas e trincas, por exemplo) e microflambagem das fibras. Este grupo de materiais compósitos sofre um complexo fenômeno térmico, químico e mecânico acoplado durante a cura do polímero, intensificado pelo comportamento exotérmico da reação química termoendurecível, o que pode levar a importantes gradientes do grau de cura e mudança de propriedades nos materiais, mais especificamente em compósitos espessos. Foram realizadas simulações numéricas no *software* comercial COMSOL Multiphysics®, baseado no Método dos Elementos Finitos, para a investigação do processo de cura de um sistema epóxi LY 556 espesso considerando os acoplamentos químicos, térmicos e mecânicos. Os parâmetros de cura e propriedades do material, que evoluem com a cura, foram assim avaliados. Ensaios experimentais para obter epóxis com diferentes níveis e gradientes de cura também foram realizados variando a temperatura e o tempo de cura para cada amostra. Concordâncias entre as previsões numéricas, dados experimentais e resultados numéricos anteriores reforçam o modelo apresentado e a capacidade promissora da simulação multifísica do processo de cura de epóxis.

PALAVRAS-CHAVE: Cura. Método dos Elementos Finitos. Sistema epóxi LY 556. Simulação multifísica.

LIST OF FIGURES

LIST OF TABLES

LIST OF ABREVIATIONS

FRC	Fibre-Reinforced Composites
UFPE	Universidade Federal de Pernambuco
ENSTA	École Nationale Supérieure de Techniques Avancées
FEM	Finite Element Method
MMC	Metal Matrix Composite
PMC	Polymer Matrix Composite
CMC	Ceramic Matrix Composite
CBN	Cubic boron nitride
SAP	Sintered Aluminium Powder
TD-nickel	Thoria Dispersed-Nickel
T.T.T	Time–Temperature–Transformation
DGEBA or BADGE	Bisphenol A Diglycidyl Ether
TGA	Thermogravimetric Analysis
TG	Thermogravimetry
DTG	Derivate Thermogravimetry
IR	Infrared Spectroscopy
DDA	Dynamics Dielectric Analysis
TBA	Torsional Braid Analysis
DMA	Dynamic Mechanical Analysis
DSC	Differential Scanning Calorimetry
DEA	Dielectric Analysis
DMA	Dynamic Mechanical Analysis
FEA	Finite Element Analysis
FE	Finite Element
BC	Boundary Condition
API	Application Programming Interface
EMC	Epoxy Moulding Compounds
CNT	Carbon Nanotube
ODE	Ordinary differential equation
CTE	Coefficient of thermal expansion

LIST OF SYMBOLS

ρ_c	Composite density
f_i	Volumetric fraction of the composite constituent
ρ_i	Density of the composite constituent
l_c	Critical fibre length
d	Fibre diameter
σ_f^*	Tensile strength of the fibre
τ_e	Shear strength of fibre-matrix interface or Matrix's yield stress to shear
f_{matrix}	Matrix volumetric fraction
ρ_{matrix}	Matrix density
f_{fibres}	Fibres volumetric fraction
ρ_{fibres}	Fibres density
α	Degree of cure
T_g	Glass transition temperature
T_{g0}	Glass transition temperature at $\alpha = 0\%$
$T_{g\infty}$	Glass transition temperature at $\alpha = 100\%$
$T_{g\,gel}$	Temperature where gelation and vitrification coincide
μ	Viscosity of the material
α_{gel}	Degree of cure at gelation
H	Enthalpy
C	Capacitance
t	Time
T	Temperature
$H(t)$	Reaction's enthalpy at instant t
H_U	Reaction's total enthalpy (dynamic mode)
dH/dt	Measured heat flux
$d\alpha/dt$	Conversion rate of the polymerization / reaction rate
K_1	Rate constant of the catalytic process (or at the initial moment)
K_2	Rate constant of the auto-catalytic process
B	Molar ratio epoxy/amine
m	Order of the auto-catalytic reaction
n	Order of the catalytic reaction

A_1, A_2	Pre-exponential constants
E_1, E_2	Activation energies
R	Universal constant of perfect gases
f_d	Diffusion factor
α_f	Conversion at the end of the isothermal cure
b	Empirical diffusion constant
κ, μ	Lamé coefficients
$\boldsymbol{I}$	Identity tensor
$\boldsymbol{\varepsilon^e}$	Second-order strain tensor
ρ	Density of the resin
c_p	Specific heat capacity of the resin
k	Thermal conductivity of the resin
q	Heat flow imposed by the oven
$\Delta \mathrm{H}^r$	Enthalpy of the reaction
α_T	Coefficient of thermal expansion of the resin
ϕ	Heat flow produced by the chemical reaction
$\boldsymbol{\sigma}$	Stress tensor
E	Young's modulus
ν	Poisson's ratio
$\boldsymbol{\varepsilon}$	Total strain tensor
G	Elastic shear modulus
K	Bulk modulus
$\boldsymbol{\varepsilon^{ch}}$	Chemical strain tensor
$\boldsymbol{\varepsilon^{th}}$	Thermal strain tensor
ε_{ii}^{th}, ε_{ij}^{th}	Normal and shear components of thermal strain tensor
ΔT	Temperature increment over time
λ	Parameter from DiBenedetto's equation
h	Coefficient of heat transfer by convection
T_e	External temperature
flux_epoxy_1	Heat flow produced by the chemical reaction for $T < T_g$
flux_epoxy_2	Heat flow produced by the chemical reaction for $T > T_g$
$c_p(0,T)$, $k(0,T)$	Specific heat capacity and thermal conductivity for the uncured resin
$c_p(1,T)$, $k(1,T)$	Specific heat capacity and thermal conductivity for the fully cured resin
fd	Diffusion factor (only with positive values)

fd_t	Total diffusion factor (with negative values included)
alpha	Degree of cure in the simulations
alphaf2	α_f in the simulations
b2	b in the simulations
m_r	Mass of resin
K1	Rate constant of the catalytic process in the simulations
K2	Rate constant of the auto-catalytic process in the simulations
A1, *A2*	Pre-exponential constants in the simulations
E1, *E2*	Activation energies in the simulations
R_g	Universal constant of perfect gases in the simulations
e_a, d_a, f	ODEs coefficients in the simulation
Tg_ep	Glass transition temperature in the simulations
lambda	λ in the simulations
Tg0	T_{g0} in the simulations
Tginf	$T_{g\infty}$ in the simulations
H_T	Reaction's total enthalpy (isothermal mode)
Te(t)	External temperature in the simulations
$\alpha_T(0,T)$,$\alpha_T(1,T)$	CTE for the liquid and fully cured resin
beta_fce_after	CTE for the fully cured resin for $T > T_g$ in the simulations
exp_ep	Resin's CTE in the simulations
e_ch	Chemical shrinkage in the simulations
K_ep	Bulk modulus in the simulations
G_ep	Elastic shear modulus in the simulations
E_ep	Young's modulus in the simulations
nu_ep	Poisson's ratio in the simulations

CONTENTS

1 INTRODUCTION

1.1 INITIAL CONSIDERATIONS

Composites have become a focus of many studies, representing nowadays a great deal for industrial applications. They are not a new class of materials, though. Since Classical Antiquity, humans seek out new materials with specific desired properties. One of the first uses of composites was by Mesopotamians for construction purposes, such as bricks of mud reinforced by chopped straws, or of clay reinforced by wood. Mongol warriors of the 12th century made archery bows with bamboo, silk, cattle tendons, horns, and natural pine resin, nearly as strong as modern bows.

The emergence of composites from synthetic raw materials occurred in late 19th century, when resins that could be converted from a liquid to a solid state by polymerization were developed. These first resins included celluloid, melamine and Bakelite. Other high-performance resins, epoxy resins for instance, were already available by the late 1930s and early 1940s. Also at that time, the fabrication process of glass fibres was developed. The combination of this material with polyester resins gave birth to strong and lightweight composites, giving birth to fibre-reinforced composites (FRC) and revolutionizing boating industry.

World War II strongly boosted the incipient composites industry due to the military need of weight cut of air and water crafts as well as increase of strength, durability and resistance to weather conditions. Once the war was over, the benefits of composites, being corrosion resistance one of the main ones, spread among the market, with particular regard to oil industry. Other composites applications became more and more common in various products: boats, automobiles, pipelines, storage tanks, sports equipment and so on (ACMA, 2017).

Today, the industry of composites is quite active, notably replacing metal and reducing costs in aerospace, marine, construction and energy sectors, besides becoming a part of our everyday life. There is a large variety of composite materials but the most known are probably the fibre-reinforced resins, in which the strong, stiff fibres mainly carry the tensile stresses and the resin transfer the loads to the fibres and protects them from the external environment. In Figure 1, the history of composites can be briefly observed.

Figure 1: Brief history of composites.

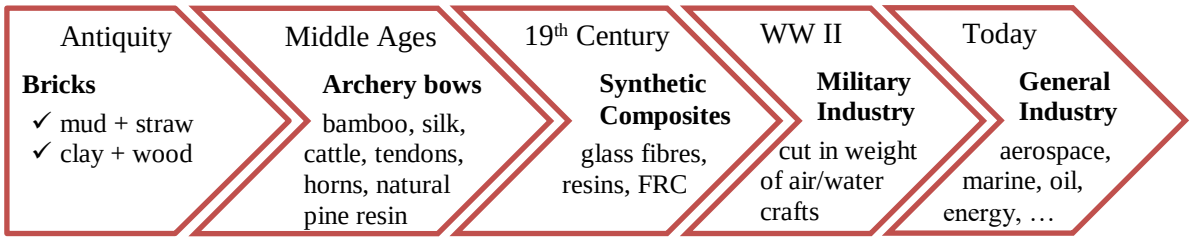

Source: Author.

According to ROESELER et al. (2007), we keep the same basic principles of working with composite materials, as mud and straw housebuilding changed to steel and concrete. The difference remains on the characteristics and mechanical properties of basic constituent materials. Therefore, we can find composites with high-performance fibres as carbon, glass or boron, embedded into a thermoplastic or thermoset matrix like epoxy, polyester or Nylon for special and/or demanding applications.

However, in order to obtain materials with the desired performance, as well as improve design and optimize costs, knowledge of material properties and fabrication process must be mastered (JOCHUM, 2009). An important phenomenon to consider in thermosetting polymer matrix composites reinforced with fibres is the process of curing of such matrix.

The cure of thermosetting polymers usually consists of an exothermic reaction, involving coupling of thermal, chemistry and mechanics. Material properties of the final product depend on the cure process. Nevertheless, during the cure internal stresses are also generated, and those may cause the appearance of quality defects, including bubbles, cracks and fibre waviness, leading to a decrease in the product's mechanical performance. At Figure 2, we can see an application of a carbon/epoxy composite for the fabrication of pipes for the extraction of petroleum at high depths (riser), where the composite shows the presence of defects (bubbles, pores, fissures, local dislocations, among others) through its thickness. This witnesses the phenomenon of stress development in the material during curing, which impairs the mechanical quality of the final product.

Figure 2: Defects through thickness in a carbon/epoxy composite riser (80-mm thickness).

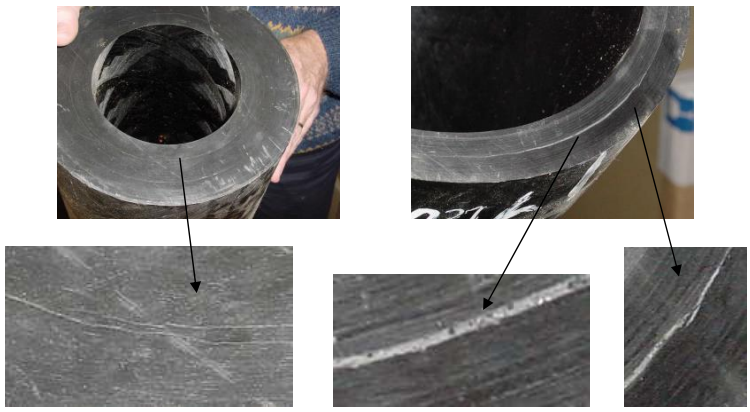

Source: JOCHUM, 2009.

Such defects become more relevant on the manufacturing of thick laminates for structural purposes – with thicknesses generally above 4-5 mm –, which are constantly increasing in naval and offshore applications (RABEARISON et al., 2009). Thermal degradation triggered by internal overheat and viscoelasticity are factors also involved in the process which affect the final state of the polymer. Hence, studies have been carried out so that the cycle of cure is optimized, and manufacturing processes ensure better mechanical properties for the composites. This can be predicted by knowing the internal state of the material at the end of cure.

The Finite Element Method (FEM) has been proven to be a helpful tool and more and more applied to predict material properties and internal stresses developed during the curing process. This numerical method has the potential to simulate the cycle of cure considering the coupled thermal, chemical and mechanical phenomena, providing reliable predictions. Studies with such tool are frequent in the literature, and the constant improvements in FE software and speed of computers are an additional impulse for their use.

As a result, this work addresses the numerical modelling of curing of thermosetting polymer matrix composites. The aim was to evaluate the process of cure involving several physics, for a reliable and realistic prediction of the material's behaviour, thanks to the COMSOL® computational software, and to benchmark it against a more traditional solver like Abaqus. The investigation gathered numerical results and experimental data for a better understanding of the process as well as the evaluation of curing parameters effects on the final material.

1.2 RESEARCH ISSUE

The research focuses on the cure of fibre-reinforced composites, with epoxy resin and carbon fibres as their constituents, a typical composite material in offshore industry nowadays. This work is limited to the analysis of the matrix curing itself, as a part of material behaviour's characterization for structural integrity evaluation.

Furthermore, the studied composites consist of thick parts and structures, where not only there is a non-homogeneity of the material specs but also the appearance of quality defects is intensified. Fibre undulations, one of the defects for instance, draw the attention to the display of stresses at the end of cure. Therefore, a mechanical analysis must be included for a proper behaviour prediction of the matrix mechanical properties as well as of the composite. Defects can also have origins on the thermal degradation process of the material under curing, which may happen as a consequence of the high internal temperatures registered in the matrix. This is another topic of investigation in this research.

For this purpose, a numerical modelling of the curing of a LY 556 epoxy resin was developed with coupled thermal, chemical and mechanical phenomena. The study involves the simulation of the cure with COMSOL Multiphysics®, firstly considering thermal and chemistry together, and then implementing the mechanics, for an analysis in the framework of elasticity. Results are benchmarked against previous studies performed with Abaqus, aiming a less time-consuming simulation with COMSOL Multiphysics, as being a more specialised tool for these kinds of couplings.

1.3 RESEARCH MOTIVATION

As commonly known, the use of composite materials in industry in general is extensive. It becomes interesting due to the possibility of designing materials with combinations of superior material and mechanical properties than those found in metals, polymers and ceramics individually, along with the ability of achieving these properties in desired directions according to the material's fabrication process, providing an anisotropic aspect. Choosing the ideal components also allows the production of economically feasible composites. The low weight, compared to metallic materials, leads to fuel economy and, then, rise in load capacity in aeronautics and aerospace, for instance. Consequently, besides the growing mastery of fabrication techniques, this class of materials has spread its applications in several areas.

Particularly in the oil industry, applications may include risers – structures in charge of transporting oil from offshore wells to platforms – coated cylinders for storage of natural gas for vehicles, offshore platform grids/gratings (Figure 3a) and metallic parts coatings with thermosetting polymeric resin composites. Their benefits commonly reside in a good strength to weight ratio and protection against weather and environmental conditions such as corrosion. In addition, another applicability of composites in this sector concerns repairs of steel pipes (Figure 3b) as a way of integrity maintenance of both the structure and the components, characterized by easy utilization and exemption of welding in this case.

Figure 3: Composites applications: (a) fibreglass grating; (b) composite wrap (glass and carbon fibres).

(a)

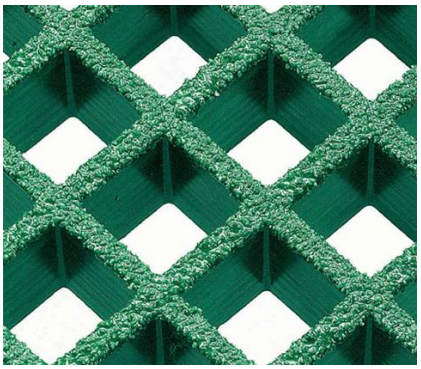

Source: Dura Composites Ltd, 2017.

(b)

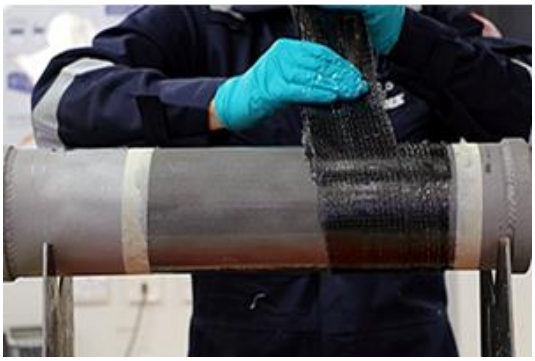

Source: MA Business Ltd, 2018.

Fibre reinforced composites represent the most important, technologically speaking, for they show high tensile strength limits. These are found not only in the greatest variety of applications but also in larger quantities, mainly to their properties at room temperature, ease of manufacture and cost. There are several combinations of fibre and resin in the world market. Epoxy resins, generally known as araldite, are the most efficient matrices, providing fine adhesion and relatively good mechanical properties (SMAALI, 2005). They also allow a broad range of properties and processing capabilities, contributing to their versatility (MAZUMDAR, 2002).

Fibre glass/epoxy is one of the most frequent composites due to the relatively low-cost of the fibre. Carbon fibres, although more expensive, represent a higher-performance material, since they have the highest specific module (elastic modulus to weight ratio) and specific strength (tensile strength to weight ratio), which are better preserved under high temperatures. Moreover, they are not affected by humidity or a wide variety of solvents, acids and bases; they show many physical and mechanical characteristics which allow specific designed properties to the composite; and relatively low-priced and cost-effective fabrication processes for the

fibres and the composites have been developed (CALLISTER, 2008). All of this contributes to the constant use of carbon/epoxy composites for more and more structural applications, especially in the offshore industry sector.

Despite the wide application of carbon/epoxy composites and the improvement in fabrication processes, there is still a lack in the knowledge and study of the complete curing cycle of the thermosetting polymer matrix. Epoxy resins can be cured in different cure rates and temperatures, for example, and this significantly affects the final properties of the material. Experimental studies for optimization of cure cycle and manufacturing processes can ensure better mechanical properties for the composites; nonetheless, it is an empirical knowledge, not being able to be expanded to different and specific uses.

The Finite Element Method (FEM), in such cases, becomes a powerful tool for behaviour analysis and material's internal state determination at the end of cure. Commercial software based on this method can particularly simulate the curing process and are in constant research and development for efficiency in material's design. The research takes place in both industry and academic community, improving the description of constitutive laws and the modelling of composite materials (JOCHUM, 2009).

In this context, COMSOL Multiphysics® is a FEM based commercial software which allows the coupling of distinct physical phenomena. It also permits the user to custom-define variable input parameters and the laws of evolution of properties throughout the simulation without the need of a programming language associated to it. Hence, modelling becomes less laborious and provides faster and reliable results. Many studies investigate and simulate the curing cycle with COMSOL Multiphysics® (BALVERS et at., 2008; PATHAM, 2009; MSALLEM et al., 2010; SHEVTSOV et al., 2012).

In this work, the COMSOL® software will be used considering the coupled physics of thermal, chemistry and mechanics as a means to develop fast, realistic and reliable predictive modelling approaches and simulations which describe the epoxy behaviour and represent changes in material properties and gradients found in the curing process. Experimental tests were as well performed to collaborate in the developing and validation of the models, for different curing processes. Such numerical models are fundamental for improvement and optimization of manufacturing processes and quality of composites, as well as ensuring operation safety, for high-performance applications, which are even more current in renewable energies, naval and offshore industries, to mention a few.

1.4 OBJECTIVES

1.4.1 General objective

The present work aims to study the process of curing of a thermosetting polymer matrix, more precisely, an epoxy resin matrix, for the purpose of evaluating the actual behaviour of the material in the manufacturing process of the composite. Multiphysics effects associated to the cycle of cure were considered, coupling thermal, chemical and mechanical phenomena. The focus remains on the numerical simulations of predictive models using the FEM developed on COMSOL Multiphysics®, which are validated with experiments and previous simulations of the material. In addition to this, the models contribute to a first thermal degradation analysis to which the resin is subjected.

1.4.2 Specific objectives

The study consisted of several steps to accomplish the general objective presented. In order to complete the work proposed, the following specific objectives were conducted:

- ✓ Execution of experimental tests of the curing process of a thermosetting epoxy resin;
- ✓ Development of numerical models on COMSOL Multiphysics® describing the behaviour of the epoxy resin during the cure cycle, first contemplating coupled thermal and chemical phenomena, then introducing the mechanical coupling;
- ✓ Comparison of numerical and experimental results obtained and consequent validation of the multiphysics models developed;
- ✓ Evaluation of curing parameters and properties of the epoxy resin during the curing process;
- ✓ Evaluation of the thermal degradation phenomenon.

2 COMPOSITE MATERIALS

This chapter presents the composite materials, approaching the conceptual part and the classifications generally applied by many authors. A special attention is given to the polymer matrix composites, which is the focus of the study. All of this contributes to a better understanding of the material under investigation and its behaviour during the manufacturing process of curing.

2.1. DEFINITION

By the classical definition of the literature, a composite material, also sometimes called composition material or simply composite, is composed of two or more materials or phases, producing a better combination of properties, which would not be obtained by each material individually (ASKELAND et al., 2011; CALLISTER JR., 2008). Among the most commonly cited examples of naturally occurring composite materials are: wood, where cellulose fibres impart strength and flexibility and are enveloped and bound by lignin, both of which are polymeric in nature; and bones, made up of collagen – a resistant and soft protein – and apatite – a hard and fragile mineral.

The term *composite*, however, is usually attributed to artificially made multiphase material. Another essential feature is the presence of a distinct interface separating its phases, which must be chemically different. Various ceramic materials and metal alloys, therefore, are excluded from this category of material.

Generally, the composite materials consist of only two phases, commonly called matrix (continuous phase) and reinforcement (dispersed phase). These phases may both be metallic, ceramic or polymeric in nature. They should have chemical affinity with each other and, in combination, provide a new material with "unusual combinations of stiffness, strength, weight, high temperature performance, corrosion resistance, hardness or conductivity" (ASKELAND et al., 2011). These new properties will be function as much of the properties of the phases as of the relative amounts of each, as well as of the geometry of the reinforcement.

As for the purposes of each phase, it is the matrix to transfer the mechanical stresses to which the material is subjected to the reinforcement and to protect it from the outside. In addition, the matrix maintains the structure cohesive and guarantees the properties of toughness, fatigue resistance and corrosion resistance of the material. The reinforcement, on the other hand, supports the mechanical loads transferred by the matrix. For this reason, the chemical affinity

between the phases and, consequently, the presence of the interface between them are necessary, since the absence of adequate adhesion between matrix and reinforcement can make the reinforcement a stress concentrator in the matrix and, therefore, reduce the mechanical strength.

Some of the properties of the composite material depend only on the relative amounts and properties of their constituents. These material properties can be accurately predicted by the ***Rule of Mixtures***. The property of the material is given by the sum of each fraction by volume of constituent material multiplied by its respective property, that is, a weighted average. The density of the composite ρ_c, for example, is given by:

$$\rho_c = \sum_{i=1}^{i=j} (f_i \rho_i) = f_1\rho_1 + f_2\rho_2 + \cdots + f_j\rho_j \quad (1)$$

where $f_1, f_2, \ldots, f_j$ and $\rho_1, \rho_2, \ldots, \rho_j$ are respectively volumetric fractions and densities of each material constituent. In the case, these constituents would be the matrix and the reinforcement.

The phases of a composite must be selected according to the application of the material in order to obtain the best combinations of properties. Among the main desired properties are high Young's modulus, high fatigue and corrosion resistance and low associated weight. A polymer matrix can be efficient in this task, since this type of material has a much lower mass than metals and ceramics. As for the reinforcement, it should not only be chosen in terms of its nature but also its form. For this reason, composites are usually classified according to their dispersed phase.

2.2 CLASSIFICATION BY REINFORCEMENT

There are several classifications of composite materials in the literature. Chiaverini (1986), for example, usually classifies the composites into five types regarding the reinforcement used:

- ✓ Fibrous, in which the reinforcement consists of fibres;
- ✓ Particulate, with reinforcements in the form of particles;
- ✓ Lamellar, where laminate constituents are arranged in layers;
- ✓ Scaled, with flat scales attached by a binder or incorporated in the matrix;
- ✓ Filled, where the matrix consists of a skeletal structure filled with another material.

Askeland et al. (2011) classify them into the following categories: particulate composites, fibre-reinforced composites and laminar composites. The author exemplifies each type with common materials. Concrete fits in the first classification, being composed of cement, sand and gravel; fiberglass is composed of glass fibres embedded in a polymer matrix, consisting of a fibre-reinforced composite; Finally, plywood represents a laminar composite.

Another classification widely used by other authors, such as Callister Jr. (2008), involves the concentration of composites in three main types, which may contain other subdivisions. They are: ***Fibre-reinforced Composites***, ***Particle-reinforced Composite*** and ***Structural Composites***. Each of them is presented below. The Figure 4 illustrates this type of classification.

Figure 4: Scheme of classification of composite materials.

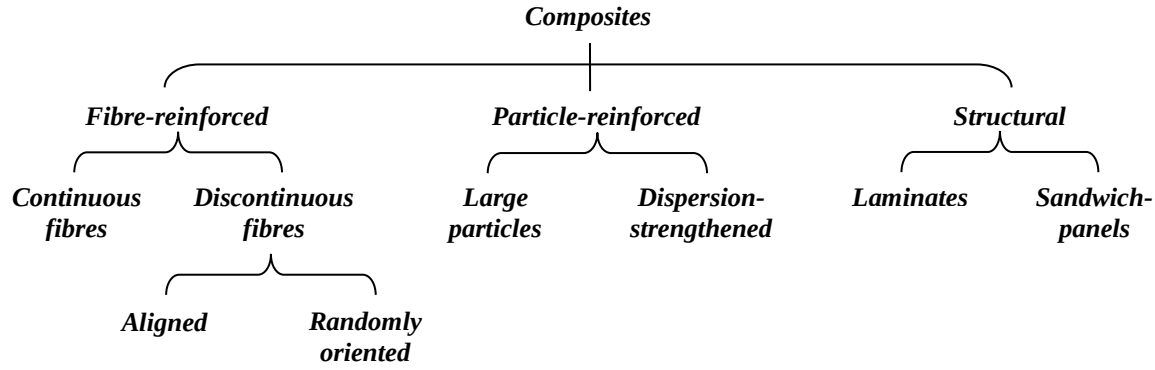

Source: Adapted from CALLISTER Jr. (2008)

2.2.1 Fibre-reinforced composites

Fibre-reinforced composites are considered to be the most important technologically, since materials of this category are common to improve properties such as strength, stiffness and Young's modulus in relation to the weight of the resulting material. This is achieved by inserting, in ductile matrices, generally low-density fibres which, although fragile, have high strength and hardness.

As explained in Section 2.1, the composite matrix is responsible for transmitting the applied force to the reinforcement, in this case the fibres, and they are the ones that support a large part of the load. The most encountered types of fibres include glass, carbon, aramid (Kevlar) and boron fibres. Whiskers, extremely expensive materials, also fit this classification,

with their constituents in the form of very thin single crystals and resulting in exceptional mechanical strength (CHIAVERINI, 1986).

The application of this class of composites is quite broad. From clay bricks reinforced with straw, as it was done in the past, to steel bars-reinforced concrete structures, usual in civil construction. In several industrial sectors, such as aerospace and petroleum, the use of polymer matrix composites reinforced with glass or carbon fibres is constant.

In fibre-reinforced composites, the mechanical characteristics are dependent on several factors. Among them are the properties of the matrix used, the union between matrix and fibres (for the effective transmission of the stresses) and the fibre characteristics. Together with these characteristics are clearly the properties of the fibres, but also their length, diameter, concentration and orientation.

Fibres length and diameter

Concerning the length, fibres can be considered as short – in which their sizes are so reduced that they do not cause significant strength improvement – or long. Hence, it is necessary to define a critical fibre length to the composite to achieve the desired effective improvement in strength and stiffness of the material. The critical fibre length l_c is dependent on the fibre diameter d, its tensile strength σ_f^*, and the shear strength of the fibre-matrix interface τ_e (or the yield stress to shear of the matrix, using the value whichever is less). The critical length expression is given by:

$$l_c = \frac{\sigma_f^* \, d}{2\tau_e} \tag{2}$$

Another way to define the fibre dimensions is through the l_c/d relation, called aspect ratio. The higher the aspect ratio, the better the composite strength. As superficial imperfections are one of the causes for fibre fracture, smaller diameters are preferred, thus obtaining smaller surface areas and, consequently, smaller possibilities of fibre failure. Furthermore, long fibres are preferred, since the ends of the fibre carry less load than the remainder of it, and reducing the ends increases the load carrying capacity of the fibres (ASKELAND et al., 2011). Critical-length fibres only reach the maximum load at their centre. With a longer length, the central length of the fibre is increased, supporting the maximum load and, thus, achieving a more effective reinforcement, as illustrated in Figure 5.

Figure 5: Increase in glass fibre strength with its growing length.

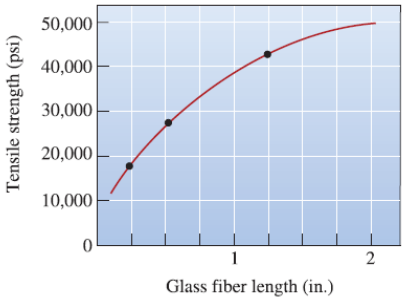

Source: ASKELAND et al. (2011).

When the fibre has a length much greater than the critical one, generally considering $l > 15l_c$, the fibre is called ***continuous***. Short or ***discontinuous*** fibres are those of length below this limit. Thus, the first subdivisions of the category are defined, shown in Figure 4.

According to diameter and nature, the reinforcement is classified into: ***whiskers***, ***fibres*** and ***wires***. ***Whiskers*** (graphite, silicon carbide, aluminium oxide, among others) have immensely high length-to-diameter ratios and, because of their small size, are theoretically defect-free, producing very high strength. ***Fibres*** have small diameters, being able to be polycrystalline or amorphous, and are usually polymeric or ceramic materials. Thin ***wires*** have relatively large diameters, used as radial reinforcement of steel in automobile tires, in high pressure hoses wound with wire and in jet engine housings rolled with filaments (CALLISTER JR., 2008).

Fibre concentration

As the Rule of Mixtures is generally applicable to strength and stiffness properties of a composite, a higher concentration of fibres implies a larger volumetric fraction, resulting in an increase of these properties (ASKELAND et al., 2011). The maximum volumetric fraction of fibres is usually about 80%, since above that the matrix is unable to completely envelop them. For fibre-reinforced composites, there are only two constituents: the matrix and the fibres. Thereby the Rule of Mixtures is reduced to the sum of only two parcels. Again, using density as an example, we have:

$$\rho_c = f_{matrix}\rho_{matrix} + f_{fibres}\rho_{fibres} \quad (3)$$

where ρ_c is the density of the composite, f_{matrix} and f_{fibres} are respectively the volumetric fractions of matrix and fibres, and ρ_{matrix} and ρ_{fibres} are their respective densities. The Rule

of Mixtures, however, is not always valid for this type of composite. Depending on the orientation of the fibres, this rule no longer applies to certain properties.

Fibre orientation

Fibres may be inserted into the composite's matrix in various orientations relative to one another. They can be unidirectional – when they are all oriented in the same direction – or they can simply be randomly oriented. If unidirectional fibres are orthogonally set, they are characterized with two-dimensional orientation, and if oriented in non-coplanar directions they are three-dimensional. In such manner, the material's strength can be improved in various desired directions.

Discontinuous/short fibres may be aligned, partially or randomly oriented. Randomly-oriented discontinuous fibres – used in cases of multidirectional stresses – offer a relatively isotropic behaviour in the material. Continuous fibres are unidirectionally aligned, producing property anisotropy and good strength and stiffness parallel to the longitudinal axis of the fibres, but low properties in the case of perpendicular load application. That is, the maximum strength and stiffness are obtained in the direction of alignment, whereas in the transverse direction the fibres do not offer effective reinforcement.

Fibre-reinforced composites can also be classified according to their type of matrix. Thus, the three possible classifications are: ***metal matrix composites*** (MMC), ***ceramic matrix composites*** (CMC) and ***polymer matrix composites*** (PMC).

For ***matrix metal composites***, the matrix consists of a ductile metal, and these materials allow their use at higher operating temperatures than their base metals and that of polymer matrix composites. They also have the advantage of being non-flammable, but their costs are usually higher than those of other types of matrices. Their reinforcements may be in the form of fibres or whiskers.

In ***ceramic matrix composites***, the matrix offers resistance to oxidation and deterioration as benefits. However, ceramic materials have low fracture toughness. For this reason, this type of composite aims to improve this material property. This is obtained through interactions between the cracks that advance, initiated in the matrix, and the dispersed phase, which prevents or delays their propagations.

Polymer matrix composites are the most common, usually using glass, carbon and aramid fibres as reinforcement, and polymer resin as matrix. The specific low mass promotes high specific strength and/or high specific modulus to the final material. Their popularity is largely due to their ease of manufacturing and lower cost.

2.2.2 Composites reinforced by particles

As shown in Figure 4, this class of composites can be considered to contain two subdivisions. They are: ***large particles-reinforced composites*** and ***dispersion-strengthened composites***. The two types of particulate composites are characterized according to the reinforcement mechanism or increase in strength.

Large particles-reinforced composites

Callister Jr. (2008) explains that when one uses the term "large" particles in the first type, it is to indicate particle-matrix interactions. These interactions cannot be treated from the atomic or molecular point of view, leading, therefore, to the application of the continuum mechanics for such materials. For this subdivision, the author points out that the particles are usually harder and stiffer than the matrix and tend to restrict the movement of the continuous phase of the composite in the vicinity of each particle.

Generally, this type of material is designed and produced in order to obtain unusual combinations of properties rather than increase strength (ASKELAND et al., 2011). Among the main examples of this category are:

- ✓ Concrete, already mentioned. Both the continuous (cement) and the dispersed phase (sand and gravel) are ceramic materials;
- ✓ Cermets. They are ceramics-metal materials, where the most used reinforcements are refractory ceramic carbides particles, with high hardness, dispersed in a metallic matrix. They have wide application in the field of machining for cutting tools of hardened steels;
- ✓ Milling and cutting wheels, composed of alumina (Al_2O_3), silicon carbide (SiC) and cubic boron nitride (CBN). The particles have the abrasive property and to provide strength they are joined by a glass or polymer matrix. With the rigid particles wear, they are fractured or removed from the matrix, exposing a new cutting surface;

- ✓ Electrical contacts on switches and relays, made of silver reinforced with tungsten. In this case, silver is responsible for electrical conductivity and tungsten, with its rigidity, offers resistance to wear, thus avoiding bad contact;
- ✓ Car tires, manufactured with carbon black on vulcanized rubber, a classic use of polymers reinforced with particulate materials. The small particles of carbon black, carbon spheroids of 5-500 nm in diameter, improve toughness and tensile, tear and wear resistance.

Dispersion-strengthened composites

As for the dispersion-strengthened composites, particles are generally smaller, having diameters between 0.01 and 0.1 μm (or 10 and 100 nm). The mechanism of strength increase involves interactions at atomic or molecular level between the particles and the matrix, more precisely the continuous phase dislocations. The particles block the movement of the dislocations, restricting plastic deformation and increasing the yield limit, the tensile strength and the hardness, similar to precipitation hardening.

Although this increase in strength is not as pronounced as in precipitation hardened materials, these composites do not have their properties catastrophically soften by overageing, overtempering, grain growth or coarsening of dispersed phase. Their reduction in strength is a gradual effect with increasing temperature. Besides, they have a higher creep resistance than that of metals and alloys (ASKELAND et al., 2011).

One of the most cited materials in this category is Sintered Aluminium Powder (SAP). Its aluminium matrix can have its strength increased by up to 14% by alumina (Al_2O_3), according to Askeland et al. (2011). There are also metals with addition of Thoria (ThO_2) as reinforcement, such as TD-nickel (Thoria Dispersed-Nickel).

2.2.3 Structural composites

Structural composites can be classified into ***laminates*** or ***sandwich panels***. They are composed of homogeneous materials or composites, according to Callister Jr. (2008), and their properties are dependent on both their constituent materials and the geometric design of the structural elements.

Laminate composites

This type of composite is constructed by stacking two-dimensional laminas or panels with a preferred direction in each layer having high strength. The layers may be arranged so that this direction is the same in all of them or variant, according to the material design requirements. The main desired characteristics of these materials are: increased corrosion and tensile resistance, and lower costs and weight. It is important to note that these materials are always anisotropic.

An example is plastics reinforced with continuous fibres, which can be considered as laminate composites. Similarly, fabric-like materials, where cotton, paper or glass fibres are woven into plastic matrices also fit into that category.

Sandwich-panels

Sandwich panels, also called sandwich-type structural composites, have thin layers used as a coating, bonded by adhesive to a light material that acts as a filler. Although neither the coating nor the filler material is resistant or rigid, the resulting material has relatively high stiffness and strength (ASKELAND et al., 2011). The layers of the coating are called faces, while the filling is called core, which is thicker.

The core of sandwich-type composites has low density and generally low Young's modulus. It is responsible for providing continuous support to the faces of the composite, must have sufficient shear strength to withstand cross shear stresses and be of sufficient thickness to provide high shear strength, resisting to material buckling (CALLISTER JR., 2008). Rigid polymer foams and wood are usually used as core.

Among the main examples is corrugated cardboard, with a corrugated core connected on both sides to flat and thick papers. As stated, the components alone are not rigid, but when combined generate a material having this rigidity.

A typical example of this category is also the hive structure, commonly present in aerospace applications. In it, cells are formed by thin strips, which are shaped into the desired shape – such cells can take the hexagonal, square, rectangular or sinusoidal form – made of materials such as aluminium, fiberglass, paper and aramid polymers. These moulded strips can be filled with various materials, including foam and fiberglass, providing good sound and vibrations absorption. Finally, they are glued having the axes of the cells oriented perpendicular

to the planes of the faces of the composite. The final strength of the material is dependent on: cell size, cell wall thickness and material used in the hive.

2.3 CLASSIFICATION BY MATRIX

Another way of classifying the composites is based on the type of material used as composite matrix. A more general classification divides the materials into ***inorganic matrix composites*** and ***organic matrix composites***, where the latter can still be categorized into ***thermoplastic organic matrix*** and ***thermosetting organic matrix***. Regarding the types of materials, a classification already mentioned in section 2.2.1 organizes the composites into three categories:

- ✓ Metal matrix composites (MMC);
- ✓ Ceramic matrix composites (CMC);
- ✓ Polymer matrix composites (PMC).

Wang et al. (2011) uses a very similar classification, considering the first one – Metal matrix composites – and the third – Polymer matrix composites – categories equal to those presented above. The second category, however, is called by the authors as *Inorganic non-metallic matrix composites*, which include Ceramic matrix composites (CMCs) and composites based on carbon, as a carbon/carbon composite.

Some characteristics of each matrix type have already been highlighted in Section 2.2.1. In addition, since the focus of this work is concentrated on polymer matrix composites, this will be the next explored category.

2.3.1 Polymer matrix composites

Polymer matrices give the material high specific strength and specific Young's modulus (properties-to-density ratios). Wang et al. (2011) lists other advantages of composites with this type of matrix:

- ✓ Fatigue resistance: for metal matrices, it corresponds to 30% to 50% of tensile stress, whereas for a carbon fibre/polyester composite it is 70% – 80% of tensile strength and for fiberglass composites their resistance to fatigue is a value among these presented proportions;

- ✓ Damage tolerance: composite failure occurs due to a series of damages including matrix failure, fibre extraction, splitting or rupture, and interface disconnection, while the common materials exhibit the unstable propagation of the main crack and its sudden failure;
- ✓ Damping characteristics: composite materials have high frequencies of vibration – proportional to the square root of specific Young's modulus – and the fibre-matrix interface in the composites can absorb the vibrational energy well;
- ✓ Multifunctional performance: among them, superior electrical insulation performance, good friction properties and high resistance to chemical corrosion;
- ✓ Good processing techniques: the material can be designed by selecting its constituents according to its condition of use and its performance requirements, the product moulding allows to choose the processing method according to its physical characteristics and can reduce the number of mounting parts, reducing the weight of the product and the time and material expended to obtain it;
- ✓ Capacity of property design and anisotropy: fibre-reinforced composites, for example, impart greater resistance to the material in the direction of dispersed phase orientation. Thus, the material is designed in a way that meets the design requirements, and reinforcing the material in a desired direction helps to optimize its design.

The negative aspects of the polymer matrix composite are the low degree of automation and mechanization processes, low consistency of material properties and stability of product quality, imperfection of quality testing methods and weak long-term high temperature and aging resistances. Among the most used in the matrices and most economically feasible polymer resins are the polyesters and the vinyl esters, widely applied in conjunction with glass fibres. Epoxies tend to be more expensive, being quite present in the aerospace sector, since they offer better mechanical properties and greater resistance to humidity. Polyimide resins are recommended for applications at high temperatures (CALLISTER JR., 2008).

Glass fibre-reinforced composites embedded in a polymer matrix are most commonly produced and are known only as "glass fibres". The glass has its wide application due to the ease to stretch in the form of high strength fibres starting from its melted state, besides its availability and its economical manufacture in a reinforced plastic through several existing techniques. Glass is also chemically inert when associated with different plastics and is useful in corrosive environments (CALLISTER JR., 2008). Although glass fibres provide high strength, the composites created with them are not very rigid, and the polymer matrix makes it

impossible to operate at elevated temperatures (above 200°C) due to the beginning of its yield or deterioration. They are widely applied in automotive structures, storage containers and aircraft fuselage and wings, resulting in lightweight and resistant materials.

Carbon fibres polymeric composites, the famous "carbon fibres", are another option. Some of the benefits of them are higher specific modulus (elastic modulus/weight) and higher specific strength (tensile strength/weight) between the fibre reinforcements, maintaining their properties at elevated temperatures; the fact that they are not affected by humidity at room temperature; and its diversity of physical and mechanical characteristics, making it possible to design composites with specific properties (CALLISTER JR. 2008). These materials may have high manufacturing costs but are ideal when high specific strength and modulus is required with applications in the civil, automotive, aerospace, oil and high-performance sports industries.

Polymer matrix composites may be made with only one type of polymer or a mixture of them. They can be further divided into two classes: ***thermoplastic polymer matrix composites*** and ***thermoset polymer matrix composites***.

Thermoplastic polymers are of high molecular weight and non-crosslinked – being semi-crystalline or amorphous – having structures of straight or branched chains. As temperature rises, they soften and melt, and harden when temperature is reduced, consisting of reversible processes. Although they have strong intramolecular bonds, intermolecular bonds aren’t so (AGARWAL et al., 2006). For this reason, by increasing the temperature, the secondary bonds between the molecules decrease and facilitate the relative movement of adjacent chains with the application of a stress (CALLISTER, JR., 2008). Among them are polyethylene, polystyrene and nylon.

Thermosetting polymers, on the other hand, have a cross-linked structure (three-dimensional molecular chains) and covalent bonds between all molecules. The crosslinking process, given by curing, occurs with the solidification of the material. Therefore, when heated, thermosetting polymers do not melt, but decompose, and cannot be remoulded, configuring solidification as an irreversible process. Typical examples are epoxies, polyester resins and phenolic resins (AGARWAL et al., 2006).

Thermosetting resins are usually harder and more resistant than thermoplastics and have better thermal and dimensional stability. Mazumdar (2002) shows basic properties of some thermosetting resins, epoxy being the one with greater tensile elastic modulus and strength, as observed in Table 1.

Table 1: Typical Unfilled Thermosetting Resin Properties.

Resin Material	***Density (g/cm³)***	***Tensile Modulus (GPa)***	***Tensile Strength (MPa)***
Epoxy	1.2 – 1.4	2.5 – 5.0	50 – 110
Phenolic	1.2 – 1.4	2.7 – 4.1	35 – 60
Polyester	1.1 – 1.4	1.6 – 4.1	35 - 95

Source: MAZUMDAR (2002).

Thermosetting resins, however, must be produced with due attention and control to obtain their final properties because of the impossibility of remoulding. The crosslinking effect involves a thermosetting chemical reaction, which occurs with the demanded heat supply, characterizing the material curing. The production of thermosetting polymeric matrix composites must therefore have the necessary control during curing, so that both the desired matrix performance is achieved, and the reinforcement is not adversely affected (SMAALI, 2005).

3 THE PROCESS OF CURING

As mentioned, epoxy resins, the central issue of this research, are a customary example of thermosetting polymers, passing through the curing process during the formation of the desired composite material with this type of matrix. Afterwards the particularities of this process will be presented, as well as its intrinsic phenomena and parameters effects.

3.1 EPOXY RESIN

Wright (2002) defines epoxy resins as "a group of crosslinked polymers, and are sometimes known as the oxirane group, which is reactive toward a broad range of curing agents." That is, under the activity of various curing agents, this low molecular weight polymer undergoes a chemical reaction, called curing, and transforms into a thermosetting three-dimensional structure with relevant properties.

Epoxy is a synthetic resin with numerous applications, including adhesives, coatings and fibre-reinforced composite matrices, current in mechanical, chemical, aerospace, naval, offshore and other industrial sectors. According to Wang et al. (2011), it is an organic prepolymer with molecules containing two or more epoxide groups, given by the structure below:

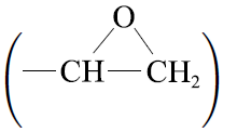

Still according to the authors, these epoxide groups may be located either at the end or in the middle of the molecular chain or in a ring structure. Moreover, the fact that they are capable of cross-linking with various curing agents is due to the active epoxide group of the molecular structure.

The main characteristics and properties of epoxy resins listed by Wang et al. (2011) are:

- ✓ Great variety, with respect to resins, curing agents and modifying agent systems;
- ✓ Ease of curing: depending on the curing agent selected, curing of the epoxy resin is carried out in the temperature range of 0ºC to 180ºC;
- ✓ Strong adhesion, due to the inherent polarity of the structure, having a high adhesion to various substances;

- ✓ Low shrinkage: epoxy resin, unlike other thermoset polymer resins, does not produce sub products during curing and has a high degree of association in the liquid state. With this, the cure is performed by direct addition reaction, showing a small shrinkage;
- ✓ Excellent mechanical properties of the cured resin;
- ✓ Electrical properties: the cured epoxy resin has good electrical performance over a wide range of frequencies and temperatures, being a good insulating material;
- ✓ Strong chemical stability of cured resin;
- ✓ Dimensional stability;
- ✓ Resistance to fungi; it can withstand most fungi and be used under harsh tropical conditions.

They are the most widely used resins, having varying grades of epoxies with varying levels of performance. Another advantage associated with this material is its ability to be formulated with other materials or mixed with other epoxies to meet a specific performance need. Their material properties can be changed with the formulation of the epoxy: cure rate, processing temperature requirement, time of cycle, toughness and temperature resistance, no mention a few.

Epoxies are more costly than other resins, such as polyester and vinylesters, which leads to their applications for specific performance demands instead of cost-sensitive markets. These materials can form composites with good performance at room and elevated temperatures, being able to operate well up to temperatures of 90 to 120 °C. There are also epoxies which can perform well up to 200 °C, offering as well good chemical and corrosion resistance, but costs increase (MAZUMDAR, 2002).

As a means to obtain a large part of the properties and characteristics, the epoxy resin must first be cured, as observed. The curing process will therefore be subsequently presented.

3.2 CURING TRANSFORMATIONS

Thermosetting resins, when exposed to high temperature, from room temperature to approximately 230 °C, undergo the process of cure, or polymerization, which consists of an irreversible chemical reaction and where the hardening occurs through the structure's cross-linking (WRIGHT, 2002). This supply of energy given by raising the temperature is necessary for the reaction to start, or it is also possible to use a curing agent, also called a hardener. The

resulting material from curing, initially in the viscous flow state, soluble and capable of melting, is an insoluble, three-dimensional, non-melting solid (WANG et al., 2011).

The curing of a resin is both thermoactivated and exothermic, and the reaction usually occurs from a mixture of three components: the epoxy prepolymer, the hardener and the accelerator. Commercial prepolymers, “epoxy resin” as called on Section 2.4.1, are numerous, with the Bisphenol A Diglycidyl Ether (DGEBA, or BADGE) as one of the most regularly found in naval and offshore industries for thick epoxy composites and the one selected for this work. They show an initial linear structure. Hardeners form the three-dimensional network when reacted with epoxy, amines and anhydrides being representatives of this category. They present a quite variable chemical nature and determine the type of chemical bonding and the network’s degree of cross-linking – hence, the cure characteristics and properties of the final product (MAZUMDAR, 2002).

Finally, accelerators promote the cross-linking of the prepolymer/hardener mixture, reducing the total time of the reaction. They do not modify physicochemical mechanisms of polymerization, as total enthalpy and glass transition temperature. The reaction’s final degree of cross-linking is not affected as well (RABEARISON, 2009).

The cross-linking density of molecular chains is commonly called degree of conversion as a way to characterize the cure kinetics. The degree of cure (α), therefore, varies from 0 – the initial liquid state of the resin – to 1, or 100% – fully cured resin. During the chemical reaction of cure, resin starts in the liquid viscous state, changes to a rubbery state solid and, afterwards, becomes a solid in a glassy state. The Time–Temperature–Transformation (T.T.T.) Diagram in Figure 6 represents these phase changes along an isothermal cure at 120°C, for example.

Figure 6: LY 556 epoxy T.T.T Cure Diagram.

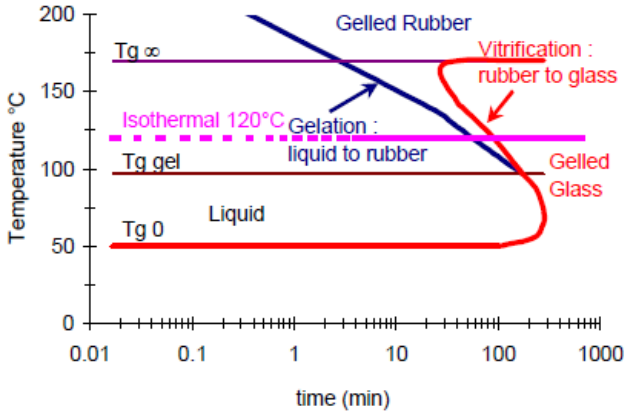

Source: JOCHUM et al. (1999).

Parameters T_{g0} and $T_{g\infty}$ are, respectively, the glass transition temperatures for the resin system with unreacted components (degree of conversion of $\alpha = 0\%$) and for the system with completely reacted components ($\alpha = 100\%$). Below T_{g0} the system is nonreactive, and can be considered as the storage temperature of the material. $T_{g\infty}$ represents the maximum glass transition temperature, being the maximum limit of glass transition temperature, T_g.

The diagram highlights two phenomena which occur during curing of thermosetting systems: ***gelation*** and ***vitrification***. $T_{g\ gel}$ represents the temperature where they coincide, occurring simultaneously. Gelation and vitrification play an important role in the curing process and, consequently, on the final properties of the material. Thus, the process characterization must be performed, and these phenomena ought to be studied for the purpose of correct properties prediction.

3.2.1 Gelation

Gelation refers to the change of the material under curing from liquid to a cross-linked gel, or rubber. It is characterized by the initial formation of a macromolecular network, where the thermosetting material starts to lose its ability to flow. The material's viscosity grows exponentially due to cross-linking, with the reaction reaching a critical conversion which is called "gel point". At gel point, the material is not liquid but not quite solid yet; it is a mixture of a soluble phase giving way to the insoluble one in formation – a gel of macroscopic size. For the appearance of the gel, the material can be considered as a viscoelastic solid (RABEARISON, 2009).

After gelation, the cure process becomes slower on account of the increase in cross-linking density, restricting, thus, the system mobility. Cross-linking density rise also enlarges glass transition temperature and mechanical properties (COSTA et al., 1999). Moreover, above gel point the material can no longer be processed. The gelation process is, therefore, irreversible. The gelation of a chemical reaction of cure doesn't take long, only a few minutes (called gelation time). It can be seen in Figure 7 from the starting increase of viscosity (μ) to its divergence to considerably greater values. The elastic modulus can also be verified to greatly increase after gelation.

Figure 7: Viscosity and Elastic Modulus evolutions of the epoxy resin in the chemical reaction of polymerization.

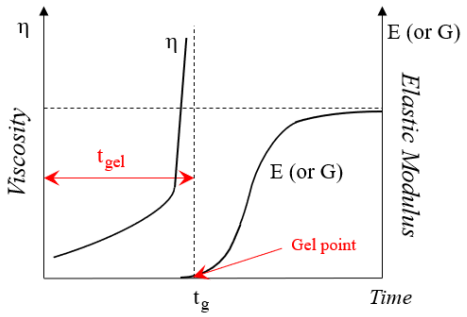

Source: Adapted from RABEARISON (2009).

According do Wang et al. (2011), Flory's gel theory says the degree of cure for any cross-linking reaction is a constant at gel point, not related to reaction temperature or experimental conditions. Rabearison (2009) highlights that the degree of cure at gelation, called α_{gel}, is comprised between 40% and 80% for epoxy systems. For the LY 556 epoxy blend, the subject of this work, Jochum et al. (2008) identified the start of gelation at a degree of conversion of α_{gel} = 55%.

3.2.2 Vitrification

As long as the glass transition temperature, T_g, is below the reaction temperature, the material remains at rubbery state. During curing, however, at a certain point T_g equals (and then overcomes) the temperature of the system, giving space to vitrification. The transformation associated to this phenomenon is the transition of the material from rubbery to glassy state. Unlike gelation, vitrification is a reversible process by heating, and a glassy state may return to rubbery state.

At glassy state, system mobility is further reduced as densification of the forming network increases while thermal agitation reduces. Reaction becomes more and more controlled by diffusion of reactants. Hence, keeping reaction temperature above T_g enables curing to remain at rubbery state, achieving a greater reaction rate and a maximum degree of cure. A conventional fabrication process involves a post cure, where cure temperature is increased in order to augment cross-linking density and, consequently, improve the degree of cure and mechanical as well as physical properties.

Aside from structural and state transformations, the process of curing involves the occurrence of shrinkage and viscoelasticity. They greatly affect the quality of a fibre-reinforced composite, for it is proven that resin shrinkage is directly related to generation of residual stresses and, so, fibre waviness (RABEARISON et al., 2008; LORD & STRINGER, 2009; MSALLEM et al., 2010), as viscoelastic behaviour of the resin induces stress relaxation effects, rightfully studied at several works (WISNOM et al., 1999; EOM et al., 2000; JOCHUM et al., 1999; 2007; 2008; RABEARISON et al., 2009; PATHAM, 2009; 2012). These effects will be then discussed.

3.2.3 Shrinkage

Cross-linking and temperature changes are the two driving forces of volume variation in a thermosetting polymer during curing. The chemical shrinkage accounts for the first cause, as molecular chains are configured in a more compact – denser – rearrangement, while the second cause consists of a thermal shrinkage that takes place at the cooling and final stage of cure, when the cured polymer at a higher temperature at the end of the chemical reaction returns to room temperature.

Several studies show that shrinkage in a fibre-reinforced composite leads to development of internal stresses and fibre waviness. Nevertheless, stresses emerge at the hot stage of cure, not on the cooling one. Jochum et al. (1999) observed the mechanism of fibre waviness in a single fibre carbon/epoxy composite. They established it as being the consequence of fibre microbuckling phenomenon, created by resin shrinkage during the hot phase of curing. Experiments were carried out at different cure cycles but with the same cooling phase. The sample with a fast cure presented fibre instability, as the one with slow cure didn't, which led to the conclusion that thermal stresses don't trigger fibre microbuckling phenomenon during cooling. This is an evidence that internal stresses are mainly generated due to chemical shrinkage of the matrix from the reaction of cure, before exposing the cured composite to room temperature – thermal shrinkage at cooling stage.

Thereafter, Jochum et al. (2007) measured experimentally fibre instability at the hot stage of cure. The authors registered in real time video the undulation evolution of a long carbon fibre in a LY 556 epoxy resin, characterizing the undulations according to wavelengths measured from a sinusoidal-like behaviour. Recordings show lower wavelengths – and so higher amplitudes – at the hot stage of cure, indicating the development of stresses. In a

following work (JOCHUM et al., 2008), authors claim that fibre instability is triggered at local heating rates above 3°C/min, coinciding with the maximal chemical shrinkage observed prior to glass transition. Hence, slower cure rates at lower temperatures provide a more uniform degree of cure, temperature distribution and shrinkage, reducing internal stresses. Afterwards (JOCHUM et al., 2013; 2014; 2016), the authors kept on investigating internal residual stresses development during curing of thick epoxies, where there is a greater heterogeneity. They simulated samples exposed to laser induced shock waves for internal stress level and damage prediction, registering internal stresses around 10 MPa.

Wang et al. (2011) state that only a part of curing affects internal stresses, as the resin before gel point is in its liquid state. Molecules are free within the mould and are not yet fixed on the surface of fibres, which cannot produce internal stresses. The same is affirmed by Jochum el at. (2007; 2008), Rabearison (2009) and other authors: internal stresses start appearing at gelation, where the polymer structure begins to form, chemical shrinkage is produced, and resin elastic modulus evolves.

As for the volume change in epoxy resins, Li et al. (2004) presents three stages (Figure 8). Stage ***a-b*** corresponds to the thermal expansion which the resin undergoes when at an initial temperature it is heated up to the curing temperature. At stage ***b-c***, chemical shrinkage occurs, and the volume intensely decreases. Stage ***c-e*** refers to thermal contraction, when the resin is cured to room temperature. At point ***d***, there is the volume at glass transition temperature, at which the coefficient of thermal expansion suffers an extreme change.

Figure 8: Schematic of volume change of epoxy resins during cure.

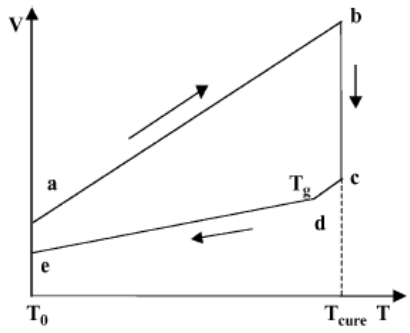

Source: LI et al. (2004).

The authors performed an in-situ measurement of chemical shrinkage of an epoxy resin. They came to the conclusion, from different cure cycles, that it is a function of degree of cure alone, regardless of time and temperature, being applicable to a wide range of materials. The Li et al. approach is acknowledged by the scientific community and defines chemical shrinkage

as a bi-linear relationship fitted to experimental data. The break-point is found at a degree of cure of 28% – related to the gel point of the studied resin –, with a corresponding chemical shrinkage of 3%. Extrapolation of results to a degree of cure of 100% showed a total chemical shrinkage of 6.9% (Figure 9).

Figure 9: Chemical shrinkage versus degree of cure for Li et al.'s bi-linear fit to a 100°C isothermal cure.

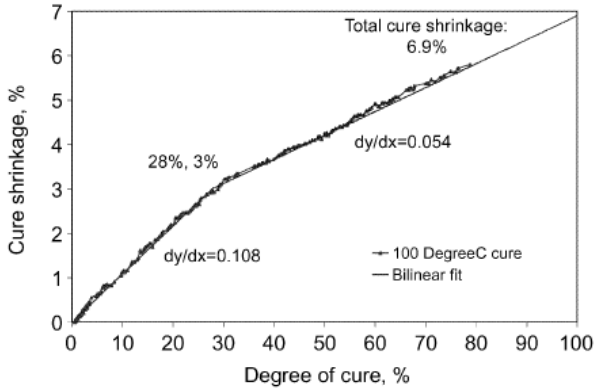

Source: LI et al. (2004)

3.2.4 Viscoelasticity

The property of viscoelasticity enables materials to show both viscous and elastic characteristics when under deformation. The relationship between stress and strain depends on time (or frequency, for a frequency domain). The slope of a stress-strain plot, thus, depends on the strain rate. Viscoelasticity is a still growing subject in composites studies, and recent works show relations between viscoelasticity and generated residual stresses in fibre-reinforced composites.

Eom et al. (2000) characterized the evolution of elastic modulus of an epoxy/amine system during cure, it being described with a phenomenological model for prediction of levels of internal stresses. The authors performed experimental tests for cure kinetics determination and viscoelastic properties measurements. The proposed model accurately predicts the relaxation modulus of a thermosetting system over the complete range of cure (at any moment and at any cure temperature), providing a full description of instantaneous viscoelastic properties during curing.

Further investigating fibre undulations evolution, Jochum et al. (2007) noticed a slight increase in fibre wavelength before and during the cooling stage to room temperature. The authors highlight the viscoelastic behaviour of the matrix as the cause of it, which enables

matrix tensile relaxation and a consequent decrease of fibre compressive stress, increasing its wavelength. Residual stresses are, therefore, reduced compared to a solution in the elastic framework.

Elastic calculations of compressive load to which fibres are submitted are overestimated, since there is evidence of viscoelasticity of the matrix. Viscoelastic effects weren't, however, explored in this work, but they are to be taken into account on further modelling approaches for epoxy resin matrix characterization as well as for fibre instability mechanism in a fibre-reinforced composite.

3.3 EFFECTS OF CURE PARAMETERS ON MATERIAL PROPERTIES

In addition to the own constituents of a composite mentioned in Sections 2.1 and 2.2, the moulding process can significantly influence the final properties of the material. As for the parameters adopted in the cure of the polymer resin, pressure, temperature and time are of paramount importance.

3.3.1 Pressure

Effects of pressure consist in making parts denser and removing low molecular weight materials, such as residual solvents, water, air bubbles and molecules released during curing, as well as accelerating and enhancing impregnation. The pressure point in the formation of a composite material should be controlled when pressure is imposed on parts of the material (WANG et al., 2011).

Costa et al. (2005) state that pressure should be imposed when the resin does not gel, but almost gel. This permits fibres to be properly wet and promotes the compaction of the laminate. If pressure is imposed before this, the material will have a large empty fraction due to resin loss. If it is imposed after that, the pressure will not be able to remove air bubbles, because the resin has already gelled, and the material will have a non-compact and low adhesion between the layers, as well as great porosity.

3.3.2 Temperature

The curing temperature is related to the chemical reaction activity of resins and curing agents. In thermosetting polymers, reaction is usually centred in the curing agents and irradiated to the surroundings, causing the area around the curing agent to have a high crosslinking density and this density is reduced in other parts of the polymer in formation. In curing, the influence of temperature refers to curing performed in several steps or in a single step.

In cases of pre-cure at low temperature, reaction is slow, allowing macromolecules to move and the curing agent to completely react with the surrounding resin. The result of this is the presence of more reaction centres and, consequently, a uniform structure with more uniformity in crosslink density. After this pre-cure, there is a cure at high temperatures, which can improve mechanical properties and heat resistance of the matrix.

Cures performed only at high temperatures lead to rapid cross-linking reactions. Although reduction in cure time by increasing cure temperature may seem an advantage in industrial processes, it can lead to significant loss in the product quality of the composite. Effects may comprise augmentation in residual stresses, shape distortions and delaminations (SHEVTSOV et al., 2012). At higher cure temperatures, the curing agent is concentrated and unable to react with more distant macromolecules. Unlike the first case, the generated solid becomes more heterogeneous, presenting different densities of crosslinking and greater thermal gradients during curing, leading to higher internal efforts.

In thick-walled matrices, the effects of a higher cure temperature are intensified. In Figures 10 and 11, the results of it can be observed. Epoxy cylinders with a 32-mm diameter, poured into a 6.5 mm thick steel cylinder mould, submitted to cycles with cure temperature of 140°C show the heterogeneity of conversion from a cut of the cylinder's bottom surface – Figure 10a –, which is noticed by the concentration of orange tones in the centre. The centre has a higher degree of cure as the resin's low thermal conductivity doesn't allow the heat produced by the exothermic reaction to be easily dissipated. Hence, with higher temperatures, so is the cure rate and the degree of cure. In Figures 10b and 11, light diffraction evidences presence of cracks developed by the stress state in the material, which will drastically have an impact on the composite strength. As cure temperature augments, the epoxy shows a darker coloration, tending to hide these defects and making visual inspection more difficult.

Figure 10: LY 556 epoxy cylinder of 32 mm diameter cured with an isotherm of 140°C: (a) bottom-cut surface and (b) full cylinder.

(a)

Source: Author.

(b)

Source: Author.

Figure 11: LY 556 epoxy half-cylinder of 32 mm diameter cured with a heating rate of 3°C/min followed by an isotherm of 140°C.

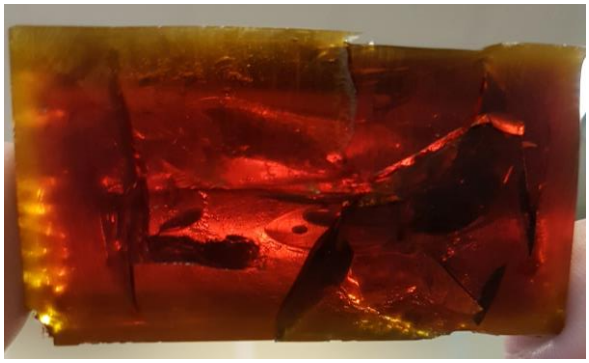

Source: Author.

Another phenomenon related to high cure temperature is thermal degradation, as polymers degrade when overheated. Polymer chains may be ruptured and produce components which react with one another, changing the properties of the polymer. The great values of temperature that remain in the material, since the heat generated cannot diffuse, may reach a critical value at which the polymer suffers thermal degradation. Consequences of the process include loss of mass and production of gases, inducing the emergence of bubbles and increasing internal pressure, leading to cracks. It is probable that most cracks in Figure 11 were a result of thermal degradation.

Some works in literature present studies on cure temperature effects over a thermosetting polymer. Junior et al. (2012) performed experimental tests on fibre glass-reinforced composites with a polyester matrix. They highlight the appearance of residual stresses due to chemical shrinkage of the matrix, which directly affects the fibres. Cure

temperatures were 40°C, 60°C, 80°C, 100°C, 120°C and 140°C. The authors carried out impact tests and detected a growing impact strength with cure temperatures from 40°C to 100°C. Although less cross-linking leads to higher toughness, higher temperatures promote adhesion fibre/matrix, positively influencing impact resistance. For 120°C and 140°C it was expected that this property would increase as well but it reduced instead. The reason for this was thermal degradation of the polymeric matrix, found in this paper. Balvers et al. (2008) verify through finite element numerical simulations thermal degradation on thick-walled epoxies. As anticipated, increasing thickness shows a more severe heating leading, thus, to degradation of the matrix.

A good knowledge on thermal degradation temperature can help avoid the quality defects provoked by it by ensuring that temperatures along the resin are below this limit. One of the techniques for establishment of the critical temperature where degradation starts is Thermogravimetric Analysis (TGA). In this destructive technique, a sample is heated in a controlled environment while measurements of the sample's mass are made throughout the increasing temperature. As mentioned, when the sample degrades, its mass reduces. Figure 12 shows the evolution of mass loss in a TGA of a LY 556 epoxy resin sample.

Figure 12: Thermogravimetry and Derivate Thermogravimetry of a LY 556 epoxy resin.

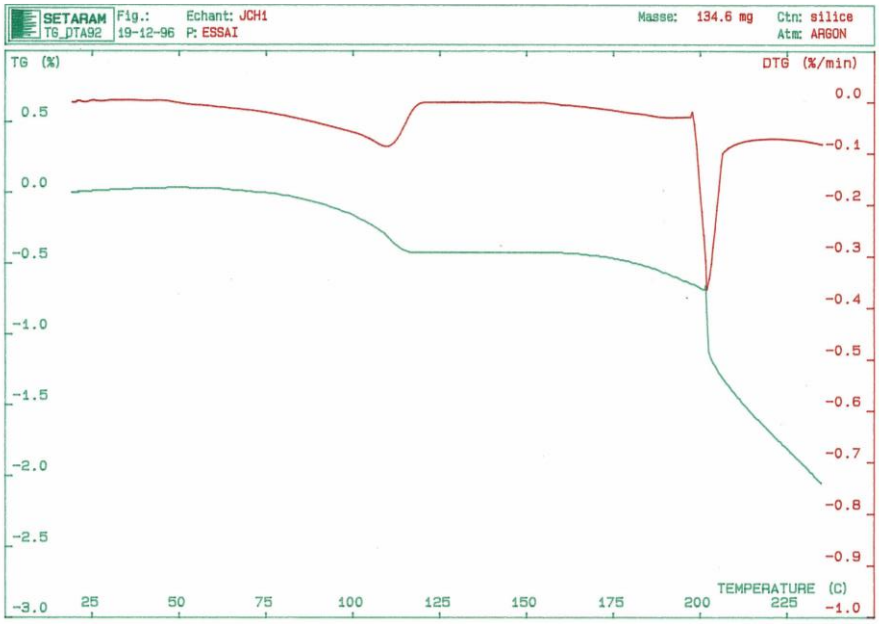

Source: Courtesy of ENSTA Bretagne.

The curve in green represents the loss of mass percentage (TG), where the red curve is its derivate over time (DTG). There is a first drop on TG curve up to around 120°C, which is probably loss of mass regarding evaporation of water within the resin. As measurements

proceed, mass of the sample keeps constant until after 150°C, decreasing once again. A slight change in DTG curve inclination can be observed with respect to this fall, indicating the beginning of thermal degradation process. At the vicinity of 200°C, TG – and DTG – drops drastically, clearly evidencing the degradation of the material. Data on the process can be better visualized at DTG. The peak area on the red curve consists of the mass variation of the material while the peak itself is the temperature in which mass variation is maximum in the process. The determination of the point where degradation begins is fundamental for curing optimization studies.

Taking all reported information into account, fabricants preferably carry out the multiple-step curing process. It's a way of avoiding temperatures within the resin which might overcome the limit of thermal degradation initiation. As thermal reaction reaches its peak around gelation, the solution consists of carrying out curing at a lower temperature until the resin is gelled. It favours total resin impregnation and eliminates air bubbles at the composite interface. Moreover, during the low temperature step, the reaction, as already mentioned, is slow and facilitates control of the pressure point of the material. Afterwards and before material turns to glassy state, temperature is gradually risen to a higher platform level, a process also known as post-cure, in order to further improve cross-linking degree and mechanical properties, as well as relaxing internal stresses (WANG et al., 2011).

4 CURE CYCLE OF AN EPOXY RESIN

For characterizing and further modelling the cure process of an epoxy resin, cure kinetics must be investigated and established. Local temperature and degree of conversion predictions enable quality description of the polymer. Therefore, a following overview on cure kinetics is presented, along with the determination of parameters, to fully describe a thermo-chemical-mechanical analysis of curing.

4.1 CURE KINETICS

Characterization and monitoring of curing processes of thermosetting polymers can be performed by several techniques, such as Infrared Spectroscopy (IR), Dynamic Dielectric Analysis (DDA), Viscosity Analysis, Dielectric Spectroscopy, Torsional Braid Analysis (TBA), Dynamic Mechanical Analysis (DMA) and Differential Scanning Calorimetry (DSC). Wang et al. (2011) present a table – Table 2 – with some of these techniques, their indicators and transformations through the stages of curing.

Table 2: Characterization of the curing stages by a few techniques.

Technique	**Indicator**	**(A)**	**(B)**	**(C)**	**(D)**
DSC	dH/dt	Endothermic-melting	Get to the peak value	Exothermic slowly	No significant changes
	Dynamic $\mu - t$	Gradually get to the lowest point	Go up rapidly	Go up slowly	No significant changes
DDA	Capacitance $C - t$	Gradually get to the level step	Get down rapidly	Get down slowly	No significant changes
IR	Concentration of functional groups	A little change	A big change	No significant changes	No significant changes
Viscosity	$\mu - T$	Get down to the lowest point	Go up rapidly	Go up	Difficult to determination

(A) from ungelled glass state to viscous flow state; **(B)** from viscous flow state to the gel point; **(C)** from the gel point to glass state; and **(D)** solid-phase reaction within glass state

Source: Adapted from WANG et al. (2011).

Differential Scanning Calorimetry is one commonly, if not the most, applied technique, where the amount of energy absorbed (endothermic process) or released (exothermic process) by a sample and a reference submitted to heating or cooling are measured. For this technique, a metal capsule containing a few milligrams of the sample and an identical empty capsule – the reference sample – are placed in two identical micro-ovens, which submit the samples to the

same thermal cycle T(t). Differential heat flux necessary to keep a temperature difference of zero between the micro-ovens is registered. Over the years, literature works constantly report the use DSC to monitor cure kinetics of epoxy resins (OLCESE et al., 1975; HEISE & MARTIN, 1990; MONTSERRAT & MALEK, 1993; COSTA et al., 1999; KARKANAS & PARTRIDGE, 2000; RABEARISON et al., 2011; HARDIS et al., 2013).

Olcese et al. (1975) study curing kinetics of two different epoxy systems, evaluating their influences on the rate of curing. Heise & Martin investigate a blend of epoxy with imidazole instead of amines and determine the reaction kinetics with DSC and Fourier Transform Infrared Spectroscopy (FTIR), developing a model for describing the cure behaviour of such system. Cure kinetics for a reaction in non-isothermal conditions was the topic addressed by Montserrat & Malek (1993). For Karkanas & Partridge (2000), four epoxy/amine systems were explored under both isothermal and dynamic curing conditions, using DSC to determine cure kinetics.

Rabearison et al. (2011) identified all parameters for an Araldite LY 556 epoxy for a complete, temperature dependent cure kinetics by isothermal and non-isothermal DSC, consisting of a strategic step for use in further finite element analysis of the curing. Hardis et al. (2013) use Dielectric Analysis (DEA) and Raman spectroscopy for in-situ cure monitoring, comparing the degree of cure with data obtained from DSC and achieving good agreement in the three results. The authors, however cite the fact that DSC is performed in laboratories under ideal conditions, which is an obstacle for in-situ cure monitoring.

Whatever technique applied, they all come to the same point: the determination of the degree of cure. This parameter can be achieved experimentally or by cure kinetics modelling. There are two types of modelling approaches: mechanistic models and phenomenological models. According to Rabearison (2009), mechanistic models take into account reaction mechanisms, but their use is more complex, especially for epoxy chemical reactions. Appropriate modelling can be achieved by phenomenological models due to their agreement with experimental results. They don’t, however, consider chemical phenomena, hence being, in principle, limited to the time and temperature zone studied for their determination. In the following sections, degree of cure and cure kinetic models will be discussed.

4.1.1 Degree of cure

Degree of cure, or degree of conversion (α), is used to characterize and monitor the cure process of thermosets. This parameter is strongly influenced by cure temperature, as previously said, and heat exchanges with the environment. Processing DSC measurements, the degree of cure at a particular time t is defined as the ratio between the reaction's enthalpy at that instant – $H(t)$ – and the reaction's total enthalpy for a fully cross-linked resin – H_U. It is expressed by:

$$\alpha(t) = \frac{H(t)}{H_U} = \frac{1}{H_U} \int_0^t \left(\frac{dH}{dt}\right) dt \tag{4}$$

where dH/dt is the measured heat flux, in power units.

The degree of cure can also be written in a formulation in terms of the reaction/cure rate $d\alpha/dt$ $[s^{-1}]$, that is how fast polymerization takes place and α increases, assuming the following form:

$$\frac{d\alpha}{dt} = \frac{1}{H_U} \left(\frac{dH}{dt}\right) \tag{5}$$

As previously exposed, the higher the cure rate, the lower the process cycle. Besides, the higher cure temperature, the higher the maximum degree of cure of the resin, obtaining a denser material. In fact, degree of cure rarely achieves unity (100%). Hence, it is considered that the curing process reaches its end as the degree of cure – and material properties since they depend on α – are stabilizing.

4.1.2 Horie's mechanistic model

Cure reaction can also be characterized by models. As mentioned, mechanistic models consider the mechanisms of reaction that take place during curing. There may be two of them: mechanism of addition – an addition reaction between the hydrogen of a primary amine and an epoxy group, forming a secondary amine which reacts again with another epoxy group, resulting in a tertiary amine – and mechanism of etherification and homopolymerization – etherification reaction is catalysed by tertiary amines and hydroxyl groups and occurs for high polymerization temperatures and at the end of the reaction, when there's excess of epoxy rings and all hydrogen atoms of the amine groups were previously consumed.

Horie's model (HORIE et al., 1970) relies on these mechanisms, taking into account concentrations of reaction's chemical species. He proposed the following equation to describe the kinetics of polymerization of an epoxy/amine resin:

$$\frac{d\alpha}{dt} = (K_1 + K_2\alpha)(1-\alpha)(B-\alpha) \tag{6}$$

where $d\alpha/dt$ is the conversion rate of the polymerization, representing the rate of cross-linking. K_1 and K_2 are the rate constants of the catalytic process (or at the initial moment) and of the auto-catalytic process, respectively; they follow the Arrhenius Law. As for B, it is the molar ratio epoxy/amine. For a reaction with stoichiometric compositions ($B = 1$), the conversion rate equation becomes:

$$\frac{d\alpha}{dt} = (K_1 + K_2\alpha)(1-\alpha)^2 \tag{7}$$

4.1.3 Kamal's phenomenological model

Phenomenological models obtain their parameters through adjustment of experimental curves to usually linear regressions by imposing a minimization criterion. The adjustments for one formulation won't be the same for another one. Among the various cross-linking kinetics available in literature, Kamal's model (KAMAL, 1974) – also known as Kamal and Sourour's model – stands out. The author proposed an empirical formulation based on Horie's rate of conversion equation. For Kamal's formula, both catalytic and auto-catalytic effects of the reaction are included. Kinetics of the reaction is given by:

$$\frac{d\alpha}{dt} = (K_1 + K_2\alpha^m)(1-\alpha)^n \tag{8}$$

Once again, $d\alpha/dt$ is the rate of degree of conversion α, and K_1 and K_2 the rate constants of the catalytic and auto-catalytic processes. Exponents m and n are respectively the orders associated with the auto-catalytic and catalytic reactions. The sum $m + n$ is the global order of the reaction. As mentioned, the formulation shows that reaction rate is dependent on the amount of resin not yet reacted – factor $(1-\alpha)$, catalytic – and the amount of reacted resin (reaction product) – factor α^m, auto-catalytic.

Rabearison (2009) states that for most studies on epoxy systems, n varies between 1 and 2, while m usually assumes values of 0.67 up to 1. An interesting observation is that for $m = 1$

and $n = 2$ the formulation is similar to the mechanistic model of Horie previously presented. Since rate constants follow the Arrhenius Law, they can be written as:

$$K_1 = A_1 exp\left(\frac{-E_1}{RT}\right) \tag{9}$$

$$K_2 = A_2 exp\left(\frac{-E_2}{RT}\right) \tag{10}$$

A_1 and A_2 are pre-exponential constants [1/s], while E_1 and E_2 are the activation energies [J/mol]. Reaction site temperature T must be considered in absolute values, being inserted into the equation in Kelvin. Lastly, $R = 8.314\ \mathrm{J/(mol * K)}$ is the universal constant of perfect gases.

4.1.4 Diffusion phenomenon

Kamal's model tends to a final degree of cure of 100%. Nevertheless, experimental results don't follow this tendency for they rarely achieve such conversion. This formulation is acceptable for the beginning of evolution of the degree of conversion, where the reactivity of the molecules is dominant, but not so at vicinity of the end of the thermosetting reaction – starting at vitrification. In fact, as curing evolves, reaction becomes more and more controlled by diffusion of reactive species and reduced in molecule mobility, slowing down the reaction rate.

For the purpose of adding diffusion effects to cure kinetics, which can't be disregarded as previously observed, Fournier et al. (1996) introduced a diffusion factor f_d to Kamal's model. f_d is a semi-empirical relationship and a function of degree of conversion. The extended model is represented by:

$$\frac{d\alpha}{dt} = (K_1 + K_2\alpha^m)(1-\alpha)^n . f_d(\alpha) \tag{11}$$

Diffusion factor is expressed by:

$$f_d(\alpha) = -1 + \frac{2}{1 + exp\left(\frac{\alpha - \alpha_f}{b}\right)} \tag{12}$$

where parameter α_f is the conversion at the end of the isothermal cure and b in an empirical diffusion constant of the material. Thus, for the complete characterization of cure kinetics with the extended model, eight parameters must be identified: m, n, A_1, A_2, E_1, E_2, α_f and b.

4.2 CONSERVATION LAWS AND PARAMETERS

The curing consists of an exothermal reaction, where the heat produced helps its activation. This leads to a coupling of two physics: thermal and chemistry. A simple coupling of these physics can be represented by the addition of a heat flow equivalent to that released by the chemical reaction, as the focus remains on the evolution of degree of cure and temperatures, not on the way chemical species are reacting. As discussed, the curing generates internal stresses, which leads us to adding the mechanics into our modelling. A thermo-chemical-mechanical coupled problem must meet both mechanical balance and heat transfer equations. Therefore, the following conservation laws are involved:

$$div\{\kappa(tr\boldsymbol{\varepsilon})\boldsymbol{I} + 2\mu\boldsymbol{\varepsilon}\} = \mathbf{0} \tag{13}$$

$$\rho c_p \frac{dT}{dt} = div\{k[\boldsymbol{grad}\, T]\} + q + \rho\Delta\mathrm{H}^r \frac{d\alpha}{dt} - T\{(3\kappa + 2\mu)\alpha_T\} tr\dot{\boldsymbol{\varepsilon}}^{\boldsymbol{e}} \tag{14}$$

Equation 13 is the *equation of motion*, in which the linear momentum balance is met considering only stresses, without the application of external forces. $\dot{\boldsymbol{\varepsilon}}^{\boldsymbol{e}}$ is the second-order elastic strain tensor and $\boldsymbol{I}$ is the identity tensor. The total strain tensor $\boldsymbol{\varepsilon}$ includes all of the acting strains, such as elastic, thermal and chemical strains. Lamé coefficients are identified by κ and μ. Equation 14 defines the local temperature T of the matrix during curing. Parameters ρ, c_p, k and α_T are the density, specific heat capacity, thermal conductivity and coefficient of thermal expansion of the forming matrix. Term q represents the heat flow imposed by the oven and $\Delta\mathrm{H}^r$, the enthalpy of the reaction.

The term $\rho\Delta\mathrm{H}^r(d\alpha/dt)$ stands for the heat flow (ϕ) produced by the chemical reaction, consisting of the thermo-chemical coupling. It will be expressed by:

$$\phi = \rho\Delta\mathrm{H}^r \frac{d\alpha}{dt} \tag{15}$$

4.2.1 Elastic constitutive law

The mechanical behaviour's description of the resin under the cure process, in the framework of linear elasticity with small strains, is given by the elastic constitutive law:

$$\boldsymbol{\sigma} = \kappa(tr\boldsymbol{\varepsilon})\boldsymbol{I} + 2\mu\boldsymbol{\varepsilon} = \frac{E}{1+\nu}\left\{\left[\frac{\nu}{1-2\nu}(tr\boldsymbol{\varepsilon})\right]\boldsymbol{I} + \boldsymbol{\varepsilon}\right\} \tag{16}$$

where $\boldsymbol{\sigma}$ represents the stress tensor, E is the Young's modulus, ν stands for Poisson's ratio, $\boldsymbol{I}$ is the identity tensor and $\boldsymbol{\varepsilon}$ is used as the total strain tensor. Material properties E and ν are laborious to obtain along the cure process of a resin. Therefore, they are calculated through the elastic shear modulus G – achieved by Dynamic Mechanical Analysis (DMA) – and the bulk modulus K – available in literature –, by the following equations:

$$\nu = \frac{3K - 2G}{6K + 2G} \tag{17}$$

$$E = 2G(1 + \nu) \tag{18}$$

The total strain tensor $\boldsymbol{\varepsilon}$, once again, is given by the sum of all strains presented in the process. It comprises the elastic (ε^e), chemical (ε^{ch}) and thermal (ε^{th}) strains, that is:

$$\boldsymbol{\varepsilon} = \boldsymbol{\varepsilon^e} + \boldsymbol{\varepsilon^{ch}} + \boldsymbol{\varepsilon^{th}} \tag{19}$$

Elastic strain is a result of the internal stresses generated in the curing process, while chemical strain comes from chemical shrinkage and thermal strain is due to temperature gradients along the cure. As formerly introduced, chemical shrinkage of an epoxy resin was determined by Li et al. (2004) and fitted to a bi-linear relationship function dependent on the degree of cure, which can be used for cure modelling. As for the thermal strain, it is the effect of a temperature increment over time ΔT, resulting in a volumetric deformation defined by the linear equation:

$$\varepsilon_{ii}^{th} = \alpha_T \, \Delta T \; ; \quad \varepsilon_{ij}^{th} = 0 \tag{20}$$

ε_{ii}^{th} and ε_{ij}^{th} are, respectively, the normal and shear components of the thermal strain tensor. Once again, α_T is the coefficient of thermal expansion of the material in formation.

4.2.2 Glass transition temperature

As a resin during curing undergoes structural and phase changes, which affect directly material properties, the glass transition temperature must be properly described, for according to earlier discussions this parameter is a reference to such changes – rubbery state and glassy state transformations. Glass transition temperature, however, is not constant throughout the process. It changes instantly and can be predicted by DiBenedetto's equation (DIBENEDETTO, 1987; PASCAULT et al., 2002):

$$\frac{T_g - T_{g0}}{T_{g\infty} - T_{g0}} = \frac{\lambda\alpha}{1 - (1 - \lambda)\alpha} \tag{21}$$

Parameters T_{g0} and $T_{g\infty}$ are the glass transition temperatures for a resin at degree of cure $\alpha = 0\%$ and $\alpha = 100\%$, respectively, as shown in Section 3.2. T_{g0} can be interpreted as the temperature below which the reaction is in a glassy state, being slow to occur; it is used to define the maximum storage temperature for the unreacted resin. λ is an adjustable parameter which generally assumes values between 0.46 and 0.58 for most epoxy/amine systems (SMAALI, 2005).

4.3 CURE MODELLING VARIABLES

All the required parameters and properties for complete characterization and monitoring of the cure process are summarized in Table 3. The attributed values and expressions for each one will be presented in a future section.

Table 3: Cure process variables.

Field	***Variables***
Cure Kinetics	$A_1, A_2, E_1, E_2, m, n, \alpha_f, b$
Material Properties	$G, K, \alpha_T, k, \rho, c_p,$
Chemistry	ϕ, ε^{ch}
Environmental Conditions	q
Glass Transition Temperature	$T_{g0}, T_{g\infty}, \lambda$
State variables	$\boldsymbol{\alpha, T, t}$

Source: Author.

5 FINITE ELEMENT MODELLING

Finite Element Analysis (FEA) is a computational tool more and more employed for integrity evaluation of components and structures. Although it requires training of people involved in simulations and result analyses, pointing out difficulty in operation, commercial software based on the Finite Element Method (FEM) has been showing significant improvements. Some of them include better and easier user interfaces and reduction in processing time, leading to less expensive studies in computational and money terms and popularizing this kind of assessment.

FEA has a strong application in literature works for several areas – composite materials, for instance – frequently showing accurate and reliable results. The following sections are dedicated to an explanation on the FEM as well as its application on composites characterization.

5.1 THE FINITE ELEMENT METHOD

The FEM emerged in the 1950s in aerospace industry for stress analysis of aircraft wing plates, and today it turns out to be a helpful technique for structural integrity assessment. Fields of application of the method are diverse, including applications in mechanics aerodynamics, heat transfer and electrical and magnetic potential.

According to Fish & Belytschko (2009), the FEM is a numerical approximation with which partial differential equations that represent a certain phenomenon can be approximately solved, for their analytical resolution may be difficult, and generally almost impossible for arbitrary geometries. The solution of this approximate method is carried out until a defined degree of accuracy is reached.

The approach behind the Finite Element Method is to discretize a continuous medium into a finite set of elements, and each element has a specific number of nodes connecting one another. Elements can be of varied shapes based on the nature of the problem (Figure 13); common examples are beams (1D element), triangles, quadrilaterals (2D elements), tetrahedrons and hexahedrons (3D elements).

Figure 13: Representative finite elements: (a) beam, (b) triangle, (c) quadrilateral, (d) tetrahedron, (e) hexahedron.

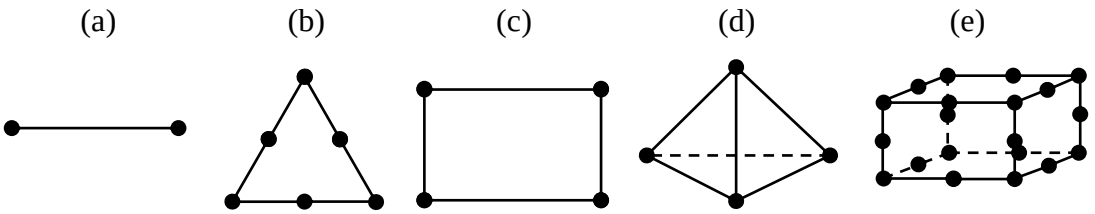

Source: Author.

The discretization elements compose the mesh, and as the mesh is refined – that is, as the number of elements increases, or they are better represented – the discrete model behaves more similarly to the continuous model. The obtained field variables from the method are computed at each node; all the non-nodal points of the geometry are then approximated by interpolation functions, called shape functions, with the element's nodes. Thus, the FEM consists of a system of algebraic equations that represent – for a mechanical problem, for instance – the equilibrium of each individual node instead of the infinitesimal equilibrium by differential equations of the continuum medium, and the field variables are the nodal displacements through which strain and stresses are thereafter calculated. In the following Figure 14, there's a summary of the stages taken by the method.

Figure 14: Stages of the FEM.

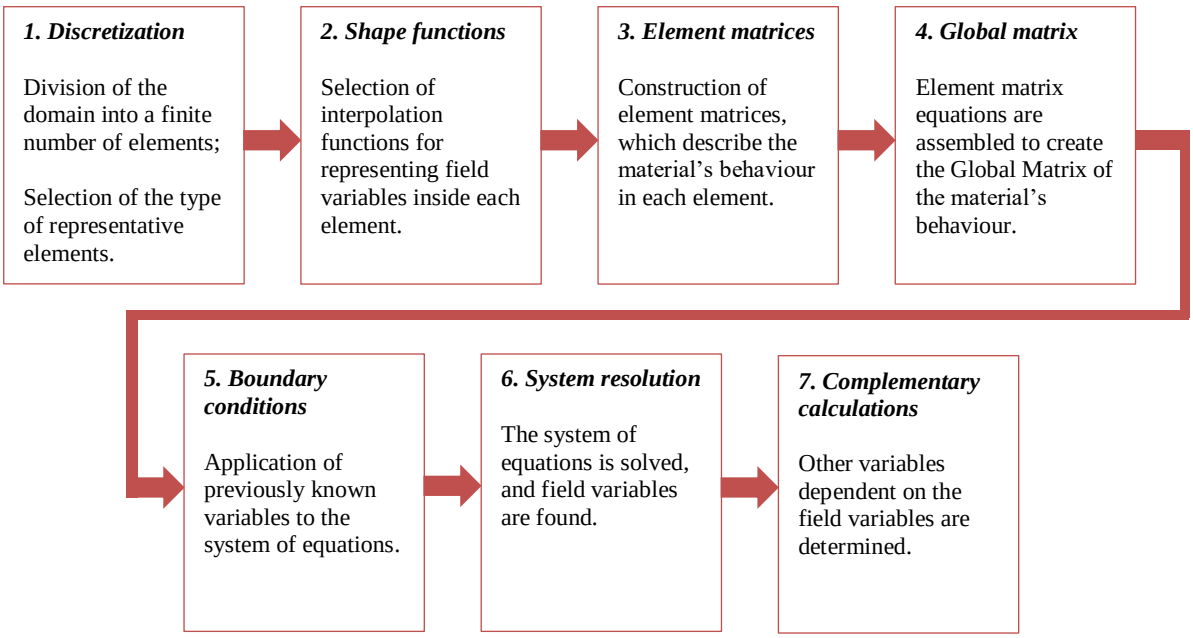

Source: Author.

During ***Stage 6.***, the great number of degrees of freedom and, consequently, of equations involved can become significantly larger as the domain mesh is refined. For the feasibility of the FEM application, the system's solution shouldn't be manually calculated, revealing the utmost importance of computational resources at this stage in special. The development of finite element commercial software, hence, arises in this context.

5.2 FEM-BASED SIMULATION

One of the first FE programs widely used was developed by E. Wilson in the 1960s, which gained popularity due to being free, a common practice at that time for the current commercial programs. It was limited to two-dimensional stress analyses, and was used and modified by several academic research groups and industrial laboratories.

In 1956, NASA started a project for development of a FE program named NASTRAN, which could perform stress analysis in two and three dimensions for complex structures, as well as vibrational analysis and transient responses of dynamic loads. Although the project was of public domain it had a great deal of problems. The NASA project was terminated, and the software was released to the public; after that, MacNeal-Schwendler Corporation started to not only fix its problems but also market and support the software as ***MSC Nastran*** (FISH & BELYTSCHKO, 2009). Now, it is widely applied in the aerospace, automotive and maritime industries.

Ansys appeared at almost that same time, created by John Swanson for Westinghouse Electric Corp. for analysis of nuclear reactors. The software was later launched on the market by Swanson, having the ability to solve linear and nonlinear problems, and being quickly adopted by several companies. Recently, Ansys acquired numerous engineering design companies, presenting technologies for structural mechanics, heat transfer, electromagnetism, fluid dynamics, among others.

A company named HKS founded in 1978 developed ABAQUS with the initial focus on nonlinear applications. For that reason, the program has today an extensive range of material models such as elastomeric material capabilities. Capabilities for linear applications were also gradually added to the software. The company introduced ports into the program, allowing users to add new models and elements, which contributed to its wide use by researchers. The software now belongs to *Dassault Systèmes* under the name ***Abaqus FEA***, with applications in the field of automotive, aerospace and industrial products (FISH & BELYTSCHKO, 2009). The

commercial program has a broad usage due to its ability to be customized, its wide modelling capability and good collection of Multiphysics capabilities.

COMSOL Multiphysics® is another FE commercial software known to the market since 1998. The company was founded in 1986 in Sweden and offers solutions in software for multiphysics modelling. The company is expanding internationally, being present in countries of Europe, Asia and America. The software's modules include structural mechanics, electromagnetism, fluid flow, heat transfer, chemical reactions, acoustics, among others (COMSOL INC., 2017a).

Nowadays, FEA is used in structure design, integrity evaluation, simulation of experiments and manufacturing processes, just to mention a few. In special regard to designing new products, parts or structures, the time consumed decreased drastically, as fabrication and testing of prototypes are not required anymore for all stages of a design, usually being performed at the last stages. FEA also contributes to competitivity in the industry.

McKinley (1979) states the FEM had a revolutionary effect for many reasons. The method, along with the use of software, allows dealing with large amounts of processing in a short time, including automating incoming data and graphically displaying output data. The author also remarks the ability of the user to gather the properties of a large and complex structure from a number of elements with simple properties, as well as handling static dynamic, nonlinear and stability problems for a wide range of structures.

In fact, the exponential increase in computers' speed combined with the still greater cost decline in computational resources helped the FEM in these revolutionary changes. Fish & Belytschko (2009) mention that only after the 1960s computers had enough power to perform reasonably well finite element calculations. They cite the most powerful computer in 1966, Control Data 6600, being able to treat about 10,000 elements in several hours, which a current PC does in minutes, or even seconds. Along with low speed, computers also had low memory. These improvements provide ways of spreading the field of studies with the FEM, not only limited to industrial applications, but also in researches and academic works.

5.2.1 FE simulation process

A commercial FE software involves three distinct steps comprising all the detailed stages of the FEM. They are: ***Pre-Processing***, ***Processing*** and ***Post-Processing***.

At ***Pre-Processing***, the modelling of the problem is carried out. The user defines the model geometry and the material properties, selects the shape and size of the elements and mesh refinement. The type of element must be proper, and the mesh should have a refinement which not only ensures accuracy of results but also allows solving in a reasonable time. Boundary conditions and constraints are added to the model as well as solver information on the kind of analysis that will be run. The model should also be validated, verifying if the model was correctly built. The pre-processing can be the most time-consuming phase for it is where the user must define the mesh that best reproduces accurate results.

Meshing may still represent a tiresome activity for most problems. Accuracy of the model is given by the use of the element which offers the lowest possible volume, in which the distribution of the energy gradient undergoes less variation. This is achieved by increasing the number of elements for a given volume of the model, resulting in a longer simulation time and a greater memory need due to the enlargement in the system's number of nodes and, therefore, in its total number of degrees of freedom.

This process, called mesh refinement, has limitations, especially for three-dimensional simulations, in which there are more degrees of freedom. Such limitations in terms of computational time and computer memory required in Processing stage are extremely relevant, since a very refined model may be impractical to be simulated. Hence, creating a finite element mesh may be laborious and must be made cautiously, choosing the most appropriate type of mesh and its element sizes.

Some structures, however, don't need too many elements to describe their behaviours; increasing the number of finite elements on the model would just lead to a longer processing time without any significant changes in the accuracy of the results. For that reason, some features are employed for computational time and memory improvements. Simplifying the problem and the geometry is one of them. Symmetry planes should be identified in order to simulate just a part of the structure and replicate results to the rest of it. A common option in commercial software is using a 2D-axisymmetric geometry instead of 3D; the model is simulated in the two-dimensional space and graphical results are automatically reproduced to the revolution of the geometry. Another application consists on using a more refined mesh in the area of interest – the one which shows higher gradients of field variables –, and proceed with a coarser mesh in the remaining part of the model that doesn't show these higher gradients. That's the case of structures with geometric discontinuities such as cross-section changes, cracks, sharp edges and holes, for example.

The ***Processing*** stage incorporates the calculations of the simulation, where the extensive system of linear equations is generated and numerically solved until convergence of the results is obtained, leading to the solution. The software automatically assembles the matrices of each element and gathers them in a global matrix, it applies constraints and boundary conditions (BCs) to the global matrix reduction of unknown field variables, and finally solves the system. As mentioned, the type of problem and, consequently, the number of elements belonging to the discretization mesh are the factors that dictate the amount of equations involved in this stage, affecting solving time of the simulation.

The final stage, named ***Post-Processing***, involves the visualization and evaluation of obtained results from the previous stage. The solutions for the model are represented in computer graphics, allowing a clearer understanding for the user. Graphical results generally show the model in colours related to the behaviour of the structure. Among the displayed output data, there are the field variables along with other variables derived from them. In mechanics we can visualize displacements, strain and stresses while in heat transfer problems the displayed variables can be temperatures and heat flows, for instance. Moreover, commercial software enables the user to visualize the structure's behaviour through animations, showing the evolution of the model's variables with time.

During post-processing, it is critical to check the final model to see if its behaviour matches the actual behaviour of the material and whether results are relatively accurate. This check can be performed by comparisons with experimental results or previously validated numerical results. If accuracy is not achieved, modifications must be carried out in the pre-processing stage, which involves: creation of the geometric model, generation of the finite element mesh, material definition and application of boundary conditions and constraints. Once the model is coherent, the simulation process finishes (MELCONIAN, 2014). A summary of the simulation stages is found below in Figure 15:

Figure 15: Stages of the FE Simulation Process.

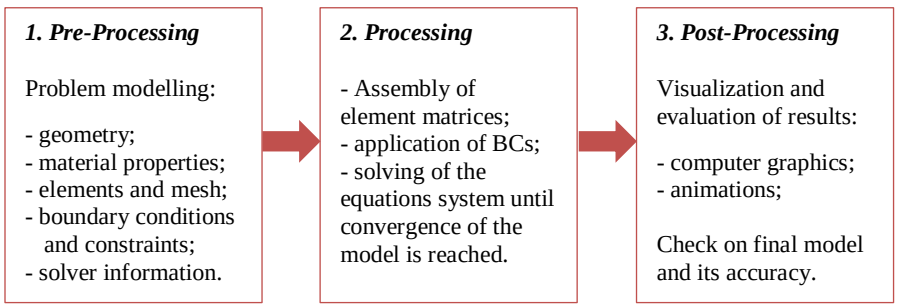

Source: Author.

Although the FEM is a great analysis tool for mathematical models of continuous medium problems, the responsibility of developing the physical system, determining the appropriate mathematical model and rightly interpreting and using the obtained results lies with the engineer performing the simulation. The evolution and increasing sophistication of software and computer performance involved in the analyses contribute to the expansion of employment of this numerical method; however, it does not dismiss the necessary human reasoning associated with it.

5.3 FEM IN THERMOSETTING POLYMER MATRIX

The FEM has been more and more used in behavioural analysis of materials, also helping to achieve efficiency in their design stage. FE simulations are performed both in industrial sector and academic community, demonstrating the applicability of the method together with the computational resource. In composite materials with thermosetting polymer matrices, there is a vast field of study with the aid of commercial FE software, encompassing experimental test reproductions, manufacturing process simulations and polymer matrix curing.

Nirbhay et al. (2014) simulated on Abaqus FEA a tensile test in a carbon fibre reinforced plastic material. The purpose of the study was to understand the mechanical strength and strain at failure of composite materials. The authors investigated carbon/epoxy, carbon+glass/epoxy and glass/epoxy composites with ply lamination in three different orientations: 0°, 45° and 90°. They identified no significant changes between carbon/epoxy and carbon+glass/epoxy composites; however, these materials showed a higher stiffness and strength than the glass/epoxy. Moreover, ply orientation affects the strength and stiffness of the composite, where cross ply laminates (0° and 90°) exhibit better properties than angle ply laminates (45°), as the latter tends to deflect more. Results were compared with predicted results and available experimental and theoretical data in open literature, revealing good agreement. The authors also highlight the occurrence of fibre waviness and variation in thickness as the two most common types of defects associated with complicated manufacturing processes of composites, and the fact that these material imperfections can lead to premature failure of the composite laminates due to strain in that region that may increase abruptly.

In the field of fabrication of composites, Andrade et al. (2000) studied the pultrusion process of carbon fibres reinforced with epoxy resin. They numerically simulated specimens using circular cross-sectional moulds, solving the algebraic equations iteratively combining

Conjugate Gradient and Newton-Raphson methods. The authors observed the influence of the volume fraction of fibres on the temperature distribution and final degree of cure of the composite. It was verified that, in the centre line, for lower fibre volume fractions – and so, higher resin volume fractions – the temperature peak is more pronounced due to the greater heat release from the exothermic reaction. Moreover, for lower fibre volume fractions, cure reaction is retarded, but since exothermic heat is greater the final degree of cure is higher as well, an intrinsic result of the polymerization reaction, not of the heating provided by the mould.

Still with the focus on manufacturing, Usui et al. (2014) simulated a composite machining with finite elements. Authors presented a finite element scheme using a nonlinear, large deformation Lagrangean formulation with an explicit time integration for the drilling process of a carbon fibre reinforced plastic. The study demonstrates the emergence of material damage, such as microcracking, fibre debonding, delamination and fibre pull-out, during drilling. It was verified that these damages are highly dependent on the orientation of the fibres, validating the simulation procedure with experimental results.

In the work of Duleba et al. (2014), a carbon cloth/epoxy resin and carbon nanotubes composite were simulated using NX8 and Nastran solver. It was found that the presence of carbon nanotubes in a carbon cloth/epoxy system improves the mechanical properties of the composite at one-directional tensile test. Comparison of simulation results with tensile tests showed higher numerical values of tensile strength than the experimental ones. An explanation given relies on the fact that this may be a result of microscopic air bubbles in the samples, reducing the strength of the composite. Authors suggest the removal of the bubbles by using a stronger autoclave or by selecting other method of preparation of the material.

Sousa et al. (2013) turn their attention to FE modelling of epoxy moulding compounds (EMC), which are widely used as encapsulation materials in electronic packages, protecting Silicon chips from environmental conditions. The paper analyses the curing of the epoxy in a two-dimensional simulation on Ansys, representing an EMC under thermal loading. Authors investigated the shrinkage resulting from the chemical reaction of curing. In the simulations, cure shrinkage was added by introducing an artificial CTE. Thermal expansion experiments were carried out at several temperatures, which were subsequently compared with simulations, showing good agreement in the results.

Simulations on Ansys were also performed by Singh et al. (2016), focusing on FE analysis of carbon nanotube (CNT) reinforced epoxy based composite subjected to thermo-mechanical loading. Similar to Sousa et al. (2013), the field of application of such composite

materials is electronics, for CNT/polymer composites exhibit thermal properties of particular interest in applications like conductive polymer films and electronic components. The study showed that long CNT embedded in an epoxy matrix further improve thermal conductivity than short CNT, proving to be a better reinforcement for nanocomposites subjected to thermo-mechanical loading.

The prediction of the temperature profile and the curing behaviour of a natural fibre reinforced thermoset matrix based composite during the moulding process was the subject presented by Behzad & Sain (2007). A multiphysics finite element package from software COMSOL® 3.2 was employed on hemp fibre/acrylic composites for 1D and 3D models without using user written programs. The analysis consisted of a nonlinear transient heat transfer FE model combined with cure kinetics, simulating the curing behaviour of the composite material. The authors carried out experiments to verify the simulated results, proving the numerical procedure to be valid and stable and provide reasonably accurate predictions. Another finding in the paper was that 1D heat transfer model is not applicable, which leads to a consideration of the 3D model for accurate predicted results.

COMSOL Multiphysics® was applied as well by Shevtsov et al. (2007) for epoxy curing investigation. The development of a mould heating distributed control model for polymerization of a helicopter main rotor blade was implemented in coupled software MATLAB – COMSOL®. The kinetic model of cure epoxy resin was designed based on DSC experiments. In a posterior work (SHEVTSOV et al., 2012), COMSOL® software was again used, this time for an epoxy-based thick-walled composite, for the proposition of a mathematical model of such structure during curing. COMSOL® modules Heat Transfer and Partial Differential Equation were coupled for thermal and chemistry representation of the material and the transitions from liquid to gel and further to solid state, with distributed exothermal heat source and kinetics equation for conversion. DSC and DMA experimental data were used to correctly build the kinetic equation. The developed model allowed the authors to determine that the critical factors such as cure temperature controlled the quality parameters of the composite, which can lead to greater residual stresses and shape distortions as cure temperature increases.

Balvers et al. (2008) direct their study to thick-walled fibre reinforced composite structures, which induce larger problems on the fabrication process compared to the thin-walled composites. Authors cite the increased ratio of volume to surface and the low thermal conductivities of both fibres and resin as an obstacle to the diffusion of released heat during the

exothermic reaction, increasing reaction temperature and favouring thermal gradients, which leads to higher residual stresses. They also highlight the appearance of another structural defect in thick-walled composites due to chemical shrinkage, which is microcracking. Simulations of curing on COMSOL Multiphysics® were performed on an epoxy/amine system (RTM6 resin, especially developed for aerospace industries) involving coupled thermal and chemical phenomena for predicting the behaviour of the material. Cure kinetics was investigated at different isothermal cure temperatures – 140°C, 150°C, 160°C, 170°C, 180°C and 190°C – with an initial ramp of 40°C/min, being validated with numerical models from the literature. In order to avoid convergence problems with the software, interpolation tables for instantaneous thermo-physical properties and cure kinetics were used instead of the direct equations. The authors mention that heating up becomes more severe for increasing thickness, which could lead to thermal degradation of the matrix. With this in mind, a maximum reliable thickness was obtained for a 160°C cure temperature equal to 33 mm in order to avoid reaction temperature overcoming the degradation temperature of the material, estimated in 220°C.

In the work of Zhang et al. (2009), temperature and degree of cure field were analysed in a 3D FE model, simulating a thick epoxy cylinder casting part during cure process. The model was based on software Abaqus and its subroutines, accounting for thermal and chemical interactions during curing. Simulations were validated with a literature example and experimental data, resulting in good agreements. The authors mention that in previous works the commercial software Ansys was used for curing predictions of resin matrix composites and casting resins; however, it demanded a large amount of code, while Abaqus can deal with nonlinear coupled problems using subroutines in FORTRAN. They also cite the automatic decoupling of heat conduction equation and cure kinetics equation as an advantage of Abaqus. A further investigation consisted on the effect of non-uniform temperature and degree of cure field within epoxy casting part on hardness of the material. It was concluded that this mechanical property is related not only to the degree of cure but also to the thermal history during curing process.

Generation of residual stresses are a constant in studies of thermosetting polymer curing, as it has been already proved in many papers that they appear during the hot stage of the curing. Moreover, stresses lead to fibre waviness in fibre-reinforced composites, which leads to a decrease in the final product's quality.

Lord & Stringer (2009) developed a prediction tool for a unidirectional AS4 carbon fibre embedded in a Hexcel 8552 epoxy, commonly used in aerospace composite structures. A 3D

model was simulated on Abaqus with its subroutines for prediction of residual stresses and distortions during and after cure, considering the resin chemistry and structural analysis. Cure kinetics was modelled with data obtained experimentally. The U-shaped geometries were submitted to a single step cure at 180°C and a two-step cure with isotherms at 210°C and 180°C. Similar components were manufactured in an autoclave process for validation of numerical results. The authors highlight the importance of modelling the full cure cycle, since if the analysis starts from the gel point the expansion and cure shrinkage accumulated in the fibre and resin up to gel point are ignored, and they do represent a significant contribution to distortions. At last, numerical and experimental results were in good agreement; still, as the number of elements through the thickness in the simulation increased, numerical results were predicted with higher accuracy.

The subject of residual stress generation during curing was also investigated by Msallem et al. (2010), which are more significant in thick resin parts. The cure process of a 1D simple plate thermosetting resin was simulated on FEMLAB (now COMSOL Multiphysics®) with coupled thermal, chemical and mechanical phenomena. The authors state that, generally, the gel point is considered as a criterion for residual stress formation – mainly driven by chemical shrinkage –, but they find it more appropriate to consider stresses beginning to form when the resin has a yield stress. A second study on the chemical shrinkage revealed changes in longitudinal and transverse coefficient of thermal shrinkage, indicating an anisotropic behaviour which is not shown in classical models. Consideration of anisotropic shrinkage led to lower residual stresses, as well.

Some literature works investigate the viscoelastic phenomenon in thermosetting resin matrix composites. That's the case of Wisnom et al. (1999), who analysed residual stresses throughout the cure cycle in thick filament wound tubes considering the effects of chemical shrinkage, thermal expansion, gelation and orthotropic viscoelasticity – the latter, accounting for stress relaxation. Measurements with strain gauges embedded in the tubes were performed for model validation. The simulation of a thick hoop wound E-glass/MY750 epoxy tube was run on Abaqus with separate elements for the fibre and the matrix, and provided good correlation with measured strains, but only if gelation is modelled, for that's when measurable stresses and strains start to develop. Data input of the model was produced by experimental techniques. As for the viscoelasticity, the authors initially expected it would be relevant; nevertheless, as the glass transition temperature of the matrix remained below the reaction temperature until cooldown the results displayed were the same as for an elastic analysis. The

conclusion was that, specifically for the resin used, viscoelastic parameters didn't show importance.

Patham (2009) makes use of multiphysics simulations on COMSOL®, involving heat transfer and cure kinetics, to study the evolution of cure induced stresses in a thick viscoelastic thermosetting polymeric resin. Diffusion effects were also considered in cure kinetics. The interest in a thick matrix relies on the larger temperature gradients across the thickness as a result of the exothermic reaction, which leads to the development of residual stresses and shape distortions. The author states that the isotropic stresses generated are a combination resulting from thermal stresses and chemical shrinkage. On the other hand, there's a time dependent stress relaxation during cure due to viscoelasticity. A comparison between the viscoelastic model and an equivalent elastic model showed significantly lower stress estimations for the first case. Another discussion of the paper was the instantaneous stresses, which in a linear elastic material are only governed by the instantaneous states of temperature and degree of cure. For a viscoelastic material, they are also influenced by the thermal history of the resin, as it was observed that locations with higher temperatures allowed quick relaxation of stresses produced by thermal shrinkage, leading to a slower build-up of stresses.

In a subsequent work, Patham (2012) continues the investigation of cure-induced stresses in a viscoelastic epoxy/amine thermosetting resin system. A semi-empirical cure kinetics model was included in COMSOL Multiphysics® along with heat transfer, which facilitated the implementation of the model without simplifying assumptions. Simulation results were compared with two other equivalent material models: one with a constant elastic modulus and another with a cure-dependent, time-invariant elastic modulus. The author found no differences in the stress response between the two elastic models, but, again, observed lower estimations in generated stresses for the viscoelastic model.

Lastly, Rabearison et al., in consecutive researches, performed FE simulations on Abaqus and its subroutines studying the internal stress growth during curing of a thermosetting system, where thermal, chemistry and mechanics were coupled in the framework of elasticity with small strains. The heat produced by the exothermic reaction of polymerization was added to the heat transfer equation as a heat source, inducing thermal expansion of the resin before the shrinkage from the change liquid-solid states. The degree of cure computed at each time of the curing provided the chemical shrinkage and properties evolutions, material characteristics evolution (temperature and degree of cure dependents) were deduced from DMA-TMA and

DSC experiments, and cure kinetics parameters were obtained for Kamal and Sourour phenomenological model, taking diffusion into account.

In their first work (RABEARISON et al., 2008), the chemical shrinkage followed Li et al.'s bi-linear relationship, while the rule of mixtures was used for predicting the coefficient of thermal expansion and the specific heat capacity according to the degree of conversion of the reaction. They also considered the glass temperature varying with DiBenedetto's equation. Two simulations were carried out, with its respective experiments for model validation. The first one consisted of an epoxy resin filling a steel tube with 32 mm of diameter up to 30 mm of height, placed in an oven and heated with a 3°C/min ramp followed by an isotherm of 100°C. The experimental sample had four thermocouple probes placed inside to record the internal temperature evolution, results which were compared to the simulation and validated the numerical prediction. The second model was a Pyrex test tube of diameter of 20mm filled with epoxy resin to a height of 25 mm, again with a 3°C/min heating ramp, followed by an isothermal plateau of 120°C in the oven. For the experiment, the temperature in the centre was registered, showing a peak of temperature at around 250°C due to a strong exothermal effect. Crack propagations on the Pyrex test tube walls were detected during the experiment, leading to its failure. On the other hand, numerical stress levels for the Pyrex were much higher than the failure stress of this material, consisting of a first validation of the model developed. The authors also point out the strong strain and stress gradients observed inside the matrix in formation, which after gelation were around 7–8 MPa, a confirmation of considerable internal stress development during the cure cycle of a resin. Finally, it is stated that stresses are a result of differential thermal and chemical strains appearing within the matrix due to gradients of curing produced by thermal heterogeneity.

A second investigation (RABEARISON et al., 2009) was similar to the previous one. Once more, simulations on Abaqus are compared with experimental data, showing local temperature predictions fitting well with experiments. DMA-TMA tests provided values for shear elastic modulus and loss modulus during a typical curing at 120°C. An apparent sensibility of the shear elastic modulus to the frequency of the tests was detected, indicating a viscoelastic behavior of the matrix during the cure cycle that should be taken into account in further studies for better predictive models of the internal stress state estimation. Moreover, authors state the heterogeneity of the curing process – due to the exothermic reaction – as being particularly developed as thickness increases. In the curing of thick matrices there are mass effects on the exothermic generated heat which can decrease the composite quality. For that

reason, the authors consider understanding material properties growth and gradients a strategic point, particularly for thick matrices.

The works here cited represent just a few of the possibilities of the use of FEM in composite materials characterization. The commercial FE software shows a great capacity in composites simulation, especially in coupled predictions of the cycle of cure, constantly providing reliable results.

6 EXPERIMENTAL METHODOLOGY

6.1 CURING EXPERIMENTS

Experimental curing tests were performed for the purpose of validating numerical models from COMSOL®, contributing as well to the understanding of the problem. The stainless-steel mould used in the tests is represented in Figure 16. Curing at different temperatures were carried out in collaboration with ENSTA Bretagne, and shall be presented hereafter.

Figure 16: Cylindrical mould geometry used in the experiments (in millimetres).

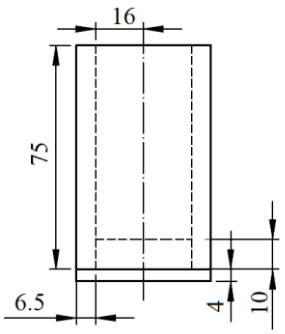

Source: Author.

6.1.1 Oven validation

Before starting the curing process of the epoxy system, the oven was validated with the process of heating and cooling of the mould filled with glycerine. This material was chosen for its similarity of thermal properties with epoxy and for being chemically and physically stable in the testing temperature range. Three thermocouples were placed in the oven: one in the centre of the glycerine, one at the mould wall and the third a little further from the mould measuring the air temperature (Figure 17). The procedure helped validating the oven and thermocouples operation, as well as the coefficient of convection tabulated by Rabearison (2009). The dimension of the sample in relation to the totality of the oven can be seen in Figure 18.

Figure 17: Sample preparation with the thermocouples (in red).

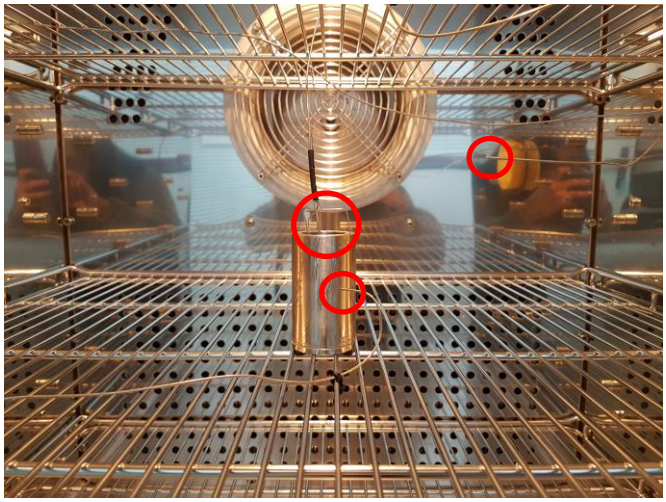

Source: Author.

Figure 18: Sample preparation in the oven.

Source: Author.

The mould was filled with glycerine – Glycerol 98% ($C_3H_8O_3$) – up to a height of 62 mm. The experiment used a 3°C/min heating ramp from 20°C to 140°C, followed by a 140°C plateau for 2 hours and a cooling rate of 3°C/min to 20°C.

6.1.2 Curing at 140°C

The first curing experiment was carried out for a 140°C plateau with a duration of 2h to ensure the complete cure of the sample. The resin system was prepared as stated by the product manufacturer: 100 parts by weight of resin (m_r) LY 556 for 90 parts of hardener HY 917 and 0.5–2 parts of accelerator QY 070. The heating ramp was set up as 3°C/min, as this is a common

practice in the industry. The total mass of the epoxy system was predicted to be 150 g, and the percentage of accelerator was chosen as 2 parts by weight. Hence, the system should follow:

$$resin + accelerator + hardener = 150\ g$$

$$m_r + 0.02m_r + 0.9m_r = 150\ g$$

$$m_r = \frac{150\ g}{1.92} = 78{,}125\ g$$

The preparation was performed on a scale with a precision of 0.0001g. The products were added and measured in the following order: first, the epoxy resin; second, the accelerator; and at last, the hardener. The respective weights to be achieved were recalculated according to the first measurement of epoxy resin. Thus, the masses described in Table 4 were obtained:

Table 4: Measurements for Epoxy Preparation #1.

LY 556:	Expected [g]:	78.125	Measured [g]:	$\mathbf{78.1482}$
	Accelerator [g]:	$0.02 * 78.1482 = \mathbf{1.5629}$	**Hardener [g]**:	$0.9 * 78.1482 = \mathbf{70.3334}$
LY 556 + QY 070:	Expected [g]:	$78.1482 + 1.5629 = 79.7111$	Measured [g]:	79.7149
LY 556 + QY 070 + HY 917:	Expected [g]:	$79.7149 + 70.3334 = 150.0483$	Measured [g]:	150.0426

Source: Author.

A silicone unmoulding lubricant spray was applied on the inside of the mould for easier cured resin removal – SI FILM HV, from Afer. The resin preparation led to the formation of bubbles. Therefore, the material was placed in a vacuum chamber for some time (Figures 19 and 20).

Figure 19: Sample in the vacuum chamber.

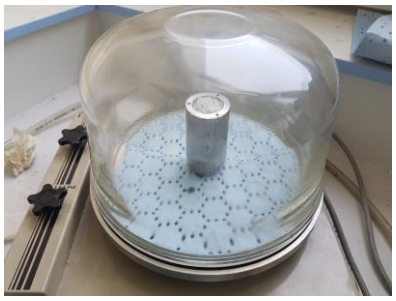

Source: Author.

Figure 20: System (a) before and (b) after bubble removal.

(a) (b)

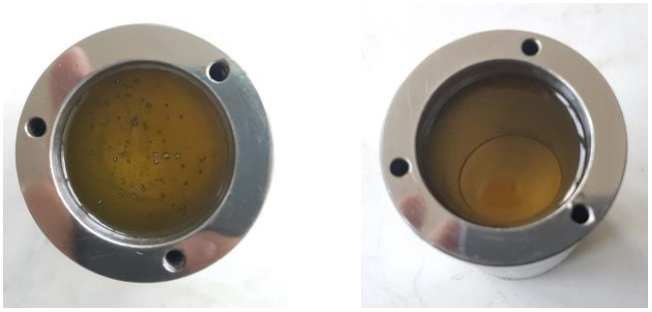

Source: Author. Source: Author.

Two experiments were performed with Epoxy Preparation #1, both with a height of resin in the mould equal to 60 mm. The first sample was inserted in a small preheated oven at 140°C for a total duration of 2 hours, being removed from it to cool at room temperature. The oven registered a curing temperature of 132°C throughout the curing (Figures 21a and 21b). This was taken as a preliminary analysis.

Figure 21: Small oven curing: (a) sample preparation and (b) during curing.

(a) (b)

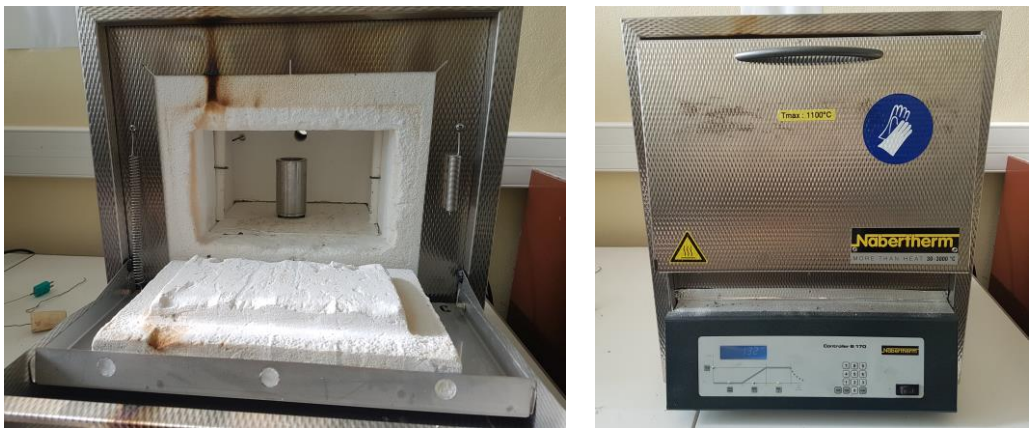

Source: Author. Source: Author.

In a first inspection, the cured resin resulting from the test showed several areas with the evidence of cracks, which can be confirmed by the diffraction of light inside the sample (Figure 22). One of the reasons may be the vacuum chamber not effectively removing all bubbles and weakening the material. However, another likely motive is thermal degradation: high temperatures achieved during curing provoking the phenomenon, leading to loss of mass, followed by the formation of gases and bubbles, which increases the pressure inside the epoxy resin and, consequently, induces cracks in the material.

Figure 22: (a) Frontal, (b) posterior, (c) lateral and (d) upper views on the cured resin at 140°C plateau [preheated oven; 2h] with the cracks detected by light diffraction.

(a) (b) (c) (d)

Source: Author. Source: Author. Source: Author. Source: Author.

The sample had its bottom part cut and the remaining was axially cut in two for better analysis of the inside. Indeed, several cracks were present (Figure 23a) and a colour gradient could be observed on the bottom cut (Figure 23b). This reveals the important role of cure temperature on the final product, which imposes higher temperature peaks from the exothermic reaction as cure temperature increases, as well as leading to higher cure gradients, detected by the darker coloration in the centre of the sample, where temperatures are more intense due to difficulty in heat diffusion out of the resin.

Figure 23: 2h curing sample at preheated oven at 140°C: (a) internal cracks at cylinder's halves; (b) colour gradient on the bottom cut of the sample.

(a) (b)

Source: Author. Source: Author.

The second sample from Epoxy Preparation #1 was placed in a larger oven – the same used for the glycerine experiment. The procedure comprised heating both oven and sample inside at a rate of 3°C/min from 20°C to 140°C, followed by a 2h plateau at 140°C, a cooling from 140°C to 20°C at 3°C/min, plus a 45 min plateau at 20°C. Just like for the oven validation with glycerine, there were three thermocouples positioned in the centre of the resin, at the wall of the mould and at the air of the oven (Figure 24).

Figure 24: Sample preparation for curing at 140°C [3°C/min, 2h] with thermocouples (in red).

Source: Author.

The results were the same as before: the cured epoxy resin had a great number of cracks inside (Figure 25). The thermocouple positioned in the centre of the mould can be seen as well in the image. This cure temperature, hence, doesn't show itself as ideal for the fabrication of a sample with such thickness.

Figure 25: Cracked sample with centre thermocouple [3°C/min, 140°C, 2h].

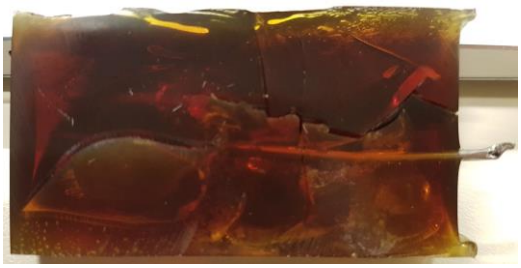

Source: Author.

6.1.3 Curing at 110°C

A cure temperature of 110°C was chosen for the next curing experiment. Initial simulations (to be presented in Section 7) showed, for such curing temperature, temperatures within the resin below 200°C, at which thermal degradation registers a more intense mass loss

on TGA graph (Figure 12). This led to the expectation of a possible crack-free sample with no signs – or very reduced ones – from thermal degradation, hence the curing at 110°C being set. A second epoxy resin system was prepared in the same way as before, achieving the following measurements in Table 5.

Table 5: Measurements for Epoxy Preparation #2.

LY 556:	Expected [g]:	78.125	Measured [g]:	**78.1181**
	Accelerator:	$0.02 * 78.1181 = \mathbf{1.5623}$	**Hardener**:	$0.9 * 78.1181 = \mathbf{70.3063}$
LY 556 + QY 070:	Expected [g]:	$78.1181 + 1.5623 = 79.6804$	Measured [g]:	79.6734
LY 556 + QY 070 + HY 917:	Expected [g]:	$79.6734 + 70.3063 = 149.9797$	Measured [g]:	149.9740

Source: Author.

Once again, the moulding was prepared with the silicone unmoulding lubricant spray and the epoxy system stayed inside the vacuum chamber for bubbles removal. As well as for the second experiment at 140°C, the oven had a 3°C/min heating and cooling rates from and to 20°C, respectively, with a 110°C plateau for 2h in-between. The resin reached a height of 60 mm in the mould. A thermocouple at the wall of the mould and another for the oven air measurements were placed. The experiment consisted of a 3h test followed by a 35min plateau at 20°C, ensuring the full cooling of the resin. The epoxy still presented cracks, as observed in Figure 26, a probable indication of thermal degradation.

Figure 26: Cracked sample [3°C/min, 110°C, 2h].

Source: Author.

6.1.3 Curing at 80°C + 120°C

The last curing experiment was carried out based on the manufacturer's recommendation, consisting of a 4h plateau at 80°C followed by a second plateau at 120°C for 4 more hours (a post-cure). Each temperature change – from 20°C to 80°C, from 80°C to 120°

and from 120°C to 20°C – was done with a 3°C/min rate. This procedure was performed for avoiding high temperatures that may lead to thermal degradation. Similar to the 110°C curing, there were two thermocouples: one at the mould wall and one for capturing the air temperature inside the oven. The resin from Epoxy Preparation #2 was used up to a height of 60 mm inside the mould, and the total duration of the test took 9 hours and 6 minutes, adding a 1h plateau at 20°C.

The resulting resin showed no signs of defects, as observed in the following figures (Figures 27 and 28). The sample was machined at the external surface; for that reason, the samples on the images present a smooth exterior. At Figure 27a, the colour difference in the centre is due to the incidence of light which was very close. The colour gradient along the radius is still visible, a result of different cure temperatures and, hence, different final degrees of cure.

Figure 27: Cured epoxy resin system [3°C/min, 80°C + 120°C]:
(a) entire geometry; (b) cut in half.

(a)

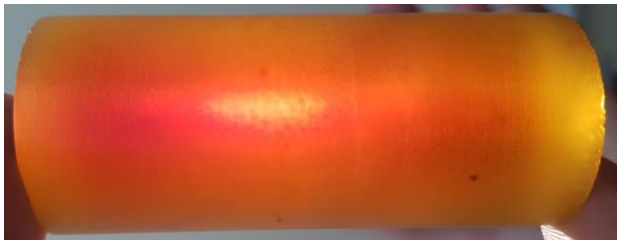

Source: Author.

(b)

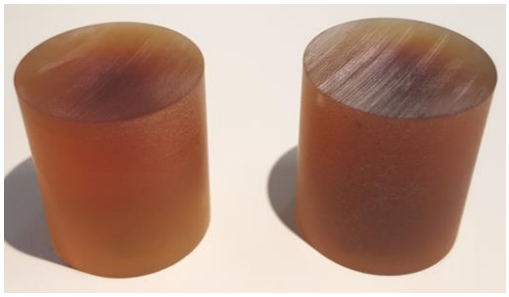

Source: Author.

Figure 28: Cured epoxy [3°C/min, 80°C + 120°C]: (a) ¼ and (b) ½ of the sample.

(a)

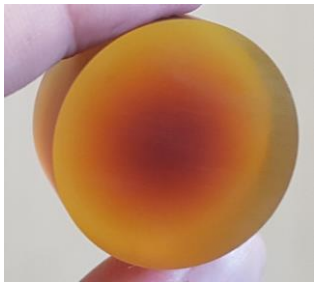

Source: Author.

(b)

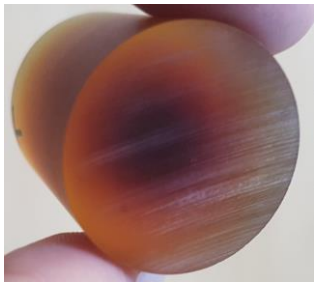

Source: Author.

7 NUMERICAL METHODOLOGY

The studied epoxy system consisted of an Araldite LY556 as prepolymer, Aradur 917 CH as hardener and DY 070 as accelerator. Several works have been carried out with this system, which gives sufficient information for comparisons. The numerical models use Kamal's phenomenological model extended by Fournier et al. (1996), including the phenomenon of diffusion. The numerical investigation consisted of a first model replication of previous simulations and the development of models, both for the thermo-chemical analysis. Subsequently, the model was improved with the inclusion of mechanics. For all cases, simulations were performed on an Intel® Core™ i5 Laptop at 2.50 GHz with 8 GB of RAM.

7.1 COMSOL MULTIPHYSICS®

The selected FE software used in the investigation presented in this work was COMSOL Multiphysics®. The program has an interesting multiphysics interface, allowing the solution of problems with coupled physics in a user-friendly interface, along with easiness in setting variant input parameters. The software will be briefly introduced, highlighting its capabilities and functionalities.

The concept of the program is that every type of simulation included in its package has the ability to be combined with any other. This compatibility ensures consistent multiphysics models. Its platform is also adaptable: when modelling needs change, so does the software. The user can include another physical effect needed or enter a required formula, for instance (COMSOL INC, 2017b). Moreover, the software has an Application Programming Interface (API) for Java and LiveLink for CAD software, MATLAB® and Excel®, which perform a fine integration between them and COMSOL® simulations. An Application Builder is provided as well for developing independent apps with custom user-interface (COMSOL INC, 2017a).

COMSOL® has several modules, including electrical, fluid and heat, mechanical, acoustics and chemical applications. It enables several space dimensions – Figure 29 – and physics – Figure 30a. Depending on the physics selected, there are types of studies possible to be run in the simulation. Figure 30b shows the studies available for Structural Mechanics → Solid Mechanics as the physics of interest.

Figure 29: COMSOL® Space Dimensions.

Source: Author.

Figure 30: COMSOL®: (a) Physics; (b) studies for *Solid Mechanics*.

(a)

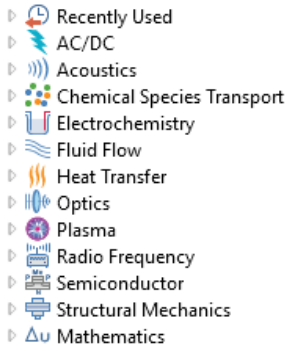

Source: Author.

(b)

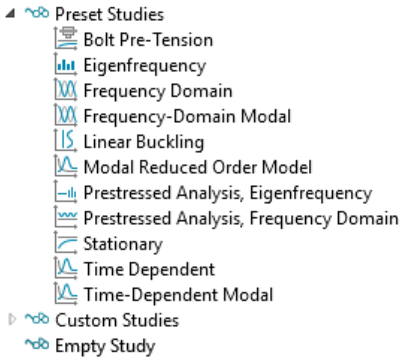

Source: Author.

Its interface shows three main windows: *Model Builder*, where the model tree is presented; *Settings*, with the characteristics of a specific selected item on the model tree to be modified by the user; and *Graphics*, showing the specific graphical interface for the model tree item selected. A toolbar above them allows the user to easily deal with the insertion of new attributes to each one of the model tree's items. A last window, below the *Graphics*, contains messages, progress and numerical results of the problem. COMSOL® interface can be observed in Figure 31, which can be customized as the user pleases.

Figure 31: COMSOL® Interface for a 2D-axisymmetric geometry.

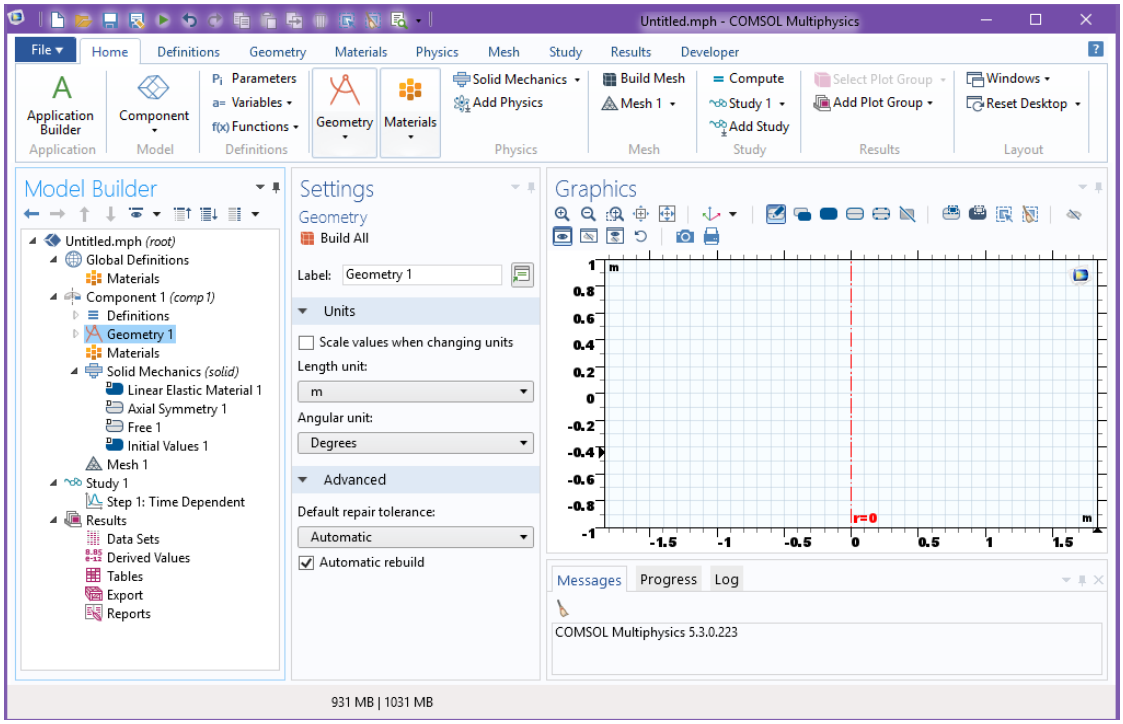

Source: Author.

The software allows the setting of parameters (constant values) as well as variables and functions. Its function library is interesting and shown in Figure 32. The user can also write functions within the settings. In Figures 33a and 33b, we can see a defined function which is used to determine the density of the material. That was found to be one of the main advantages of COMSOL® for the simulation of cure, for its parameters are in constant change; this feature of variant input data within the entire program exempts the need of programming scripts with external applications to be integrated to the software.

Figure 32: Functions library for definitions of the problem.

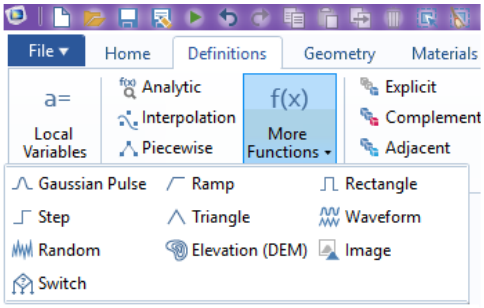

Source: Author.

Figure 33: COMSOL: (a) definition of a function c(t); (b) material density varying with c(t).

(a)

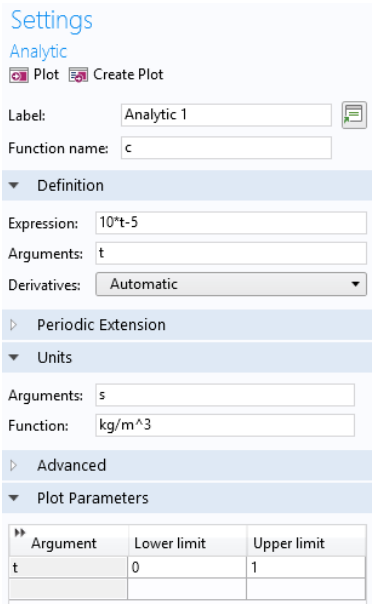

Source: Author.

(b)

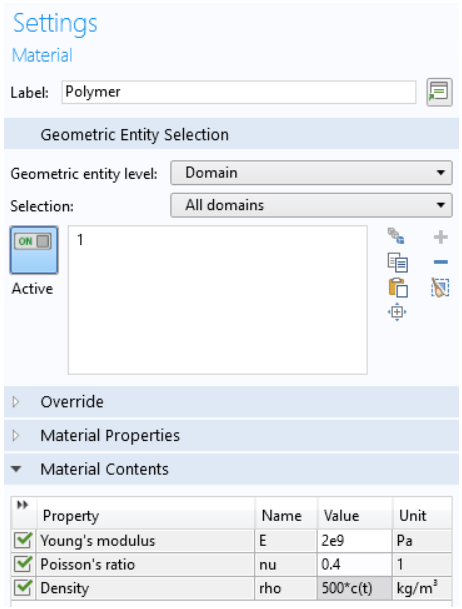

Source: Author.

In addition, COMSOL® provides relatively fast results, as the program is originally built to run coupled phenomena problems. Everything is concentrated in the program, reducing use of computer memory and computational time.

7.2 REPLICATION OF ABAQUS MODEL

A simulation provided by ENSTA Bretagne, previously run on Abaqus FEA, was used as a first verification of the thermo-chemical model created on COMSOL Multiphysics®. The aim was to reproduce the same modelling conditions, delivering a good representation of the curing process with the benefits of COMSOL®.

The geometry consisted of a block of resin with 32 mm of diameter and 58 mm of height, inserted in a steel cylinder of 6.5 mm of thickness, covered by a plate of Plexiglas of 45 mm of diameter, as shown in the following Figure 34. For modelling simplifications, the 2D-axisymmetric geometry was used on the software, which reduces meshing and computational time.

Figure 34: 2D-axisymmetric sample geometry for first verification (in millimetres).

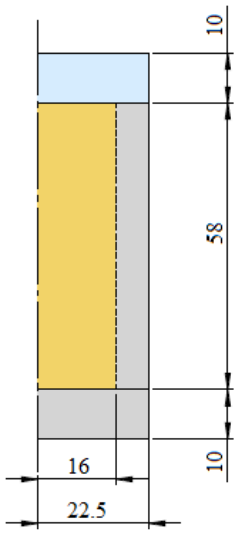

Source: Author.

For this simulation, the following parameters were defined on COMSOL®, using the same input data from previous Abaqus' simulation. This data was acquired from DSC and DMA experiments granted by the institution from the Abaqus file along with the script (programming language associated), present in Tables 6 and 7.

Table 6: Cure kinetics parameters.

A_1 [1/s]	A_2 [1/s]	E_1 [J/mol]	E_2 [J/mol]	m	n
333879.17	21042820.69	69140	72620	1	2

Source: Courtesy of ENSTA Bretagne.

Table 7: Material parameters.

R [J/(mol.K)]	T_{g0} [°C]	$T_{g\infty}$ [°C]	λ
8.3145498	-37	136	0.57

Source: Courtesy of ENSTA Bretagne.

Remember that A_1 and A_2 are pre-exponential constants [1/s], and E_1 and E_2 are the activation energies [J/mol] for the calculation of rate constants K_1 and K_2. R is the universal constant of perfect gases, m and n are respectively the orders associated with the auto-catalytic and catalytic reactions. T_{g0} and $T_{g\infty}$, the respective glass transition temperatures for a resin at degree of cure $\alpha = 0\%$ and $\alpha = 100\%$, and the adjustable parameter λ are applied in DiBenedetto's equation.

The remaining parameters and properties were added to COMSOL® as functions. Between the types used in the model, there are analytical, interpolation and ramp functions. The

heat transfer equation (Equation 14) describes the thermo-chemical behavior of the sample under curing without considering the last term, referring to the elastic deformation. The governing equation becomes:

$$\rho c_p \frac{dT}{dt} = div\{k[grad\, \boldsymbol{T}]\} + q + \rho \Delta \mathrm{H}^r \frac{d\alpha}{dt} \tag{22}$$

Once again, ρ, c_p and k are the material properties density, specific heat capacity and thermal conductivity, q stands for the heat imposed by the oven, $\Delta \mathrm{H}^r$ for the enthalpy of the reaction, and dT/dt and $d\alpha/dt$ are the temperature and degree of cure rates, respectively. All the needed terms and parameters from Equation 22 will, therefore, be presented.

7.2.1 Heat flow imposed by the oven, q

The heat exchanged between the sample and the oven is due to convection of the air in the medium. It can be expressed by

$$q = h(T - T_e) \tag{23}$$

where h is the coefficient of heat transfer by convection, T is the temperature at a certain point of interest and T_e is the external temperature. The radiation was not considered in the Abaqus simulations provided by ENSTA Bretagne and, therefore, was as well not taken into account for this case.

The convection was a boundary condition applied in the *Heat Transfer Module* to all the outer surfaces of the full geometry, i.e., the top and right edges of the Plexiglas, right and bottom edges of the steel (see Figure 35, and Appendix A for more details). The coefficient convection, h, was investigated and tabulated by Rabearison (2009) varying with the temperature according to Table 8, being inserted as an interpolation function.

Figure 35: Boundary condition of heat flux.

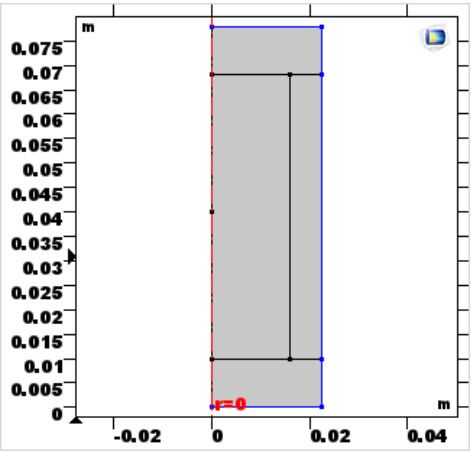

Source: Author.

Table 8: Variation of the coefficient of heat transfer by convection with temperature.

$T\ [K]$	$h\ [W/(m^2 * K]$
300.779	147.0992149
318.15	80.46560193
353.15	48.69074624
373.15	38.73839524
423.15	26.45964679

Source: RABEARISON (2009).

Lastly, the external temperature, to reproduce previous results, was set at 132°C. A ramp function was added for the change in temperature from the initial condition of the room at 20°C to 132°C in a very short time – 60 seconds –, simulating the sample being put in the pre-heated oven (COMSOL® set up at Appendix C).

7.2.2 Heat flow produced by the chemical reaction, ϕ

The term $\rho \Delta H^r \frac{d\alpha}{dt}$ was included in ϕ as the heat flow generated in the curing reaction. A boundary load of Heat Source was applied to the resin domain – also on the *Heat Transfer Module* –, consisting of a logical expression. This results from the condition attached to the heat flow, ϕ, which varies according to the nodal temperature being above or below the glass transition temperature, remembering that T_g varies with the degree of cure according to DiBenedetto's equation (Equation 21). For this, two analytical functions were created, called *flux_epoxy_1* and *flux_epoxy_2*. The resin density was considered constant and equal to $\rho = 1170.6\ kg/m^3$, as given by the Abaqus simulation file from ENSTA Bretagne. The enthalpies

of reaction, ΔH^r, are the ones dependent on the nodal temperature, which in the rubbery state – and, therefore, the reaction in progress – is a portion of the total heat released, and in the glassy state – at the end of the reaction – is approximated to the total heat produced by the chemical reaction, set in 355±25 J/g for the epoxy system. Considering the minimal total heat of 330 J/g, the functions were defined according to the source files as:

flux_epoxy_1: $1170600 * 330 * \frac{d\alpha}{dt}$, $T < T_g$ (glassy state) (24)

flux_epoxy_2: $1170600 * 330 * (0.00243 * \mathrm{T} - 0.16003) * \frac{d\alpha}{dt}$, $T > T_g$ (rubbery state) (25)

7.2.3 Glass transition temperature, T_g

Another analytical function corresponding to DiBenedetto's equation was added in the program, using the defined material parameters in Table 7. Isolating the glass transition temperature term, we have:

$$T_g = \frac{\lambda\alpha(T_{g\infty} - T_{g0})}{1 - (1 - \lambda)\alpha} + T_{g0} \quad (26)$$

7.2.4 Resin material properties: ρ, c_p, k

As stated, the density of the resin was considered as constant throughout the curing, assuming the value of $\rho = 1170.6\ kg/m^3$. The specific heat capacity and the thermal conductivity were a result of a rule of mixtures employed to each property, considering the properties for the uncured resin – $c_p(0,T)$, $k(0,T)$ – and the fully cured resin – $c_p(1,T)$, $k(1,T)$ –, expressed by:

$$c_p(\alpha,T) = (1-\alpha) * c_p(0,T) + \alpha * c_p(1,T) \quad (27)$$

$$k(\alpha,T) = (1-\alpha) * k(0,T) + \alpha * k(1,T) \quad (28)$$

The values were tabulated, and can be found in Annexes A and B. These tables were able to be inserted into the program as interpolation functions for each material property.

7.2.5 Cure kinetics

The cure kinetics parameters cited in Table 6 are applied in Kamal's extended model. Parameters K_1 and K_2 are inserted as analytical functions, following the Arrhenius Law. A function called *func* was defined for its application on the resolution of the ordinary differential equation:

$$func: \quad (K_1 + K_2\alpha^m)(1-\alpha)^n . f_d(\alpha) \tag{29}$$

The diffusion factor, however, couldn't be directly applied in *func* for it assumes negative values when inserted as an analytical function in COMSOL®, which is not realistic. Simulations carried out like this showed negative diffusion factors (Figure 36a) towards the end of curing, expressing the continuous decrease in the function values, reaching 0 but not stopping there. This resulted in a small drop in degree of cure values after it reached a stabilization, an unreal fact to occur. The diffusion factor $f_d(\alpha)$ should assume values from 1 – beginning of the reaction, where it is controlled by cure kinetics – to 0 – end of the curing, as the diffusion of reactive species dominate the reaction and the degree of cure rate becomes more and more insignificant. For this reason, a second function was created, named *fd*, assuming the value of zero whenever the diffusion factor function *fd_t* is negative (Figure 36b).

Figure 36: Graphics for (a) *fd_t(α,T)* and (b) *fd(α,T)*.

(a)

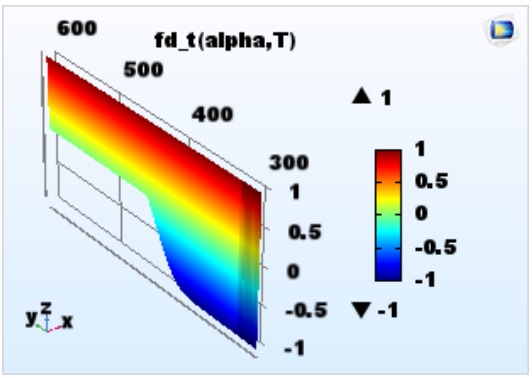

Source: Author.

(b)

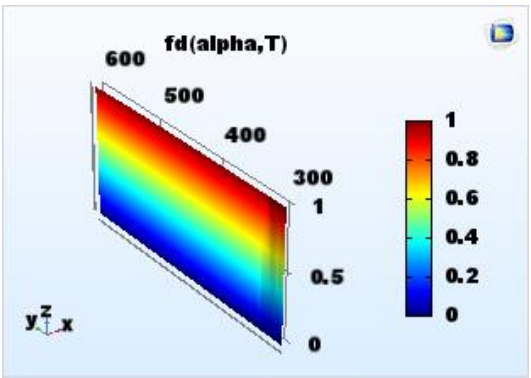

Source: Author.

$$fd = \begin{matrix} fd\_t(alpha,T)\ ,\ fd\_t(alpha,T)>0 \\ 0\ ,\ fd\_t(alpha,T)<0 \end{matrix} \tag{30}$$

The diffusion factor is also a function of parameters α_f and b – named *alphaf2* and *b2* in the program –, which are as well functions of temperature. They are defined as piecewise functions, according to:

$$\alpha_f: \quad \begin{matrix} 0.0040646 * T - 0.82434\ , \quad 293 \leq T \leq 448.8 \\ 0.0040646 * 448.8 - 0.82434\ , \quad 448.8 \leq T \leq 600 \end{matrix} \tag{31}$$

$$b: \quad \begin{matrix} 7.1588e-4 * 319 - 2.2816e-1\ , \quad 293 \leq T \leq 319 \\ 7.1588e-4 * T - 2.2816e-1\ , \quad 319 \leq T \leq 600 \end{matrix} \tag{32}$$

Both parameters were only specified for temperature ranges of 360 K to 420 K by the linear relationships. Parameter α_f, nevertheless, has a physical limitation of maximum value of the unity. This led to a restriction of the linear expression to temperatures up to 448.8 K. From this on, α_f remains constant. As for b, it cannot be zero, or the diffusion factor has an indeterminacy from the denominator of $\left(\frac{\alpha-\alpha_f}{b}\right)$. The critical temperature corresponds to 319 K, then it was decided to keep the parameter b constant for lower temperatures. The final tree of defined functions is presented below in Figure 37.

Figure 37: Defined functions in COMSOL [thermo-chemical model].

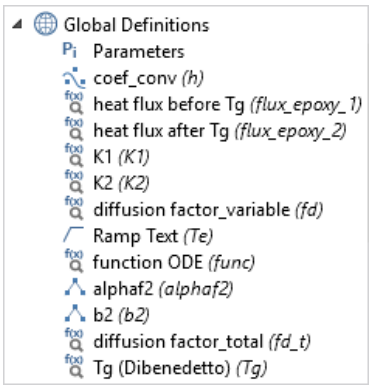

Source: Author.

7.2.6 Plexiglas and steel material properties

The required properties for the sample mould are their density, thermal conductivity and specific heat capacity. For the Plexiglas, all of them are constant; as for the steel, k and c_p are linearly dependent on the temperature, being added as interpolation functions. Table 9 exposes these properties, extracted from the literature.

Table 9: Material properties for Plexiglas and Steel.

Material	$\boldsymbol{\rho}$ $[\boldsymbol{kg/m^3}]$		$\boldsymbol{k}$ $[\boldsymbol{W/(m.K)}]$	$\boldsymbol{c_p}$ $[\boldsymbol{J/(kg.K)}]$
Plexiglas	1190		0.19	1500
		$\boldsymbol{T}$ $[\boldsymbol{K}]$		
Steel	7800	293	24	460
		773	29	540

Source: Author.

7.2.7 Ordinary differential equation

The solving of the ODE achieved by Kamal's extended model is done in *Domain ODEs and DAEs Module*, which allows the setup of a differential equation to be solved within the program. The dependent variable – *alpha* – is provided to the software, and the terms of the differential equation are defined. In Figure 38, the *Settings* window of the module is shown, with the respective values of each term of the equation. The previously defined function *func* is then inserted at this stage. Remembering that the ODE is expressed by:

$$\frac{d\alpha}{dt} = func(T, \alpha) \tag{33}$$

Figure 38: *Settings* window for *Domain ODEs and DAEs*.

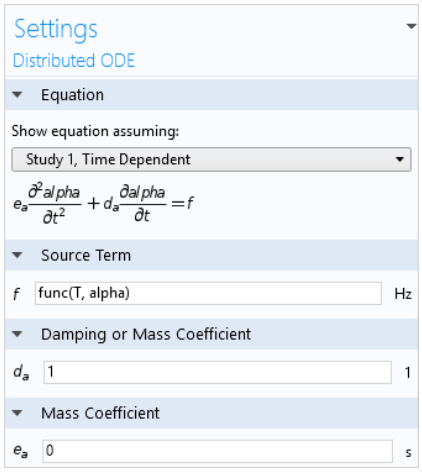

Source: Author.

7.2.8 Meshing

An *extremely fine* mesh was applied, which gave a total of 3030 quadrilateral elements (Figure 39), with the default *Quadratic Lagrange* order (quadratic Lagrange elements). Further investigation on mesh sizing wasn't performed for the Abaqus Replication, since a very refined

mesh provided fast and reliable results to be presented in Section 8 (simulations took no more than 5 minutes to be performed).

Figure 39: Geometry meshing.

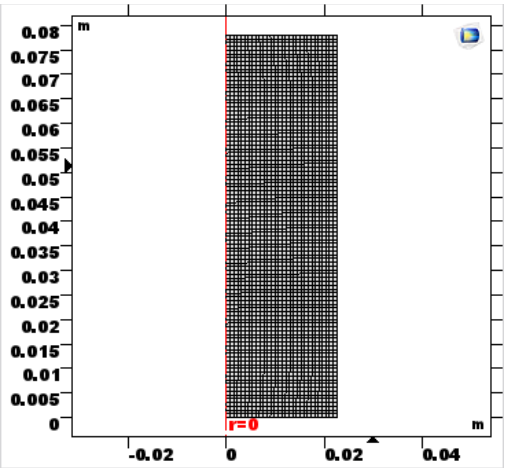

Source: Author.

7.2.9 Study

A *Time Dependent* study was setup with a total duration of 5000 s in order to fully cover the curing process. Time increments were taken as 1 s. The remaining study definitions were set as the program default.

7.3 OVEN VALIDATION WITH GLYCERINE

As a first step of the modelling process, the glycerine heating was reproduced on COMSOL® for oven validation. For the simulation, the geometry of the sample was submitted to a convective heat flux on its all external edges (Figure 40). The coefficient of convection was the same as before (Table 8 in Section 7.2.1), defined as an interpolation function. The external temperature was also added as an interpolation function, as shown in Table 10, with the same heating and cooling rates of 3°C/min from the experiment.

Figure 40: Heat flux boundary condition.

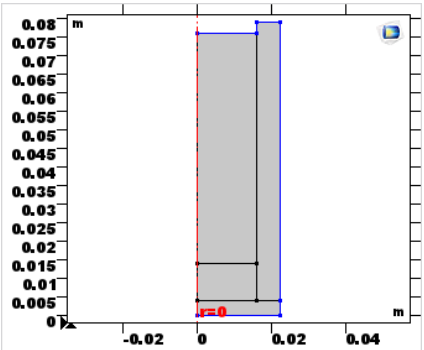

Source: Author.

Table 10: External temperature with time for glycerine experiment.

t [s]	***T [°C]***
0	20
2400	140
9600	140
12000	20

Source: Author.

Steel material properties were maintained from the previous model, with the same definitions. The glycerine properties were considered all constant, extracted from the literature, as shown in Table 11.

Table 11: Material properties for Glycerine and Steel.

Material	$\boldsymbol{\rho}$ $[\boldsymbol{kg/m^3}]$		$\boldsymbol{k}$ $[\boldsymbol{W/(m.K)}]$	$\boldsymbol{c_p}$ $[\boldsymbol{J/(kg.K)}]$
Glycerine	1261		0.286	2350
		$\boldsymbol{T}$ $[\boldsymbol{K}]$		
Steel	7800	293	24	460
		773	29	540

Source: Author.

As the simulation would run up to 12,000 s and, therefore, increasing the computational memory and time, a coarser mesh was applied for this case. The mesh convergence process was carried out for the epoxy resin, since that was the study object and more complex case. The mesh convergence test can be seen at Appendix E. For standardization, the glycerine and following simulations were performed with the same mesh distribution, obtained by the convergence test. The glycerine was, then, set to have a division of 12 elements on the horizontal edge and 30 elements in the vertical one, using a quadrilateral mesh with *Quadratic Lagrange* order as well. Since the steel doesn't represent regions of interest as the glycerine, a local triangular mesh was inserted for reduction in the total number of elements. The final mesh

presented 650 elements, as seen in Figure 41. The study was set, once again, as Time Dependent with time increments of 1 s.

Figure 41: Geometry meshing for Glycerine simulation.

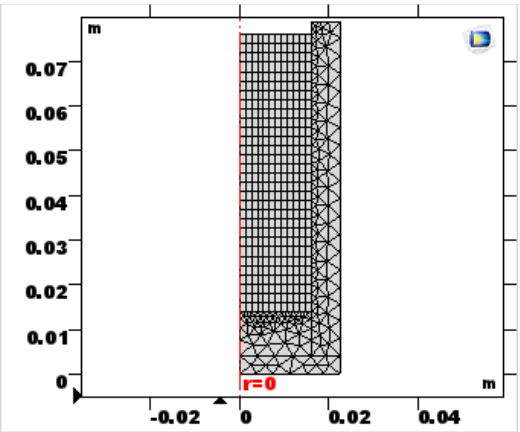

Source: Author.

7.4 MODELLING OF THE CURING EXPERIMENTS

The experimental conditions for the epoxy resin were added to COMSOL Multiphysics® for reproduction of the tests and consequent validation of the numerical results. The final developed thermo-chemical model is presented in this section, with parameters based on the literature. The studies of Rabearison (2009) and Rabearison et al. (2008; 2009) were taken as a reference for the development of the investigation. Cure parameters of the LY556 epoxy resin were identified by Rabearison et al. (2011), which were applied in the simulations.

Remembering the Heat Transfer Equation for the thermo-chemical problem, the parameters to be defined include material properties (ρ, c_p, k), the heat imposed by the oven (q), and the heat produced by the chemical reaction ($\phi = \rho \Delta \mathrm{H}^r \frac{d\alpha}{dt}$).

$$\rho c_p \frac{dT}{dt} = div\{k[grad\, \boldsymbol{T}]\} + q + \rho \Delta \mathrm{H}^r \frac{d\alpha}{dt} \tag{22}$$

From the cure kinetics expressed by Kamal's extended model, the necessary parameters are $A_1, A_2, E_1, E_2, m, n, \alpha_f$ and b, and for complete description of the glass transition temperature $T_{g0}, T_{g\infty}$ and λ must be provided. The following sections present all of this inserted into the numerical model.

7.4.1 Geometry

The geometry of the model followed the experiments, presenting the resin of 32 mm of diameter and 60 mm of height in the steel mould. In the 2D-axisymmetric modelling, the geometry of the problem is shown next in Figure 42.

Figure 42: 2D-axisymmetric geometry.

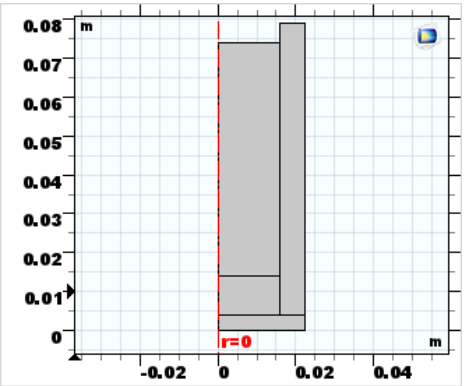

Source: Author.

7.4.2 Cure kinetics

The cure kinetics parameters, usually obtained from experimental data using data fitting methods as the least squares method, were already investigated and defined by Rabearison et al. (2011) for a LY 556 epoxy system, with HY 917 hardener and DY 070 accelerator in a mass ratio of 100:90:2. The authors used isothermal and non-isothermal differential scanning calorimetry for the characterization of the epoxy system. The study led to the following constant values for the parameters (Table 12):

Table 12: Cure kinetics parameters for the epoxy system.

A_1 [1/s]	A_2 [1/s]	E_1 [kJ/mol]	E_2 [kJ/mol]	m	n
1339879.17	21042820.69	69.14	72.62	1	2

Source: RABEARISON et al. (2011).

These constants were added to the numerical model in the *Parameters* section on COMSOL®, which admits the association of constants to a specified parameter name. Parameters α_f and b from the diffusion factor are linearly dependent on the temperature, and are expressed by the equations below, with temperature T in Kelvin:

$$\alpha_f = 4.0646e-3 * T[K] - 8.2434e-1 \quad (34)$$

$$b = 7.1588e-4 * T[K] - 2.2816e-1 \quad (35)$$

Similar to the explanation given in Section 7.2.5, α_f and b were defined for temperature ranges between 360 K and 420 K. In a physical point of view, the final degree of conversion α_f cannot exceed 100%. This limit appears at 448.8 K, and from then on α_f remains constant. Parameter b has a limitation as well, for it is a denominator and cannot be zero, or it will cause an indeterminacy. The critical temperature, achieved at 319 K, sets the parameter to assume a constant value for lower temperatures. Hence, α_f and b were set up as piecewise functions, according to:

$$alphaf2: \quad \begin{matrix} 0.0040646 * T - 0.82434\ , & 293 \leq T \leq 448.8 \\ 0.0040646 * 448.8 - 0.82434\ , & 448.8 \leq T \leq 600 \end{matrix} \tag{36}$$

$$b2: \quad \begin{matrix} 7.1588e-4 * 319 - 2.2816e-1\ , & 293 \leq T \leq 319 \\ 7.1588e-4 * T - 2.2816e-1\ , & 319 \leq T \leq 600 \end{matrix} \tag{37}$$

Parameters K_1 and K_2 were inserted as analytical functions, obeying the Arrhenius Law. The universal constant of perfect gases, $R\_g = 8.3145498\ J/(mol.K)$, was also included in the *Parameters* section, and called at the functions:

$$K1: \quad A1 * exp(-E1/(R * T)) \tag{38}$$

$$K2: \quad A2 * exp(-E2/(R * T)) \tag{39}$$

After that, an analytical function was created for the diffusion factor. Once again, it showed negative values towards the end of curing. The limitation of $f_d(\alpha)$ assuming a range from 1 to 0 throughout the curing led to the insertion of a second analytical function, in which the final diffusion factor (*fd*) follows the first function (*fd_t*), but remains zero if negative values appear. As before, this can be represented as:

$$fd = \begin{matrix} fd\_t(alpha,T)\ , & fd\_t(alpha,T)>0 \\ 0\ , & fd\_t(alpha,T)<0 \end{matrix} \tag{30}$$

Finally, Kamal's extended model was included by the analytical function *func*, defined by:

$$func: \quad (K1 + K2 * alpha\text{^}m) * (1 - alpha)\text{^}n * fd(alpha, T) \tag{40}$$

For the solving of the ODE from the phenomenological model, the module *Domain ODEs and DAEs* was added to the model. As well as in Section 6.1.7, the coefficients of the second order ODE were provided to the program, as described below:

$$e_a \frac{d^2 alpha}{dt^2} + d_a \frac{dalpha}{dt} = f \tag{41}$$

where: $f = func(alpha, T)$; $d_a = 1$; $e_a = 0$

With this, the cure kinetics is completely defined in the model.

7.4.3 Glass transition temperature, T_g

The glass transition temperature varies with the corresponding degree of cure, as previously verified in DiBenedetto's equation. The needed parameters for its definition are $T_{g0}, T_{g\infty}$ and λ. Their values were given by Rabearison et al. (2008), determined by curve fitting with experimental data, according to Table 13.

Table 13: Parameters from DiBenedetto's Equation.

T_{g0} [°C]	$T_{g\infty}$ [°C]	λ
-37	136	0.57

Source: RABEARISON et al. (2008).

These constants were added to the list of *Parameters*, where the glass transition temperature represented an analytical function, defined as:

$$Tg\_ep: \quad ((Tginf - Tg0) * lambda * alpha)/(1 - (1 - lambda) * alpha) + Tg0 \tag{42}$$

7.4.4 Epoxy's density

The epoxy system's density has a small variation throughout the curing process (less than 10%). The liquid resin ($\alpha = 0\%$) has a density of 1170.6 kg/m³, where for the fully cured resin ($\alpha = 100\%$) it is 1253.556 kg/m³. Simulations were performed with a rule of mixtures defining the density at each degree of cure α, but this didn't show significant variations in the results. Keeping such property constant seemed reasonable, especially as a way of reducing calculations within the model. Hence, $\boldsymbol{\rho = 1170.6\ kg/m^3}$ was adopted, the same value considered in previous simulations performed on Abaqus by ENSTA Bretagne and works of Rabearison (2009).

7.4.5 Epoxy's specific heat capacity

Rabearison (2009) defined the specific heat capacity of the epoxy system by a rule of mixtures:

$$c_p(\alpha, T) = (1 - \alpha) * c_p(0, T) + \alpha * c_p(1, T) \tag{27}$$

where $c_p(0, T)$ and $c_p(1, T)$ are, respectively, the specific heat capacities for the uncured and the fully cured resin. They are expressed as linear functions of the temperature:

$$c_p(0, T) = 1.8500 + 0.002625 * T[°C] \quad [J/g.°C] \tag{43}$$
$$c_p(1, T) = 1.3125 + 0.004437 * T[°C], \qquad T < T_{g\infty} \quad [J/g.°C]$$
$$c_p(1, T) = 1.8500 + 0.002625 * T[°C], \qquad T \geq T_{g\infty} \quad [J/g.°C]$$

The property was inserted into the model as an interpolation function through tabulated values, which was already available for use. The values follow cited equations, and can be seen in Annex A.

7.4.6 Epoxy's thermal conductivity

As well as the specific heat capacity, Rabearison (2009) defined the thermal conductivity of the epoxy system by a rule of mixtures. The author used literature models, which present the thermal conductivity of the fully cured resin in a linear relationship with temperature. For the thermal conductivity for the uncured resin, experimental approximations led to an assumed temperature independent value of 0.188 W/(m.°C).

$$k(\alpha, T) = (1 - \alpha) * k(0) + \alpha * k(1, T) \quad W/(m.°C) \tag{44}$$

where: $k(0) = 0.188\ W/(m.°C)$

$k(1, T) = -2.727e - 4 * T[°C] + 3555.529e - 4\ \ W/(m.°C)$

Values for the thermal conductivity of the epoxy system were also tabulated, making it possible for the insertion of the property as an interpolation function. Annex B shows these values.

7.4.7 Steel's material properties

The material properties for the steel were maintained the same as before, detailed in Table 14 below.

Table 14: Material properties for Steel.

$\boldsymbol{T}$ $[\boldsymbol{K}]$	$\boldsymbol{k}$ $[\boldsymbol{W/(m.K)}]$	$\boldsymbol{c_p}$ $[\boldsymbol{J/(kg.K)}]$	$\boldsymbol{\rho}$ $[\boldsymbol{kg/m^3}]$
293	24	460	7800
773	29	540	

Source: Author.

7.4.8 Heat flow produced by the chemical reaction

The exothermal chemical reaction of polymerization produces a heat flow derived from enthalpy variation, comprised in ϕ as $\rho\Delta H^r \frac{d\alpha}{dt}$. The enthalpy variation ΔH^r is expressed in terms of enthalpies from isothermal and dynamic modes of DSC experiments. For better understanding, we recall the definition of degree of cure:

$$\frac{d\alpha}{dt} = \frac{1}{H_U}\left(\frac{dH}{dt}\right) \tag{5}$$

This represents the formulation based on the enthalpy obtained in DSC experiments in dynamic mode, where the temperature is programmed for an evolution along with time. H_U is the total enthalpy for the complete reaction in such mode, and (dH/dt) is the instantaneous heat flux for the dynamic mode as well.

The total enthalpy of reaction can also be calculated by DSC experiments in isothermal mode, keeping the sample temperature constant. This enthalpy, named H_T, varies linearly with the considered temperature. The total enthalpy in dynamic mode H_U, however, was observed to remain constant (RABEARISON, 2009) at 355±25 J/g. The author found through experimental investigation that the ratio H_T/H_U increases in a linear relationship with temperature only until a critical temperature, in which the ratio remains constant (Figure 43). He considered such critical temperature corresponding to a value where H_T reaches its maximum in the isothermal mode, and the resulting matrix is assumed as almost completely formed.

Figure 43: H_T / H_U as function of temperature.

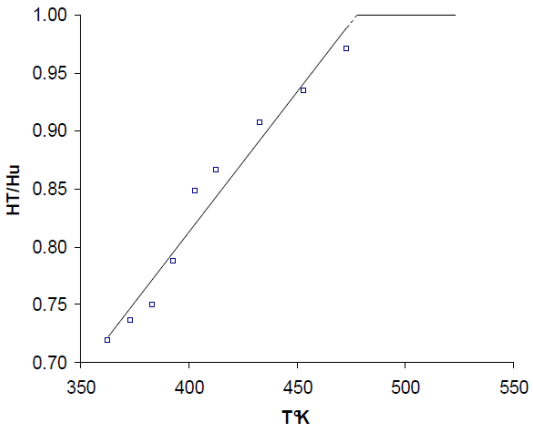

Source: RABEARISON (2009).

The matrix almost formed can be interpreted as the corresponding matrix in the glassy state. Therefore, similar to the Replication of Abaqus Model (Section 6.1), the critical temperature was taken as the glass transition temperature. The enthalpy considered in heat flow ϕ, thus, obeys the linear relationship in the rubbery state ($\Delta H^r = H_U * (H_T/H_U)$ for $T > T_g$) and is constant in the glassy state ($\Delta H^r = H_U$ for $T < T_g$). Considering the minimal total enthalpy $H_U = 330\, J/g$, the heat flow from the chemical reaction was added as two analytical functions: *flux_epoxy_1* and *flux_epoxy_2*. The linear relationship of H_T/H_U was found by Rabearison (2009) to be $0.00243 * T - 0.158$, with temperature in Kelvin. Hence:

flux_epoxy_1: $1170600 * 330 * \frac{d\alpha}{dt}$, $T < T_g$ (glassy state) (45)

flux_epoxy_2: $1170600 * 330 * (0.00243 * T - 0.158) * \frac{d\alpha}{dt}$, $T > T_g$ (rubbery state) (46)

Remembering that density is constant and equal to 1170.6 J/(kg.K). The heat flow ϕ was inserted as a Heat Source for the epoxy domain in the *Heat Transfer Module*. The general source consisted of a logical expression, where it assumes the values of *flux_epoxy_1* if $T < T_g$, and of *flux_epoxy_2* otherwise (i.e. when $T > T_g$). As heat flow is a function of the rate of cure (in both functions), at the end of the reaction the rate becomes null, and so does the heat flow. For that reason, no limitations to the stop of heat source for the cured resin were necessary.

7.4.9 Heat flow imposed by the oven

Since the oven used for the experiments (140°C, 110°C and 80°C + 120°C, with temperature changes at a 3°C/min rate) was considerably larger than the sample, radiation effects were not considered. Therefore, just the convection of the air inside the oven provokes a heat flow exchanged between the medium and the sample, defined as:

$$q = h(T - T_e) \tag{23}$$

This was added to the *Heat Transfer Module* as a Heat Flux boundary condition to all the external edges of the geometry in the model. This can be visualized in Figure 44.

Figure 44: Heat Flux boundary condition.

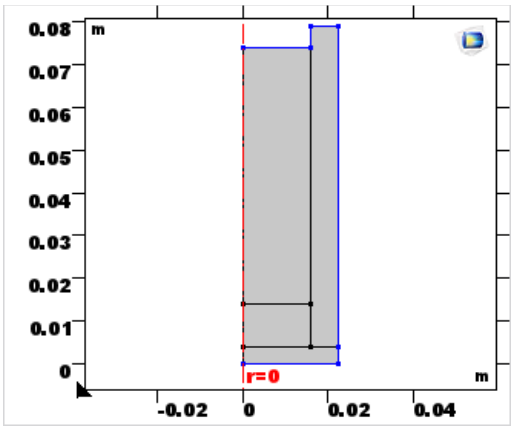

Source: Author.

Two relevant parameters must be provided to the model: the coefficient of heat transfer by convection h and the external temperature T_e. The coefficient of convection considered was the one calculated by Rabearison (2009), obtained through an oven validation with glycerine. Table 8 in Section 7.2.1 presents the values of h according to temperature. Thus, an interpolation function was inserted into the program for the definition of h.

Table 8: Variation of the coefficient of heat transfer by convection with temperature.

$T\ [K]$	$h\ [W/(m^2 * K]$
300.779	147.0992149
318.15	80.46560193
353.15	48.69074624
373.15	38.73839524
423.15	26.45964679

Source: RABEARISON (2009).

The external temperature consisted of an interpolation function as well, where the changes in temperature were carried out with a rate of 3°C/min, similar to the experiments. For the experiments with a curing temperature of 140°C, 110°C and 80°C + 120°C, the following Tables 15, 16 and 17 show the interpolation tables added to the function *Te(t)* of the model.

Table 15: Interpolation *Te(t)* for curing at 140°C [3°C/min, 2h].

***t* [s]**	***T* [°C]**
0	20
2400	140
9600	140

Source: Author.

Table 16: Interpolation *Te(t)* for curing at 110°C [3°C/min, 2h].

***t* [s]**	***T* [°C]**
0	20
1800	110
9000	110

Source: Author.

Table 17: Interpolation *Te(t*) for curing at 80°C + 120°C [3°C/min, 4h].

***t* [s]**	***T* [°C]**
0	20
1200	80
15600	80
16400	120
30800	120

Source: Author.

7.4.10 Meshing

As previously mentioned, the mesh applied for the oven validation with glycerine was kept for the thermo-chemical models. The epoxy resin was set to be divided in 12 elements horizontally and 30 elements vertically for a quadrilateral mesh. The default order of the Heat Transfer mesh elements was maintained as *Quadratic Lagrange*. A free triangular distribution was employed on the remaining of the geometry, reducing the total of elements compared with a full quadrilateral mesh. The final mesh consisted of 645 elements, as observed in Figure 45.

Figure 45: Geometry meshing for the thermo-chemical model.

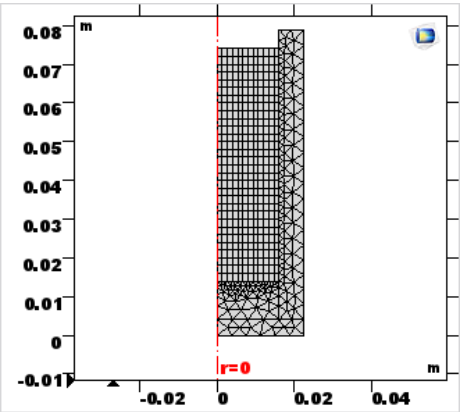

Source: Author.

7.4.11 Study

The *Time Dependent* option was selected for the setup of the study, keeping all the other configurations as the solver default. Time increments remained as 1 s. For each cure temperature simulated, the total duration in the *Study Module* was changed for the last time record of the respective *Te(t)* used.

7.5 THERMO-CHEMICAL-MECHANICAL MODEL

As mentioned before, the research progressed to the development of the curing model adding the effects of mechanics. A few more parameters are introduced, as well as new COMSOL® Modules to be subsequently explained. The final model just considers the elastic mechanical behaviour of the system during curing, and the species diffusion is only controlled by the chemistry governed by the cure kinetics model, leaving species diffusion on the mechanics as second order effects.

The thermo-chemical-mechanical model consisted of the thermo-chemical model with the addition of the *Solid Mechanics Module*, along with the *Multiphysics Module*, which allowed the coupling phenomena. In order to specify all the complementary parameters to be included in the model, we recall the constitutive equations of Heat Transfer and Hooke's Law:

$$\rho c_p \frac{dT}{dt} = div\{k[grad\, \boldsymbol{T}]\} + q + \rho \Delta \mathrm{H}^r \frac{d\alpha}{dt} - T\{(3\kappa + 2\mu)\alpha_T\} tr\dot{\boldsymbol{\varepsilon}}^{\boldsymbol{e}} \quad (14)$$

$$\boldsymbol{\sigma} = \kappa(tr\boldsymbol{\varepsilon})\boldsymbol{I} + 2\mu\boldsymbol{\varepsilon} \quad (16)$$

The last term in the Heat Transfer Equation, $T\{(3\kappa + 2\mu)\alpha_T\}tr\dot{\boldsymbol{\varepsilon}}^{\boldsymbol{e}}$, corresponds to the heat of mechanical origin. Since it is low in its effects compared to the other terms, this heat was considered negligible. Hence, in terms of Elastic Modulus and Poisson's ratio, the equations are expressed by:

$$\rho c_p \frac{dT}{dt} = div\{k[\boldsymbol{grad}\, T]\} + q + \rho \Delta \mathrm{H}^r \frac{d\alpha}{dt} \tag{47}$$

$$\boldsymbol{\sigma} = \frac{E}{1+\nu}\left\{\left[\frac{\nu}{1-2\nu}(tr\boldsymbol{\varepsilon})\right]\boldsymbol{I} + \boldsymbol{\varepsilon}\right\} \tag{16}$$

Analysing the presented equations, the remaining unidentified parameters are E and ν. The total strain is the sum of elastic strain – obtained in the solving –, thermal strain and chemical strain. The evolution of thermal and chemical strains must, therefore, be specified for the complete model development, as well as the Young's modulus and Poisson's ratio.

7.5.1 Thermal strain

The thermal strain, as previously mentioned in Section 4.2.1, can be described as

$$\varepsilon_{ii}^{th} = \alpha_T\, \Delta T\,; \quad \varepsilon_{ij}^{th} = 0 \tag{20}$$

where ΔT is the difference between the actual temperature and a reference temperature, which consists of the initial temperature of 20°C. Hence, $\Delta T = T - 293\ [K]$. The coefficient of thermal expansion (CTE) must be provided for the strain estimation along the cure. As other material properties, α_T was also included into the model by a rule of mixtures considering the contributions of the liquid resin, with a CTE of $\alpha_T(0,T)$, and the matrix already formed, with a CTE of $\alpha_T(1,T)$. As a result, α_T is expressed by:

$$\alpha_T(\alpha,T) = (1-\alpha) * \alpha_T(0,T) + \alpha * \alpha_T(1,T) \tag{48}$$

Previous works with the epoxy system in investigation (RABEARISON, 2009; RABEARISON et al., 2009) provided values for the CTE of liquid resin as constant and equal to $\alpha_T(0,T) = 5e-4\ [1/°C]$, as the CTE for the completely polymerized matrix is dependent on the temperature being above or below T_g.

$$\begin{aligned} &\alpha_T(1,T) = 450e-6\ \ [1/°C] \quad \text{for} \quad T < T_g \\ &\alpha_T(1,T) = 450e-6+4.1e-6*(T-T_g)\ \ [1/°C] \quad \text{for} \quad T > T_g \end{aligned} \tag{49}$$

In the simulations, two analytical functions were used: one for the CTE of the fully cured resin for temperatures above the changing glass transition temperature (*beta_fce_after*) and another for the instantaneous CTE $\alpha_T(\alpha, T)$ with a logical condition regarding the adequate $\alpha_T(1, T)$ to be taken into account. For $\alpha_T(\alpha, T)$ below T_g the constant value it assumes was inserted in the rule of mixtures. Thus, the following functions were added:

beta_fce_after: 450e-6+4.1e-6*(T-Tg_ep(alpha)) (50)

exp_ep: if(T>Tg_ep(alpha),(1-alpha)*beta_ue+ alpha*beta_fce_after(T,alpha),(1-alpha)*beta_ue+alpha*450e-6) (51)

7.5.2 Chemical strain

Li et al. (2004) studied the chemical contraction of an epoxy resin and achieved a bi-linear relationship of such strain with the degree of cure, where the inflexion point occurs at gelation point (Section 3.2.3). The isothermal curing temperature or cure rate were identified as not affecting the bi-linear behaviour. The concept developed by Li et al. was applied in previous works for the LY 556 epoxy system, assuming that the bi-linear evolution keeps unaffected by different non-isothermal curing temperatures, and so it was in this investigation.

Rabearison et al. (2009) exposed the chemical shrinkage using experimental data from the resin manufacturer Huntsman for a 120°C isothermal curing along with Li et al.'s model, with the break-point at gelation registered in 55% of degree of conversion (Figure 46). The total cure shrinkage is set at -6%, corresponding to Li et al.'s model for a degree of cure of 100% and not far from experimental results, which registered -5.8%.

Figure 46: Chemical shrinkage evolution with degree of cure for LY 556 epoxy system from experimental data and estimation by Li et al.'s model.

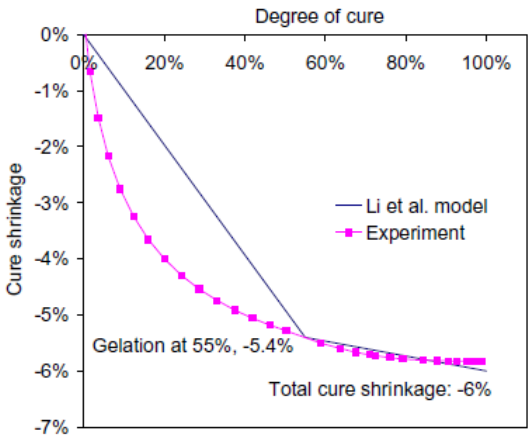

Source: RABEARISON et al. (2009).

The authors highlight a significant difference with the experiment for curing before gelation. They state a possibility of fitting the data with a polynomial function for improvement of the modelling for $0\% < \alpha < 55\%$, but this would be linked to the supposition of the data signal remaining the same for different curing conditions. Authors decided to use the bi-linear model from Li et al., since it was validated for several curing of epoxies and acknowledged by the scientific community. This same thought was kept in mind for the research, applying, as well, the bi-linear behaviour in the simulations.

Consequently, the chemical strain was added to the model as a piecewise function. The line equations defined were:

Table 18: Piecewise function for chemical shrinkage (*e_ch*).

Start	End	Function
0	0.55	-(0.054/0.55)*alpha
0.55	1	-((0.06-0.054)/(1-0.55))*alpha-0.06+(0.06-0.054)/(1-0.55)

Source: Author.

7.5.3 Poisson's ratio from bulk and shear moduli

When the Elastic Constitutive Law was presented in Section 4.2.1, it was mentioned the laborious process of obtaining the material properties ν and E along the curing of a resin. For that reason, they were achieved by the elastic shear modulus G and the bulk modulus K, as this also enables a description of the elastic constitutive behaviour on one hand and is easier to be experimentally identified on the other hand.

The bulk modulus was considered to follow a rule of mixtures with the degree of cure, with the values for the liquid resin $K(0)$ and the fully cured resin $K(1)$ retrieved from the literature as 3 GPa and 6.31 GPa, respectively (RABEARISON et al., 2009; PASCAULT et al., 2002).

$$K(\alpha) = (1 - \alpha) * K(0) + \alpha * K(1) \tag{52}$$

Parameters $K(0)$ and $K(1)$ were added to the *Parameters* list, and called in an analytical function (*K_ep*) defined according to the rule of mixtures presented.

The elastic shear modulus was achieved by DMA-TMA experiments according to the evolution of degree of cure, present in works of Jochum & Grandidier (2004), Smaali (2005), Rabearison (2009) and Rabearison et al. (2009) in Figure 47. The values were tabulated for a

frequency of 0.1 Hz, and can be verified in Annex C. These tabulated values were then inserted into the model as an interpolation function (*G_ep*).

Figure 47: Elastic shear modulus evolution with degree of cure.

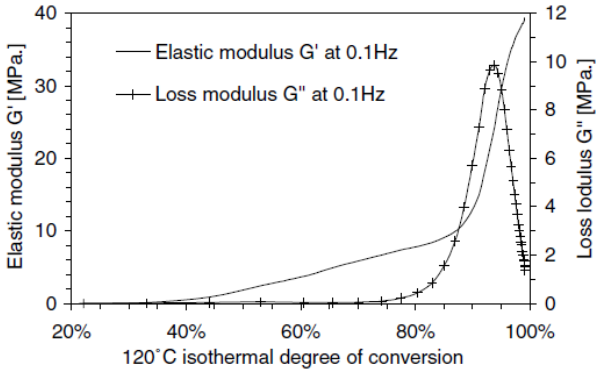

Source: JOCHUM & GRANDIDIER (2004).

From the mechanics, Poisson's ratio *nu_ep* was another analytical function set up in the model tree, assuming the form of Equation 17:

nu_*ep:* (3*K_ep(alpha)-2*G_ep(alpha))/(6*K_ep(alpha)+2*G_ep(alpha)) (53)

7.5.4 Young's modulus

The elastic modulus was the last function to be defined, also analytical, and written as Equation 18 from mechanics provided, in terms of the elastic shear modulus and Poisson's ratio:

E_ep: 2*G_ep(alpha)*(1+nu_ep(alpha)) (54)

The mechanical properties of Young's modulus and Poisson's ratio were only available for the curing cycle. An evolution of such properties for the already formed matrix submitted to cooling isn't yet fully defined. A work of Jochum et al. (2013) presented an increasing variation of the elastic shear modulus with the decrease in temperature, stating that such property reaches greater values after the cool-down of the resin. However, the evolution developed starts from a value of G around 10 MPa while the simulations carried out achieve a greater value (around 30 MPa) for the respective temperature at the end of cure. This didn't prove to be ideal, leading to an investigation limited to the end of the plateaus of the cure temperatures.

7.5.5 Mechanics coupling

As stated in the beginning of Section 7.1, the modules *Solid Mechanics* and *Multiphysics* were incorporated into the simulations for the mechanical analysis coupled with the thermo-chemical model. With properties needed already defined, a single boundary condition was applied to the model. The bottom edge of the geometry – the base of the steel cylinder – had its coordinate *z* fixed in order to avoid rigid body motion (Figure 48).

Figure 48: Boundary condition of *Prescribed Displacement* ($z = 0$).

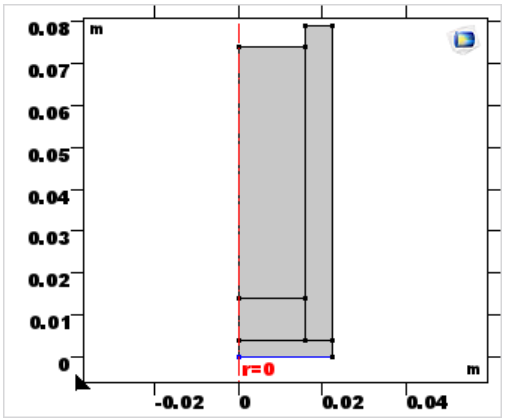

Source: Author.

In the *Multiphysics Module*, it is necessary to inform the input on the thermal expansion. As such expansion would contribute to the stress state in the geometry, it was chosen to incorporate it as *Thermal Strain*. This made possible the insertion of not only the thermal strain, but also the chemical shrinkage ruled by function *e_ch*. Hence, the expression used in this module was:

Thermal strain: exp_ep(T,alpha)*(T-293[K])+e_ch(alpha) (55)

There's also an option in the *Multiphysics Module* which can be selected named *Thermoelastic Damping*, where the heat effects caused by the mechanics can be considered into the calculation. Since these were previously disregarded in our assumptions for their low contribution, it was not the case to select it. A visualization of the *Settings* window is available in Appendix D. For this kind of setup, the multiphysics could only be applied to the resin, since the program didn't allow the addition of a second *Multiphysics Module* for the model tree created. But as the CTE of steel is considerably lower than the epoxy's – around 12.5e-6 [1/°C] – this wasn't seen as relevant for the results.

7.5.6 Meshing and study

No changes were made from the thermo-chemical model to the coupling model of thermal, chemistry and mechanics. The epoxy resin remained with a quadrilateral mesh (12 divisions on the horizontal and 30 on the vertical) and the mould with free triangular elements, resulting in a total of 645 elements. The *Time Dependent* study was kept with a time increment of 1 s and total duration defined by the last time record of the external temperature applied to the model.

8 RESULTS ANALYSIS

8.1 FIRST MODEL VERIFICATION

The initial simulations were performed for a replication of a previous model run on Abaqus FEA with integrated Fortran scripts, with results provided by ENSTA Bretagne, using COMSOL Multiphysics® features and resources for a simpler implementation of the curing process. The achieved model led to results of degree of cure and temperature shown in the following figures. Points 1, 2, 3 and 4 were defined, respectively, at the centre and half height of the resin, at the quarter (half the radius and ¾ of height), and at the top and the centre, both on the external radius (see Figure 49). These reference points were taken throughout all investigations for all types of geometry studied. Figures 50 and 51 present the result comparisons between simulations previously run on Abaqus and the ones developed on COMSOL®.

Figure 49: Location of points 1, 2, 3 and 4 in 2D-axisymmetric resin geometry.

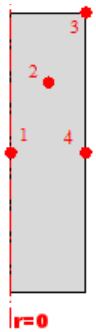

Source: Author.

Figure 50: Comparisons on degree of cure of Abaqus and COMSOL® simulations.

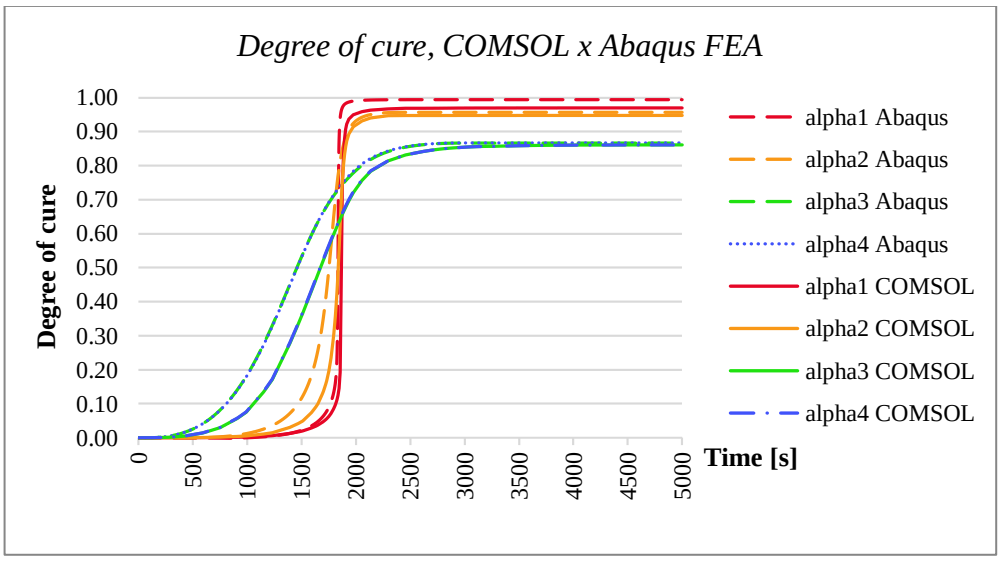

Source: Author.

Figure 51: Comparisons on temperature of Abaqus and COMSOL® simulations.

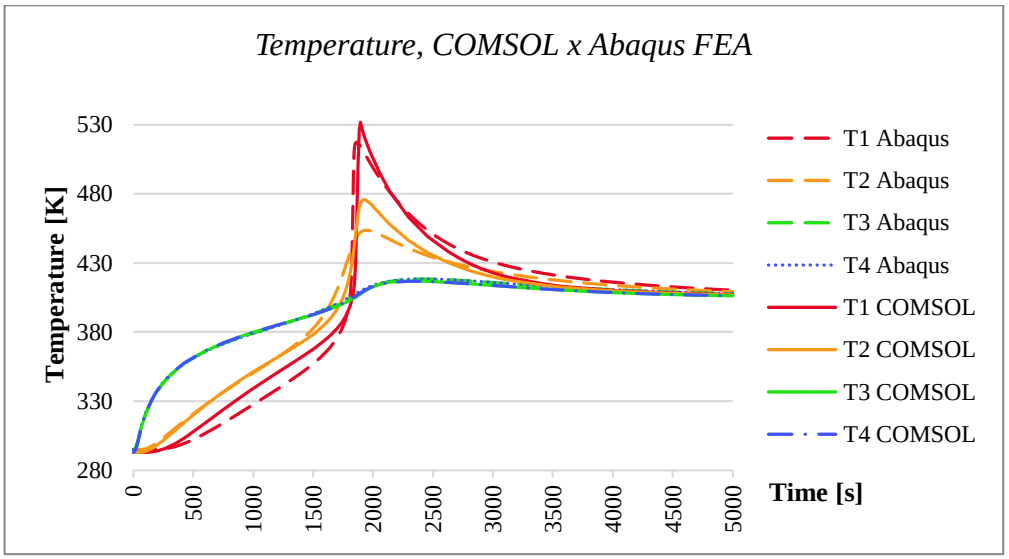

Source: Author.

Numerical results from COMSOL® are in very good agreement with simulations carried out on Abaqus FEA. This represented an initial confirmation of the model development walking into the right direction. No external script was necessary to be incorporated, facilitating the modelling process and reducing it to an application of functions and simple logical expressions, as detailed in Section 7.1. Moreover, the simulation took very reduced time in its performance, with a duration of approximately 3 minutes. Sources from ENSTA Bretagne showed that previous Abaqus simulations registered more than 20 minutes for this problem solving with a higher memory capacity computer. Hence, this step was fundamental on encouraging the continuity on the investigation of the curing process of the epoxy resin.

8.2 EXPERIMENTAL VALIDATIONS

8.2.1 Oven validation

Before validating the curing of the epoxy samples, an oven validation was carried out with glycerine, as previously explained. Results can be visualized in the following Figure 52 for both experimental measurements and COMSOL®'s predictions. The positions of the thermocouples on the wall and on the glycerine were checked on the simulation and compared with test values.

Figure 52: Temperature comparison between experimental measures and numerical prediction for Glycerine heating.

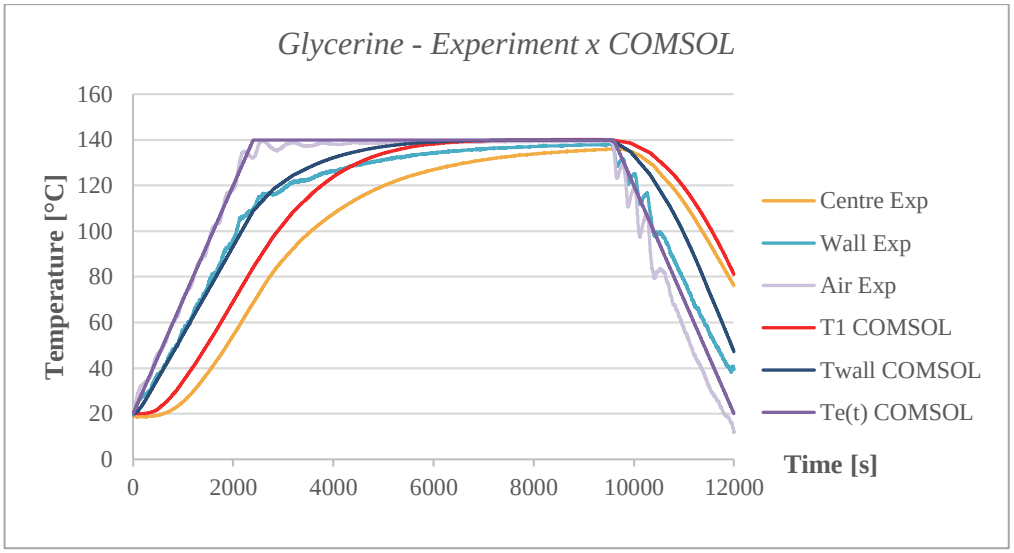

Source: Author.

The graph shows a good agreement between experimental and numerical results. Temperatures on the glycerine exhibit a few more differences than the others, but this can be a result of the thermocouple not being exactly in the centre, or due to the glycerine properties (since they are from the literature and simplified to constant values). The wall, on the other hand, with variable properties of the steel within the temperature range, achieve a better accordance, indicating a proper modelling and a validation of the coefficient of convection used for the simulation. In Figure 53, the temperature distribution can be observed at the end of the 140°C plateau (9600 s).

Figure 53: Temperature fields on the Glycerine sample at 9600 s.

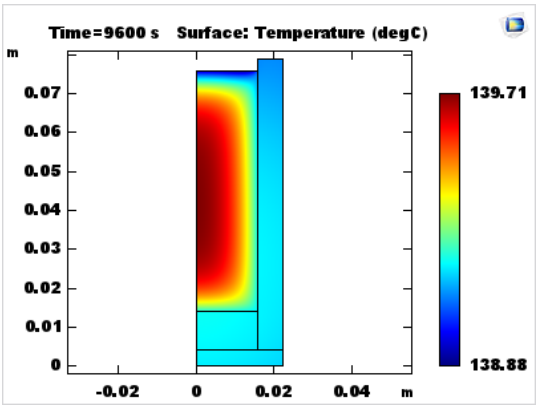

Source: Author.

8.2.2 Curing of the epoxy system

Curing experiments on three different curing temperatures were able to be performed. Due to limitations such as equipment availability and time for their performance – curing tests, as verified, take long periods of time, and a single oven was available for reproduction of results – and financial means – epoxy resin is an expensive material; each sample was equivalent to €150 –, a further experimental study could not be able to be executed. These tests, however, show their importance on a first level of investigation, which can be continued in future works for a fully experimental analysis of the curing process under several curing temperatures with a greater number of samples.

The numerical model presented in Section 7.4 was first run with an external temperature assuming a heating rate of 3°C/min and a 2h plateau at 140°C, resulting in the following values of temperature:

Figure 54: Comparisons on temperature of experimental and numerical data for 2h curing at 140°C.

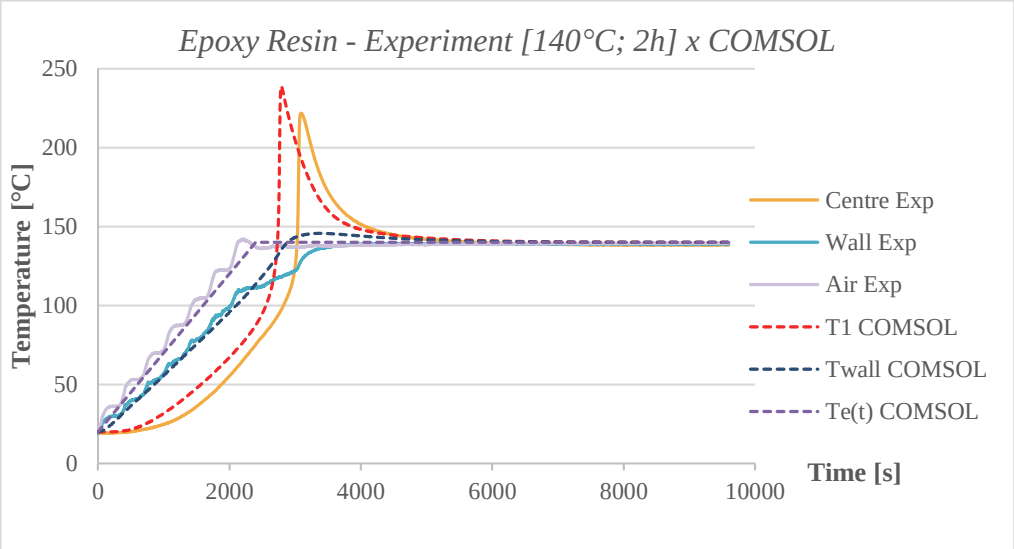

Source: Author.

The thermocouple positioned on the wall of the mould was verified and checked on the simulation. The temperature in the centre corresponds to point 1 (*T1*) in the model. Results are similar for the three experimental measurements by the thermocouples and the numerical values. The temperature peak in the centre was registered, a result of the intense exothermic reaction during polymerization, coinciding with the prediction from COMSOL®.

The wall temperatures are a little farther away from one another at the duration of the peak in the epoxy's centre temperature. A possible reason could be assigned to the coefficient

of convection h, which was added to the model from previous works based on validations with glycerine. Since glycerine doesn't have a temperature peak inside the material when heated, temperatures of the steel mould and the oven air show greater differences for the epoxy resin, leading to changes in the coefficient of convection which weren't considered.

As a matter of fact, such dissimilarities on the wall temperatures were also identified for the single step curing at 110°C (Figure 55) and the two-step curing at 80°C and 120°C (Figure 56), when comparing experimental and numerical results. For these tests, only thermocouples on the mould wall and oven air were possible to be used.

Figure 55: Comparisons on temperature of experimental and numerical data for 2h curing at 110°C.

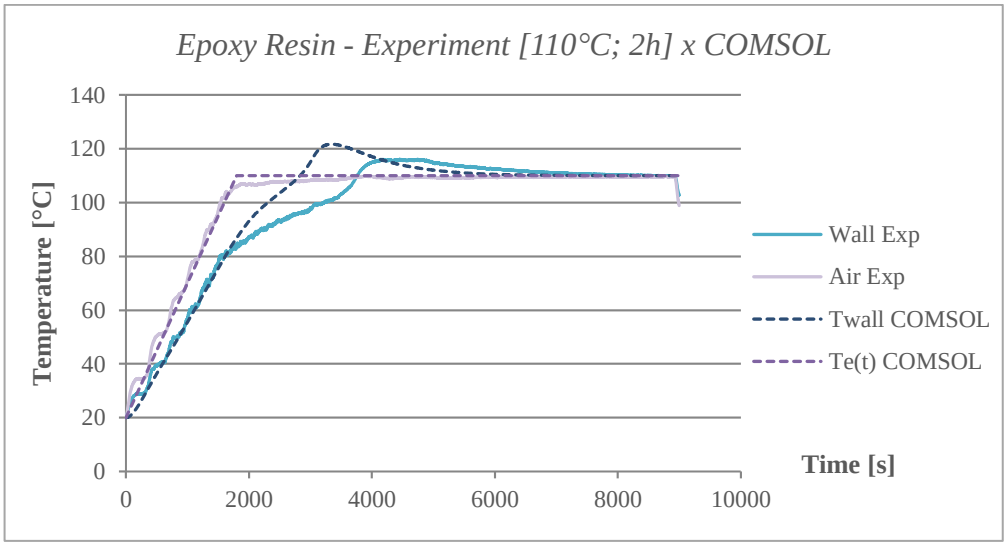

Source: Author.

Figure 56: Comparisons on temperature of experimental and numerical data for two-step curing at 80°C and 120°C.

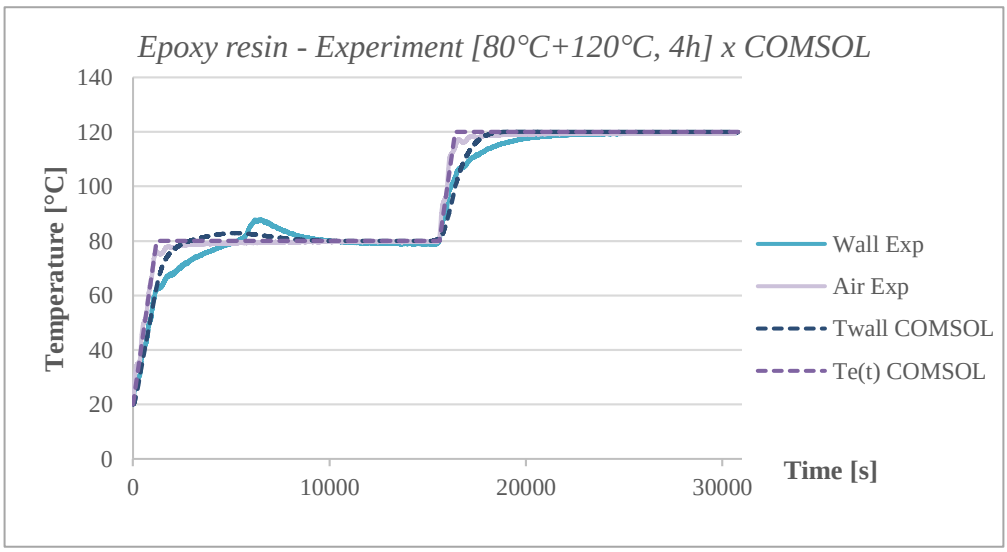

Source: Author.

These two graphs show the increase in the wall temperature due to the exothermic peak occurring a little later than simulation results, once again indicating a possible non-conform prediction of heat transfer parameters for the replication of the real curing process. For the 140°C curing case, though, the centre temperatures revealed an exothermal peak, leading to the conclusion that heat transfer inside the resin is correctly defined. In fact, as the centre of the resin is not as subjected to heat transfer as much as the external surfaces, not presenting direct effects on its temperature profile from heat convection, this evidences a required improvement on such boundary condition, more precisely, the coefficient of heat transfer by convection. Not taking into account radiation effects could also have a contribution for these results.

8.3 THERMO-CHEMICAL-MECHANICAL INVESTIGATION

Following the experimental cases, thermo-chemical-mechanical simulations were carried out for single step curing at 140°C and 110°C, and for two-step curing at 80°C and 120°C. The addition of the mechanical coupling phenomena caused the problem solution to considerably increase its computational time. The single step curing, for example, was achieved in a matter of no more than 3 minutes for the thermo-chemical model, as when mechanics was incorporated it took around an hour to be performed. As for the two-step curing, the meshing applied hasn't shown to be so effective, since the high number of degrees of freedom, connected to the multiple varying parameters and a total duration three times longer, led to a slow solving, taking almost the same time as the real curing. Thus, for further studies on multiple-step curing processes, a particular attention must be drawn to the pre-processing stage regarding the mesh development.

8.3.1 Single step curing at 140°C

The 140°C curing demonstrated high levels of final degrees of cure in the whole epoxy resin. This is, as expected, a consequence of the elevated temperatures which occurred from the exothermic chemical reaction of polymerization. The temperature gradient at the exothermic peak was significant, recording values of 25%. Results can be verified in Figure 57, where, once again, points 1, 2, 3 and 4 on the resin are defined in Figure 49.

Figure 57: (a) Degree of cure and (b) temperature evolutions; (c) final degree of cure distribution and (d) temperature distribution at exothermic peak for 140°C curing (points 1, 2, 3 and 4 on the resin).

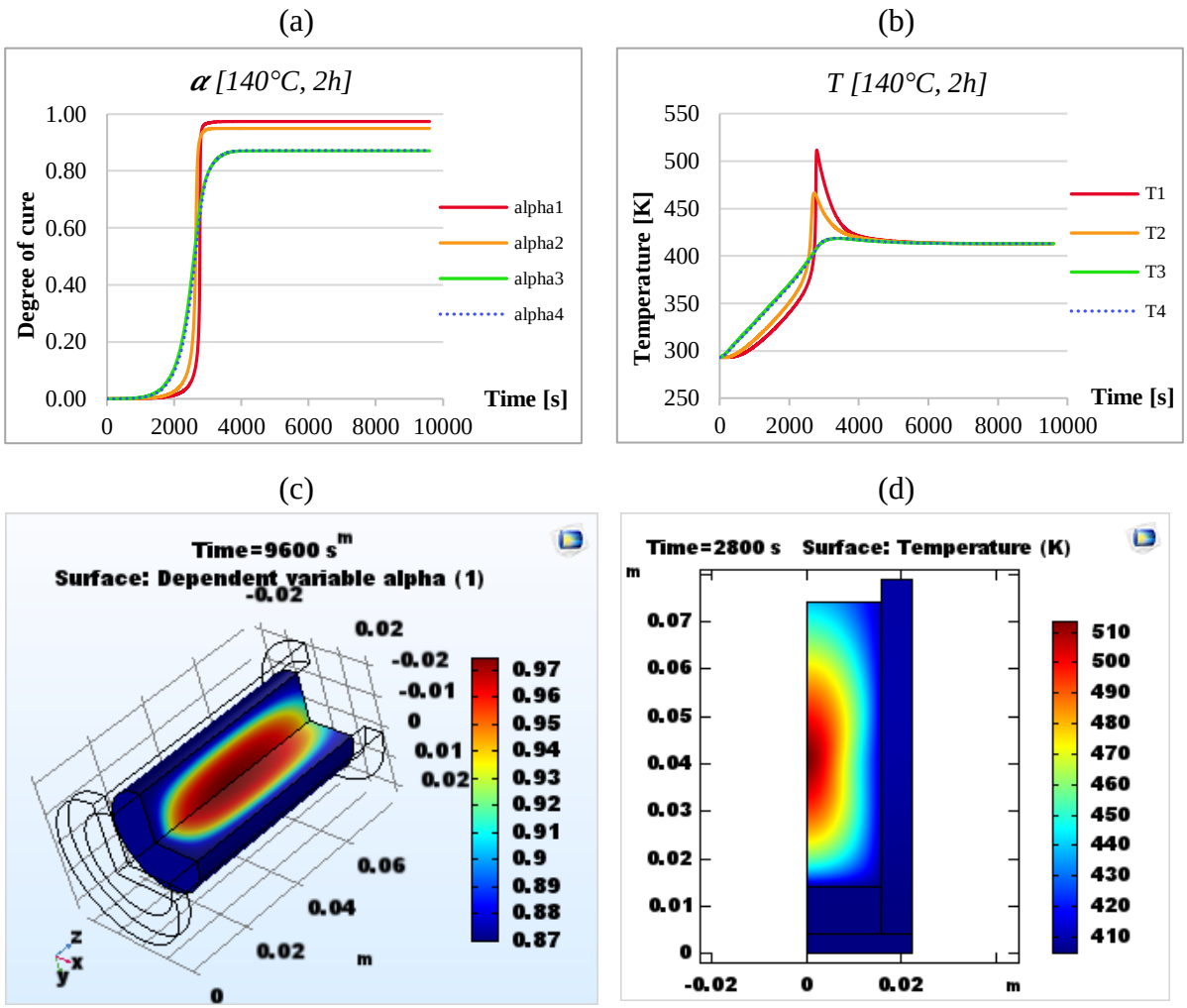

Source: Author.

The maximum temperature recorded was equal to 511 K, or 238°C. According to TGA technique presented in Section 3.3.2 for the LY 556 epoxy system, thermal degradation starts slightly at around 150°C, reaching an intense effect from 200°C. Based on simulation results, the resin is for sure thermally degraded, and this is clear in the experiments, which produced fully cracked samples. Certainly, a 140°C curing cannot be admitted in a manufacturing process of LY 556 epoxy system with such geometry. The mass effect can be rightfully verified in this investigation, which represents an obstacle for the manufacturing of thick epoxies.

As a result of the intense cure kinetics and great values – as well as gradients – of degree of conversion, thermal and mechanical parameters and properties also achieve relevant intensities. The glass transition temperature and the elastic shear modulus (Figure 58), as functions directly dependent on the degree of cure, present evolution graphs similar in form to α's. The heat source evolution denotes the exothermic peak in which the temperature in the

centre of the epoxy (*T1*) significantly rises. As the simulation was limited to the hot stage of the curing, the final mechanical property of elastic shear modulus was found a maximum of ≈36 MPa, coherent to literature results of the same nature (RABEARISON et al., 2009). The heterogeneity of the resin is as well seen on the elastic shear modulus distribution, which has values starting from ≈10 MPa.

Figure 58: Evolutions of (a) glass transition temperature, (b) heat source and (c) elastic shear modulus for 140°C curing (points 1, 2, 3 and 4 on the resin).

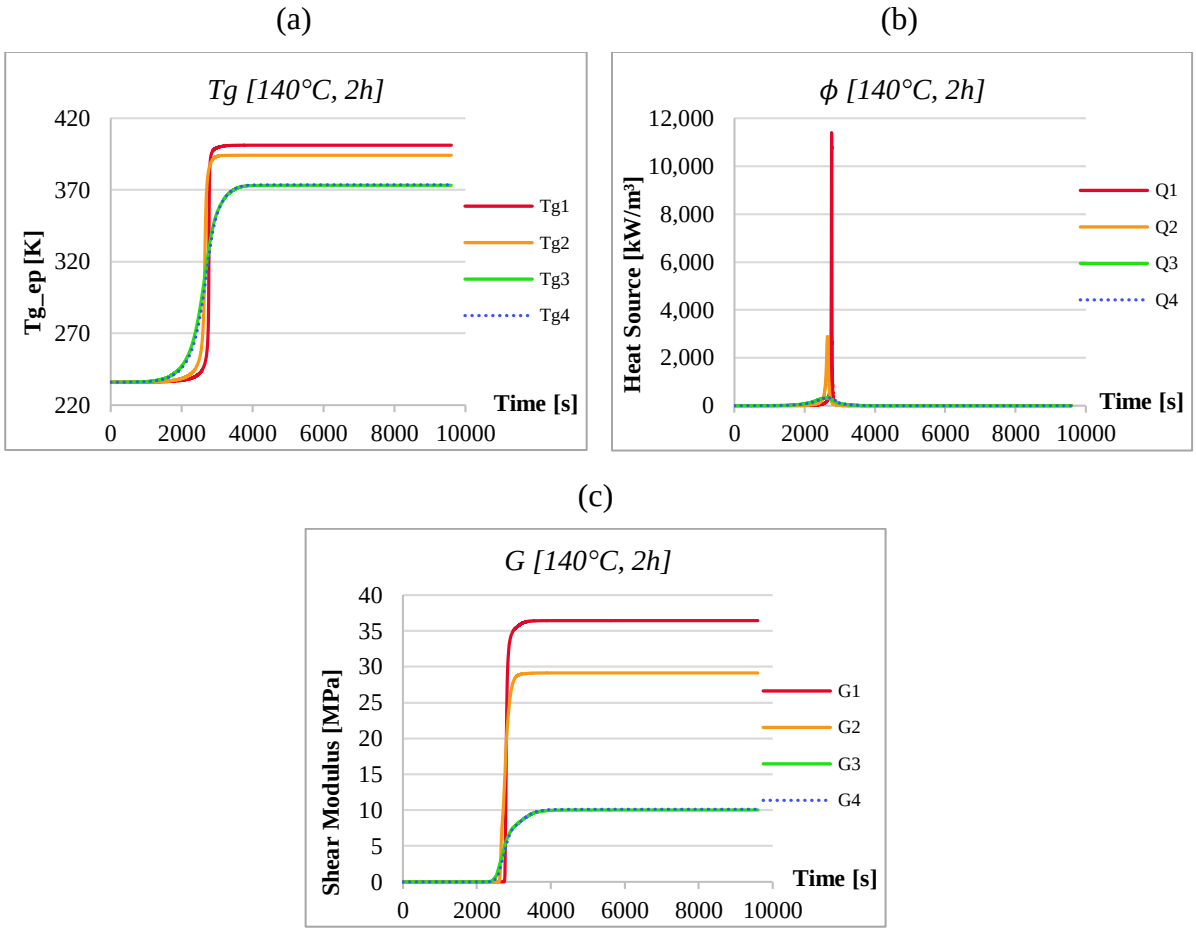

Source: Author.

Regarding the strains recorded in this curing process, the chemical shrinkage governed by Li et al.'s model follows the degree of conversion in an initially downwards concavity curve, where it reaches values close to its maximum (in absolute terms) around the temperature peak (and higher degree of conversion rate). Studies of Rabearison et al. (2009) on Abaqus achieved the same behaviour for chemical strain evolution from Li et al.'s model. As the thermal strain depends on the material temperature, its form resembles the temperature evolution. Nevertheless, since temperature gradients are intense at the 140°C curing, so are the thermal strains. Combined with fast chemical strain progression, strain gradients lead to the

development of internal stresses. For that reason, epoxy's deformation should have a particular consideration for curing studies and manufacturing processes. Both deformation evolutions are on Figure 59.

Figure 59: (a) Chemical and (b) thermal strains for the 140°C curing (points 1, 2, 3 and 4 on the resin).

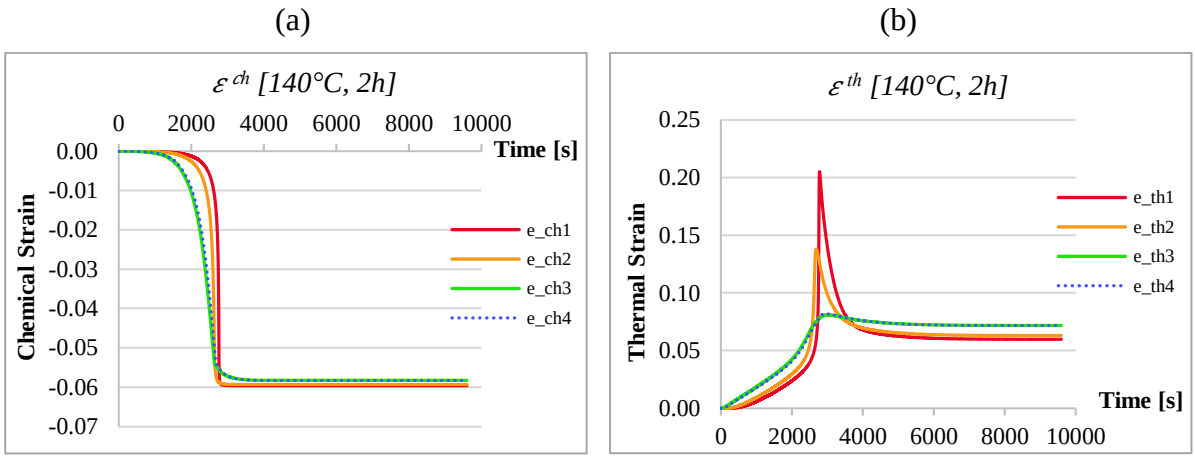

Source: Author.

8.3.2 Single step curing at 110°C

The 110°C curing simulation, evidently, led to a lower maximum final degree of cure compared to the 140°C curing, as the maximum temperature registered during curing was inferior, not contributing as much for the polymerization of the epoxy resin. The heterogeneity is still strong for these curing conditions (Figures 60a and 60c). The temperature peak, however, takes place a little later, reaching a maximum value of 472 K (199°C) – Figures 60b and 60d. Taking this numerical result into consideration, we can say that thermal degradation still makes its presence in the process. Indeed, the sample cured at 110°C shows cracks as well, although in less intensity. For a single step curing process, this temperature is not ideal yet.

Figure 60: (a) Degree of cure and (b) temperature evolutions; (c) final degree of cure distribution and (d) temperature distribution at exothermic peak for 110°C curing (points 1, 2, 3 and 4 on the resin).

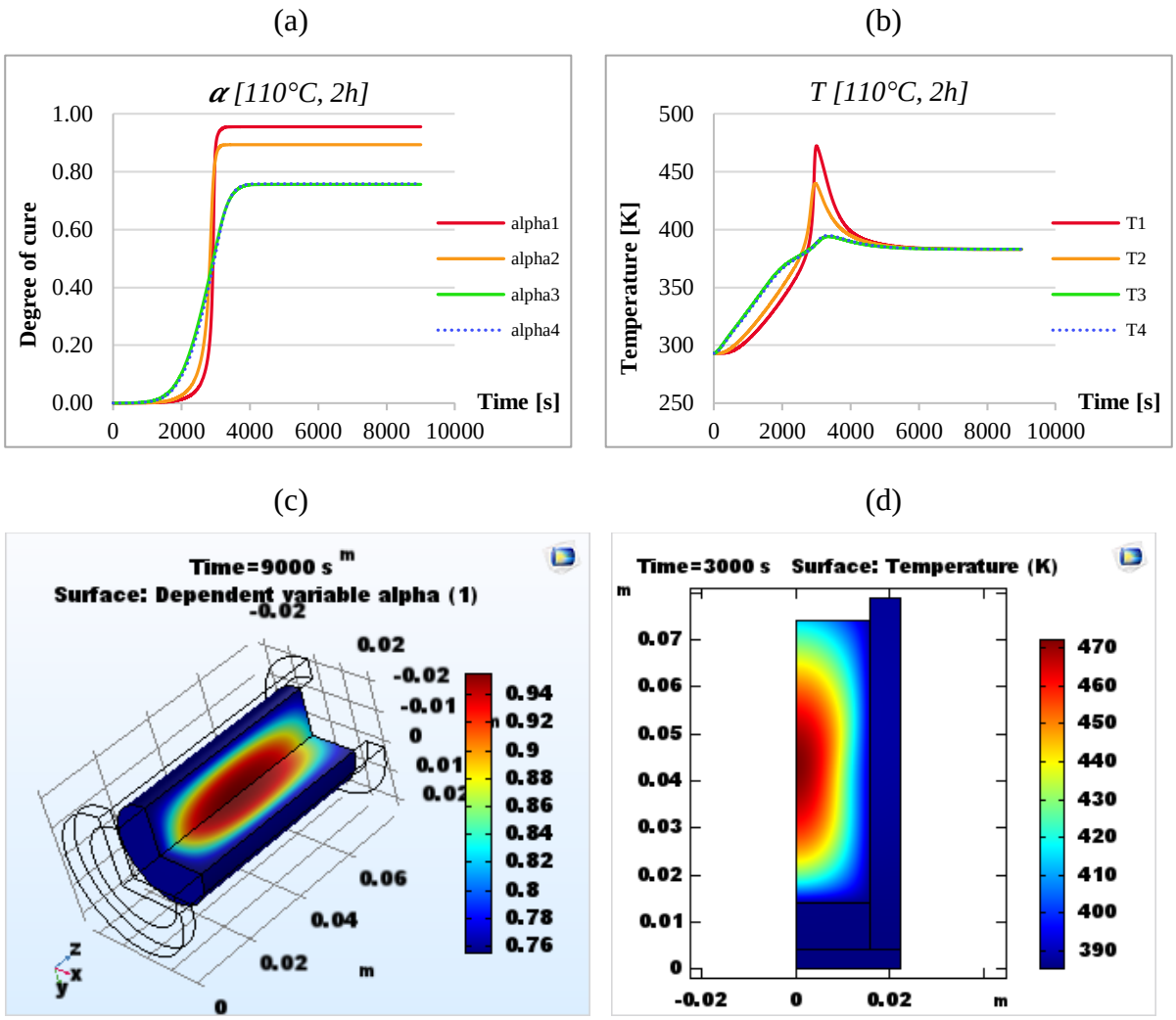

Source: Author.

Since the final degree of cure showed values ranging from 95% to 76%, a lower minimum value compared to results from 140°C curing, the lower limit of final shear modulus reduced to 7MPa (maximum was found at 31 MPa) – Figure 61. The resulting material has a reduced strength in some regions of its volume, a non-favourable aspect of the final product.

Figure 61: Evolutions of (a) glass transition temperature and (b) elastic shear modulus for 110°C curing (points 1, 2, 3 and 4 on the resin).

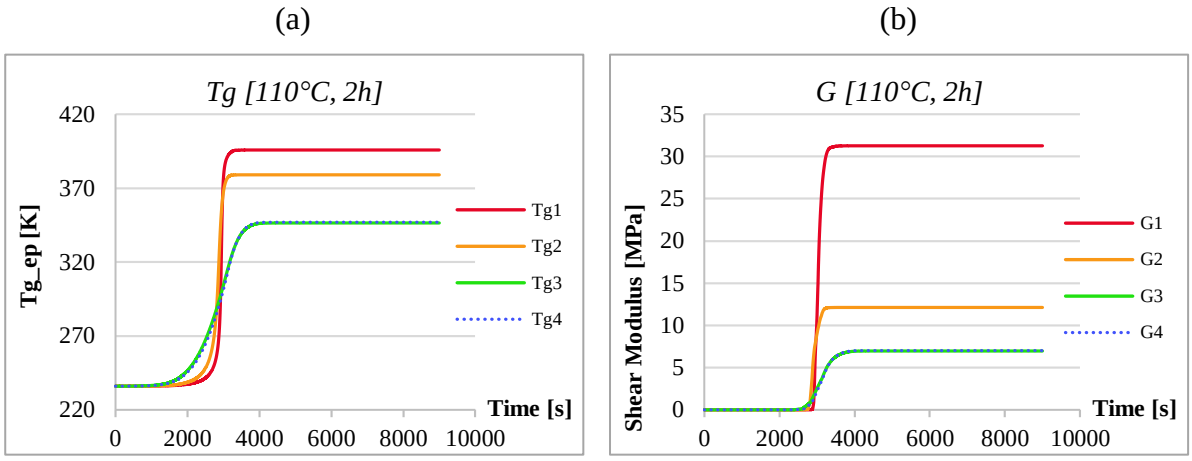

Source: Author.

Degree of conversion rate decreases a little, which can be subtly seen by the evolution of *alpha3* and *alpha4* (on the external surface of the epoxy resin) becoming less steep for 110°C curing temperature. This leads to a slower chemical shrinkage process. Temperature gradients are still high (around 22%), but showed a reduction, which directly affects the thermal strain development. All of this can have impacts on the internal stresses resulting in the process (Figure 62).

Figure 62: (a) Chemical and (b) thermal strains for the 110°C curing.

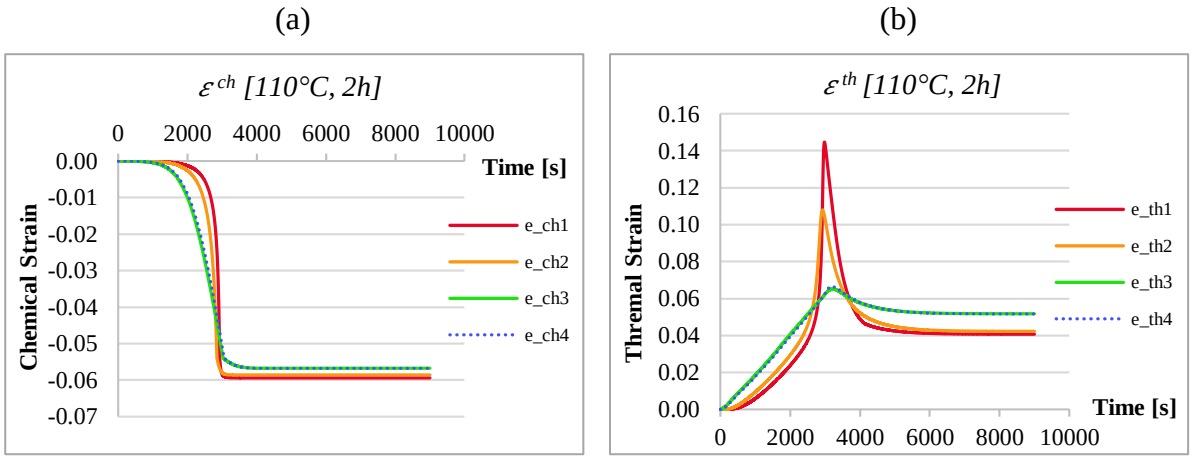

Source: Author.

8.3.3 Two-step curing at 80°C + 120°C

At last, the two-step curing experiment was reproduced on COMSOL® for the fully coupled model. As the process involved 80°C and 120°C plateaus at four hours each, solving became more time and memory consuming since the same fine mesh used at previous studies was applied. The degree of cure showed a less steep evolution (Figure 63), as expected, due to the lower curing temperature, reaching inferior maximum values at the end of the 80°C plateau. The "post-cure" at 120°C clearly enhances the polymerization of the epoxy resin, increasing the degree of conversion from 63% to 77% at point 1 (centre of the resin). A more uniform polymerization of the matrix was also achieved with this slower curing process, which guaranties more homogeneous properties to the final product.

Figure 63: (a) Degree of cure and (b) temperature evolutions; degree of cure distributions at the end of the (c) 80°C and (d) 120°C plateaus.

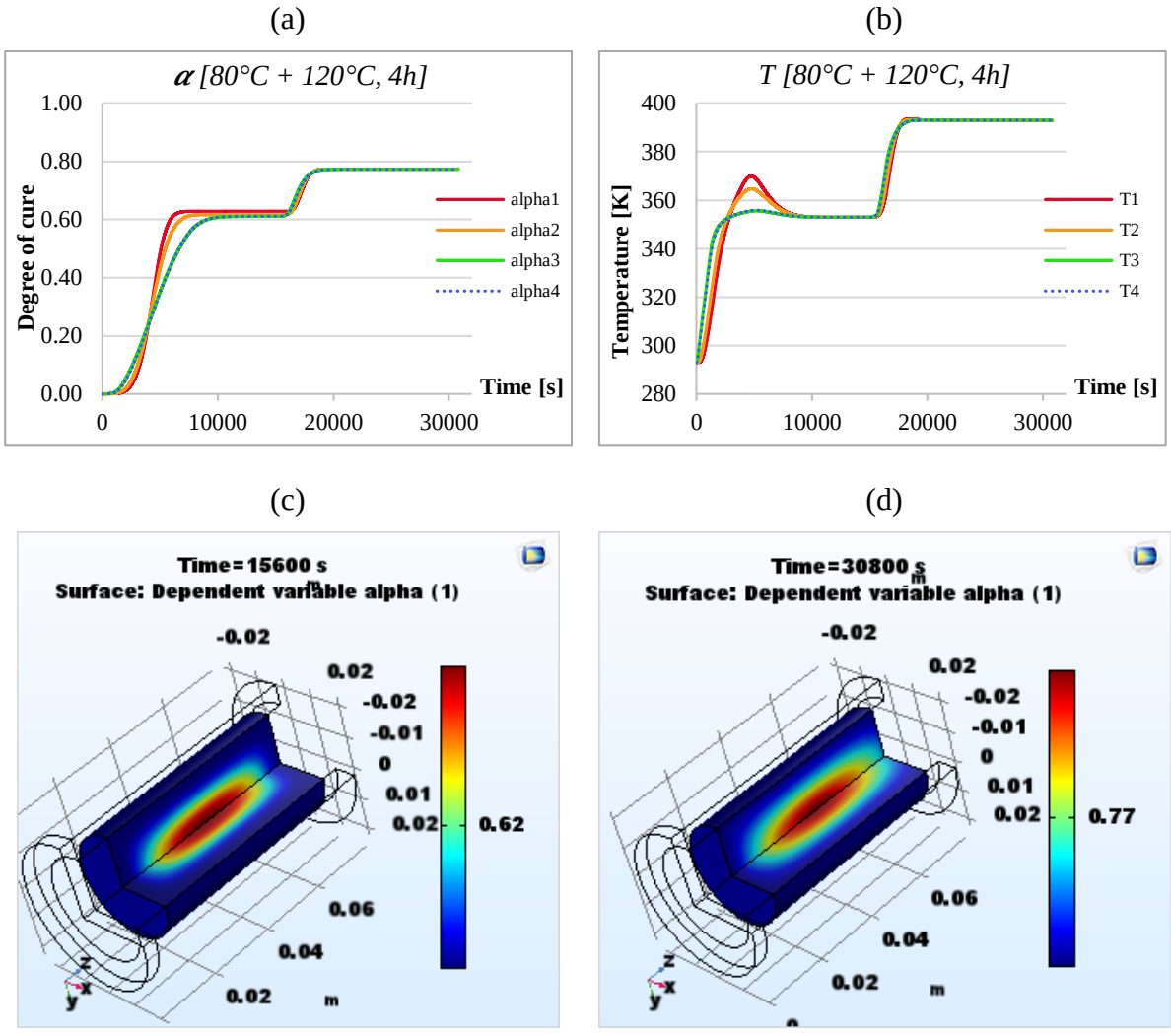

Source: Author.

Gelation occurs during the 80°C plateau, developing a significantly lower temperature peak compared to the other curing temperatures. Its maximum was recorded at 370 K (97°C), which is even below the following curing plateau. As thermal degradation is known to show its effects at temperatures from 150°C, it's safe to say the resulting cured epoxy is excluded from this phenomenon occurrence. In fact, the experimental curing resulted in a perfect sample, with no evidence of cracks. Strains from chemical and thermal origin registered a smoother evolution due to the lower degree of cure history and temperature gradients (Figure 64). Thermal strain showed significantly lower values from previous simulations, which contributes as well on the final internal stresses in the epoxy resin.

Figure 64: (a) Chemical and (b) thermal strains for the 80°C + 120°C curing.

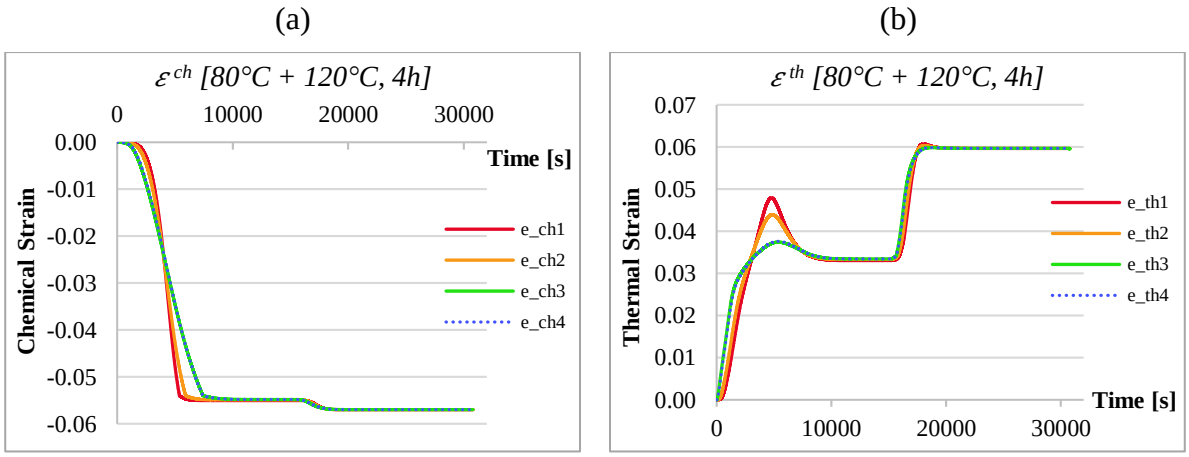

Source: Author.

8.3.4 Von Mises stresses

Assuming, as displayed by the elastic constitutive law an isotropic behaviour for the matrix in the process, as a first step, the Von Mises stresses were verified for each simulation run at this stage. Results showed that stresses are greater at gelation for the single step curing processes, registering values around 10 MPa for the 140°C curing and 6 MPa for the 110°C curing. At the end of cure, stresses were mainly about 4 MPa and 3 MPa for 140°C and 110°C curing temperatures, respectively. The two-step curing presents lower stresses, mostly around 2 MPa at the end of the 80°C plateau and 0.6 MPa at the end of cure. Results are similar to works of Rabearison et al. (2008), which found stresses in the range of 7-8 MPa after gelation and 5-6 MPa at the end of curing of an epoxy resin of 25 mm of diameter at a 120°C curing temperature.

In all cases, there's a stress concentration at the external top region of the epoxy, corresponding to point 3. This is believed to occur because of the modelling, which considered the steel mould and the matrix with coincident nodal points, as a single structure with different material properties (use of a continuous mesh with connected elements at each node of the different domains). This makes sense by assuming a perfect stick of the epoxy matrix to the steel of the mould. However, this is not the case during the real process as some anti-adhesive chemical was sprayed onto the inner steel face of the cylinder mould. Of course, a simulation with contacts condition, which is what happens in reality between resin and mould, should be conducted to take this into account. This is an arduous task to accomplish, not only by the user but also by the program, as it represents a more complex case to be solved and can lead to convergence problems more easily. We can reasonable assume that this is not worth to be simulated as the epoxy sample can easily be removed, hence is not stuck onto the steel, thanks to the anti-adhesive chemical. Furthermore, the absence of thermal deformation of the steel mould can also contribute to this scenario, although it may probably have less impact due to its lower CTE. Results can be visualized in Figure 65.

Figure 65: Von Mises stress distribution at the epoxy matrix for end of (a) 140°C and (b) 110°C curing; and the end of (c) 80°C and (d) 120°C plateaus.

(a) (b)

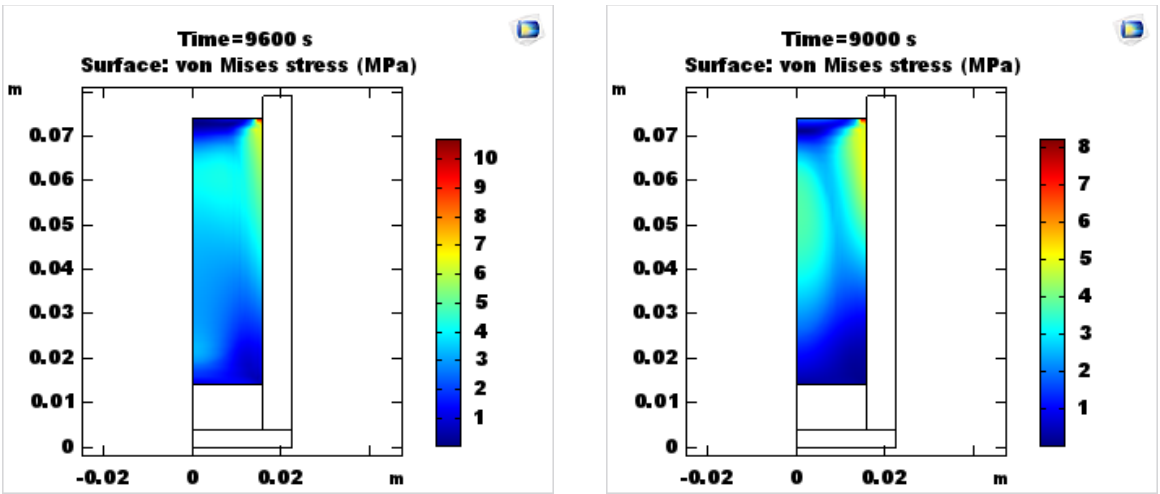

(c) (d)

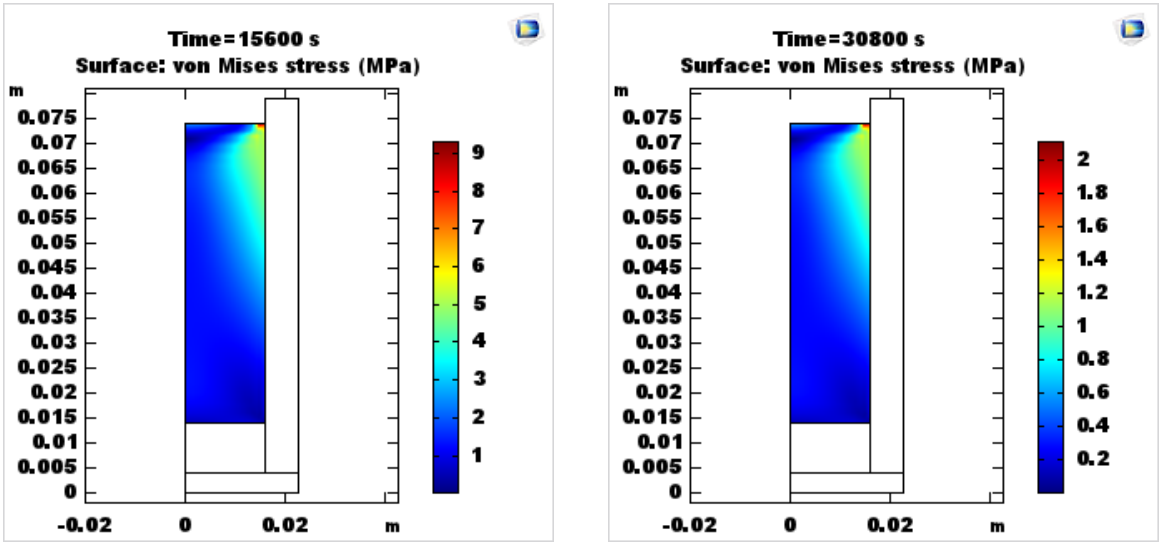

Source: Author.

Stress results reveal, once again, the relevance in pre-processing stage of modelling. Appropriate boundary conditions, as well as representative meshing, should be carried out for feasible and accurate simulations. The contact between epoxy and mould shows room for improvement on the predictive model, and would be an interesting matter for further studies.

8.4 A VIEWPOINT ON THERMAL DEGRADATION

Experiments and corresponding simulations expose the great impact of the curing temperature on the integrity of the cured matrix. Although single step curing may seem advantageous in terms of time, it can compromise the quality of the material. 140°C and 110°C curing evidence cracks, likely leading to decrease in properties of the final product.

For the geometry taken into consideration, there's a greater presence of mass effects, and the curing temperature assumes a more relevant role. Thin epoxies don't show the difficulty in heat diffusion from their insides to the medium as thick epoxies do. Hence, higher curing temperatures for boost in degree of cure of the last type of material aren't as appealing due to higher temperatures and gradients within the sample. As observed, temperatures can reach a level where thermal degradation starts, causing mass loss and, consequently, bubbles and gases, increase in internal pressure and, lastly, cracks, irreversibly damaging the structure.

An investigation of single step curing was carried out in order to evaluate the maximum allowable curing temperature in which the epoxy resin is free from the thermal degradation

phenomenon. As well as Balvers et al. (2008) achieved a maximum reliable thickness for a specific curing temperature, the process here was reversibly executed, fixing the thickness of the geometry and varying the curing temperature. Temperatures studied comprise 140°C, 110°C, 100°C, 90°C and 80°C for heating rates of 3°C/min and 2h plateaus. Temperatures in the centre of the epoxy resin (point 1) can be visualized in Figure 66.

Figure 66: Evolution of centre temperature for several single step curing temperatures.

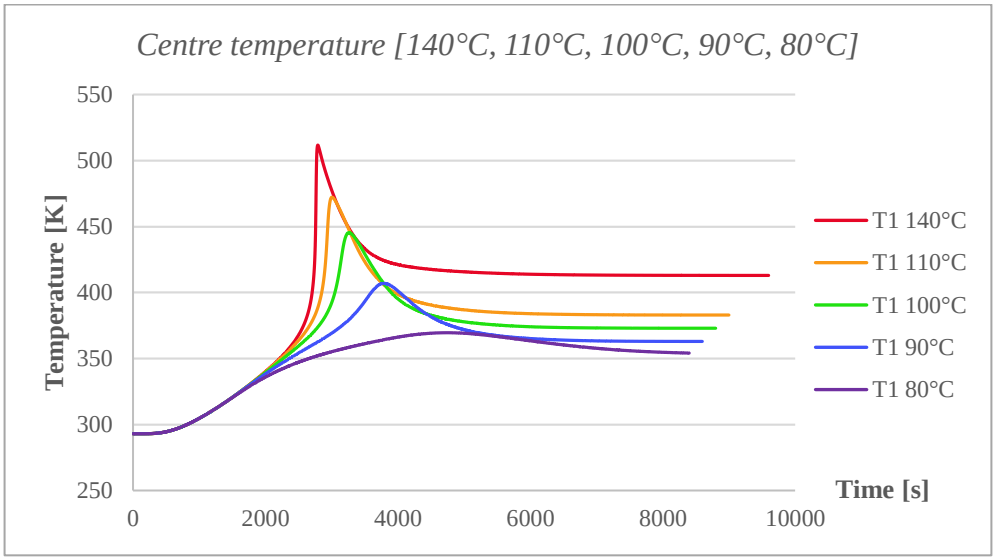

Source: Author.

Clearly, the higher the curing temperature, the more intense the exothermic peak registered in the epoxy's centre. It was verified that curing temperatures from 140°C to 100°C revealed the occurrence of thermal degradation if considering its critical value of 150°C. For those, the maximum records were, respectively, 511 K, 472 K and 445 K (238°C, 199°C and 172°C). The 90°C and 80°C plateaus are free from this effect, with maximum temperatures of 407 K (134°C) and 369 K (96°C), under the thermal degradation limit. The epoxy resin's manufacturer, therefore, suggest a safe curing process when recommending a first cure at the 80°C level, at which the epoxy resin suffers gelation and produces a lower temperature peak and, then, isn't thermally degraded. For the selected curing temperatures, the degrees of cure for points 1 and 4 (centre at half height and exterior surface, also at half height), which show the largest gradients within the geometry, are presented in Figure 67.

Figure 67: Evolution of degree of cure for several single step curing temperatures.

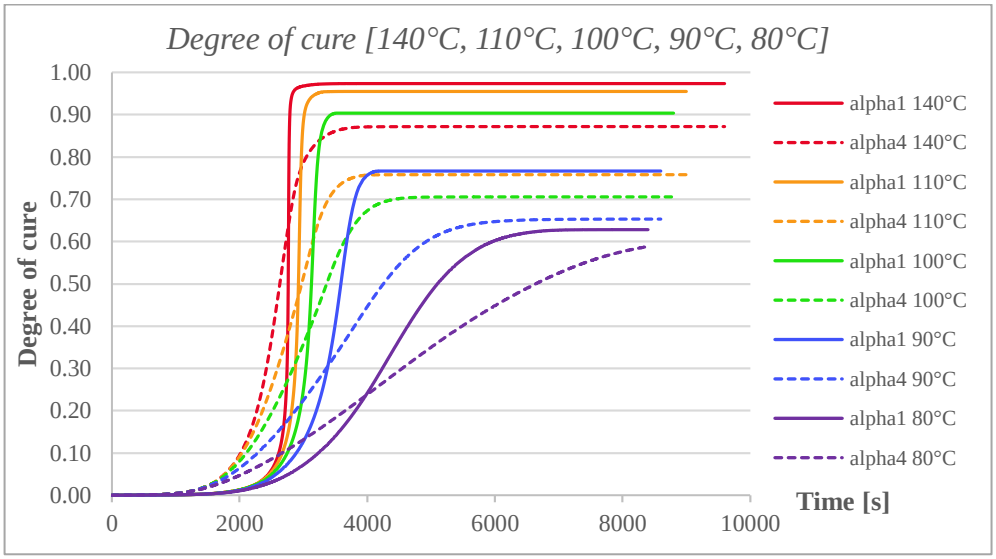

Source: Author.

The rate with which the degree of conversion increases is quite visible, reaffirming its strong connexion with the adopted curing temperature. It is also verified the anticipated growing homogeneity of the structure with the decrease in temperature of the plateau. In fact, the 80°C curing presents very similar degree of conversion values for points 1 and 4 at the end of the process. An interesting aspect to be observed is the need of more time for the stabilization of α as curing temperature becomes lower. At the smallest curing temperature, *alpha4* doesn't reach a constant profile at the end of the 2h plateau, indicating that the curing process is not over yet. Hence the manufacturer's recommendation of a 4h plateau (the double of time used in this study) at 80°C for ensuring the completion of polymerization at such temperature level.

From these results, we could suggest a single step curing process at 90°C, which guaranties the avoidance of thermal degradation and enables a faster and higher final degree of cure compared to a process at 80°C. However, simulations show the heterogeneity still present at this level, and we find areas on the epoxy with degrees of conversion ranging from 65% to 77%. The 80°C single step curing hasn't shown a stabilization but the 80°C + 120°C previously performed did, and presented a much more uniform cross-linking, reaching ranges of 61%-63% at the 80°C plateau.

For this epoxy system, the manufacturer's recommendation proves to be correctly assumed, producing a matrix with good quality. The post-cure at a higher temperature level incites more developments on the polymerization of the structure, resulting in a better final product in terms of its properties, which are mainly dependent on the degree of conversion.

Further investigations could be carried out for post-cure temperature as well as time optimization, leading to a more cross-linked structure and reduction in the process total duration.

9 CONCLUSION

The manufacturing process of a thermosetting polymer remains a focus of characterization and optimization studies, especially when it comes to thick matrices. The mass effects strongly influence the final state of the material since heat diffusion becomes more arduous to occur, leading to high temperatures and gradients and, hence, negatively interfering in its quality. The need to control and optimize the curing process for reduction and avoidance of quality defects of the matrix, as well as the composite formed by it, is crucial as the thickness of the structure increases.

Curing history has its impacts not only on the matrix itself but also on the fibre reinforced thermosetting polymer composite as a whole. The presence of cracks within the polymer does fragilize the composite; nevertheless, strain evolutions from chemical and thermal origins at the hot stage incite the development of internal stresses, which leads to microbuckling of fibres. This represents a great threat if such structures are used in special and demanding applications such as aerospace and offshore.

Both experimental and numerical investigations are current in the literature, for the curing of a thermosetting resin is still to be fully characterized. It is a complex process which involves coupling phenomena of thermal, chemistry and mechanics. The thermo-chemical analysis is the most common in studies. This research developed a fully coupled model for the curing of a LY 556 epoxy system considering thermal and chemical effects allied with elastic mechanics, employing it on COMSOL Multiphysics® for a simpler modelling with the program's capabilities. Validations were carried out by previous numerical results and experimental data.

The first thermo-chemical analysis was a reproduction of the curing model with the same conditions on a different software. Results from COMSOL® and Abaqus FEA showed good agreement with a reduced computational time when using the first software. Later on, experimental curing was performed at three different oven temperatures, producing two cracked and one perfect samples. Thermocouple measurements were helpful for the comparison with the predictive model of such materials. The numerical approach revealed good predictions, especially for the centre temperature. Wall temperature records, though, evidence room for improvement in the coefficient of heat transfer by convection, taken from the literature. The high temperature profiles inside the resin during the exothermic peak may provoke changes in such parameter which weren't considered.

The fully coupled thermo-chemical-mechanical model replicated the experimental conditions for further analysis on curing parameters and final properties. Both single step curing simulations had a visible heterogeneity in the results of degree of conversion and elastic shear modulus. The higher the curing temperature, the higher the degree of cure rate and temperature gradients, leading, respectively to faster chemical shrinkage and greater thermal strains. This reflects on the Von Mises stresses observed, which were higher for the 140°C case. The two-step curing, being carried out at a lower temperature until after gelation and producing a more uniform cured epoxy resin, had the lowest internal stresses. It also hasn't shown intense temperature peaks, staying under the limit to development of thermal degradation. Experimental samples confirm the phenomenon occurrence for the single step tests and its absence in the manufacturer's recommended process.

An extended study analysed the effect of single step curing temperature on the centre temperature and degree of cure evolutions. Indeed, the manufacturer's suggestion of a first level curing at 80°C seems appropriate, for it generates a more homogeneous matrix (and hence, homogeneous properties). Although 90°C curing temperatures remained below thermal degradation limit, it led to still significant degree of conversion gradients, which is not a desirable matter. Yet, this analysis shows room for improvement in total curing time and post-cure temperature.

In summary, this work highlights the importance of the knowledge on the curing process of an epoxy resin in terms of achievement of good final properties and material quality, as well as control and optimization of manufacturing processes of thermosetting polymer composites. The Finite Element Method shows itself as a powerful and reliable tool for curing predictions. Enhancements are constantly necessary, but numerical results already demonstrated the great potential associated to the method in this field of study.

10 SUGESTIONS FOR FUTURE WORKS

Some of the subjects which can be further explored in future studies from the research presented are subsequently cited:

- ✓ The execution of more curing tests with a greater number of samples and curing temperatures for a fully experimental analysis of the process for the epoxy system;
- ✓ Parametric studies on the curing temperature, time and cycle, aiming the further investigation and consequent optimization of the curing process;
- ✓ Study on the influence of the mould's material and its dimensions;
- ✓ Mesh studies for a better and faster prediction of the coupled phenomena, especially for the two-step curing processes with a larger time consumption;
- ✓ Improvements on investigation of the contact condition, if necessary regarding the experiments, of epoxy resin and steel mould as a way to avoid stress concentrations in numerical results which are not realistic;
- ✓ Further investigations on the boundary conditions regarding the heat imposed by the oven on the curing sample;
- ✓ Verify the evolution of mechanical properties during the cooldown phase for more accurate predictions of the final state of the cured resin;
- ✓ Analysis of the effects of thermal degradation on the material properties, followed by a model proposition for properties prediction when such phenomenon is experienced;
- ✓ Evaluation on the viscoelastic behaviour of the epoxy matrix, based namely on DMA-TMA tests and its implementation in the predictive model;
- ✓ Addition of fibre to the polymeric matrix composite for microbuckling detection, as a proof and validation of internal stress level prediction.

REFERENCES

ACMA – American Composites Manufacturers Association. *History of the composites industry*, 2017.
Available at http://www.acmanet.org/composites/history-of-composites.
Access in 4 Dec 2017.

AGARWAL, B. D.; BROUTMAN, L. J.; CHANDRASHEKHARA, K. *Analysis and performance of fiber composites*. 3rd Ed. New-Delhi: John Wiley & Sons, 2006. 576 p.

ANDRADE, C. R. et al. *Temperatura e grau de cura no processo de pultrusão de fibras de carbono reforçadas com resina epóxi*. In: Congresso Nacional de Engenharia Mecânica – CONEM, 2000. Natal: Brazil.

ASKELAND, D. R.; FULAY, P. P.; WRIGHT, W. J. *The Science and Engineering of Materials*. 6th Ed. Boston: Cengage Learning, 2011. 956 p.

BALVERS, J. M. et al. *Determination of Cure Dependent Properties for Curing Simulation of Thick-Walled Composites*. 49th AIAA/ASME/ASCE/AHS Structures, Structural Dynamics, and Materials Conference. Schaumburg, IL, USA, 2008.

BEHZAD, T.; SAIN, M. *Finite element modeling of polymer curing in natural fiber reinforced composites*. Composites Science and Technology, Vol. 67, 2007. p. 1666-1673

CALLISTER JR., W. D. *Ciência e Engenharia de Materiais: Uma Introdução*. 7ª Ed. Rio de Janeiro: LTC, 2008. 589 p.

CHIAVERINI, V. *Tecnologia Mecânica – Processos de Fabricação e Tratamento: Materiais de Construção Mecânica*. 2ª Ed. São Paulo: McGraw-Hill, 1986. Vol. 3. 388 p.

COMSOL INC. *Empresa*, 2017a.
Available at https://br.comsol.com/company.
Access in 19 Dec 2017.

COMSOL INC. *Introduction to COMSOL Multiphysics*®, 2017b.
Available at https://br.comsol.com/documentation.
Access in 20 Dec 2017.

COSTA, M. L.; REZENDE, M. C.; PARDINI, L. C. *Métodos de Estudo da Cinética de Cura de Resinas Epóxi*. Polímeros: Ciência e Tecnologia, Vol. 9, 1999. p. 37-44.

COSTA, M. L.; REZENDE, M. C.; BOTELHO, E. C. *Estabelecimento de ciclo de cura de pré-impregnados aeronáuticos*. Polímeros: Ciência e Tecnologia, Vol. 15, Issue 3, 2005. p. 224-231.

DIBENEDETTO, A. T. *Prediction of the glass transition temperature of polymers: A model based on the Principle of Corresponding States*. Journal of Polymer Science: Part B: Polymer Physics, Vol. 25, 1987. p. 1949-1969.

DULEBA, B.; DULEBOVA, L.; SPISAK, E. *Simulation and evaluation of carbon/epoxy composite systems using FEM and tensile test*. Procedia Engineering, Vol 96, 2014. p. 70-74.

DURA COMPOSITES LTD. *Fibreglass GRP grating*, 2017, il. color.
Available at http://www.duracomposites.com.
Access in 14 Jan 2018.

EOM, Y. et al. *Time-Cure-Temperature Superposition for the Prediction of Instantaneous Viscoelastic Properties During Cure*. Polymer Engineering and Science, Vol. 40, Issue 6, 2000. p. 1281-1292.

FISH, J.; BELYTSCHKO, T. *Um primeiro curso em Elementos Finitos*. Rio de Janeiro: LTC, 2009. p. 256.

FOURNIER, J. et al. *Changes in Molecular Dynamics during Bulk Polymerization of an Epoxide-Amine System as Studied by Dielectric Relaxation Spectroscopy*. Macromolecules, Vol. 29, 1996. p. 7097-7107.

HEISE, M. S.; MARTIN, G. C. *Analysis of the Cure Kinetics of Epoxy/Imidazole Resin Systems*. Journal of Applied Polymer Science, Vol. 39, Issue 3, 1990. p. 721-738.

HORIE, K. et al. *Calorimetric Investigation of Polymerization Reactions. III. Curing Reactions of Epoxides with Amines*. Journal of Polymer Science: Part A-1, Vol. 8, 1970. p. 1357-1372.

JOCHUM Ch. *Thermosetting laminates quality: from fiber waviness to FEM cure modeling*. Habilitation à Diriger des Recherches, ENSIETA, 2009.

JOCHUM, Ch. et al. *Cure multiphysic couplings effects on the dynamic behaviour of a thick epoxy*. The 19th International Conference on Composite Materials. Montreal, Canada, 2013.

JOCHUM, Ch. et al. *Estimation of the residual stress state generated during the curing of a thick epoxy matrix by pulsed laser*. 16th European Conference on Composite Materials, Seville, Spain, 2014.

JOCHUM Ch. et al. *A cut-off fracture approach for residual stress estimation in thick epoxies*. Materialwissenschaft und Werkstofftechnik, Vol. 47, Issue 5-6, 2016. p. 530-538.

JOCHUM, Ch.; GRANDIDIER, J. C.; POTIER-FERRY, M. *Modeling approach of microbuckling mechanism during cure in a carbon epoxy laminate*. The 12th Conference on Composite Materials, Paris, France, 1999.

JOCHUM, Ch.; GRANDIDIER, J. C.; SMAALI, M. A. *Experimental study of long T300 carbon fibre undulations during the curing of LY556 epoxy resin*. Composites Science and Technology, Vol. 67, 2007. p. 2633-2642.

JOCHUM, Ch.; GRANDIDIER, J. C.; SMAALI, M. A. *Proposal for a long-fibre microbuckling scenario during the cure of a thermosetting matrix*. Composites: Part A, Vol. 39, 2008. p. 19-28.

JUNIOR, J. H. S. A. et al. *Comportamento mecânico e térmico de compósitos de fibra de vidro sob diferentes temperaturas de cura*. Revista Iberoamericana de Polímeros, Vol. 13, 2012. p. 20-28.

KAMAL, M. R. *Thermoset Caracterization for Moldability Analysis*. Polymer Engineering and Science, Vol. 14, 1974. p. 231-239.

LI et al. *In-situ measurement of chemical shrinkage of MY750 epoxy resin by a novel gravimetric method*. Composites Science and Technology, vol. 64, 2004, p. 55-64.

LORD, S. J.; STRINGER, L. G. *A modelling approach for predicting residual stresses and distortions in polymer composites*. In: ICCM 17, 17th International Conference on Composite Materials. Edinburgh, UK, 2009.

MA BUSINESS LTD. *Composite wrap being used to repair metal pipes*, 2018, il. color. Available at http://www.materialsforengineering.co.uk/engineering-materials-news. Access in 14 Jan 2018.

MAZUMDAR, S. K. *Composites Manufacturing: Materials, Product and Process Engineering*. Boca Raton: CRC Press, 2002. 416 p.

MCKINLEY, J. W. Introduction to the Finite Element Method. In: _____. (Org). *Fundamentals of Stress Analysis*. Portland, Oregon: Matrix Publishers, Inc., 1979. p. 219-220.

MELCONIAN, M. V. Fundamentação Teórica: O método dos elementos finitos. In: _____. (Org). *Modelagem Numérica e Computacional com Similitude e Elementos Finitos*. São Paulo: Edgard Blücher Ltda., 2014. p. 49-63.

MONTSERRAT, S.; MALEK, J. *A kinetic analysis of the curing reaction of an epoxy resin*. Thermochimica Acta, Vol. 228, 1993. p. 47-60.

MSALLEM, Y. A.; JACQUEMIN, F.; POITOU, A. *Residual stresses formation during the manufacturing process of epoxy matrix composites: resin yield stress and anisotropic chemical shrinkage*. International Journal of Material Forming. Vol. 3, 2010. p. 1363-1372.

NIRBHAY, M. et al. *Tensile test simulation of CFRP test specimen using finite elements*. Procedia Materials Science, Vol. 5, 2014. p. 267-273.

OLCESE, T.; SPELTA, O.; VARGIU, S. *Curing kinetics of epoxy resins*. Journal of Polymer Science: Polymer Symposia, Vol. 53, 1975. p. 113-126.

PASCAULT, J. P. et al. *Thermosetting Polymers*. New York: Marcel Dekker, Inc., 2002. p. 496.

PATHAM, B. *COMSOL® Implementation of a viscoelastic model with cure-temperature-time superposition for predicting cure stresses and springback in a thermoset resin*. Proceedings of the COMSOL Conference. Bangalore, India, 2009.

PATHAM, B. *Multiphysics Simulations of Cure Residual Stresses and Springback in a Thermoset Resin Using a Viscoelastic Model with Cure-Temperature-Time Superposition.* Journal of Applied Polymer Science. Vol. 129, 2012. p. 983-998.

RABEARISON, N. *Elaboration d'un outil numérique dédié à la simulation du procédé de fabrication des matériaux composites à résine thermodurcissable - prédiction des contraintes internes*. 2009. 172 p. Thesis (Doctorate in Mécaniques des matériaux et structures) – École Doctorale SICMA, Université de Bretagne Occidentale, France, 2009.

RABEARISON, N.; JOCHUM, Ch.; GANDIDIER, J. C. *A finite element coupling model for internal stress prediction during the curing of thick epoxy composites*. The 9th International Conference on Flow Processes in Composite Materials, Montreal, Canada, 2008.

RABEARISON, N.; JOCHUM, Ch.; GRANDIDIER, J. C. *A FEM coupling model for properties prediction during the curing of an epoxy matrix*. Computational Materials Science. Vol. 45, p. 715-724, 2009.

ROESELER, W. G.; SARH, B.; KISMARTON, M. U. *Composite structures: The first 100 years*. In: 16th International Conference on Composite Materials. Kyoto, Japan, 2007.

SHEVTSOV, S. N. et al. *Cure kinetics of epoxy resin and distributed thermal control of polymeric composite structures moulding*. 3rd International Conference "Physics and Control". Potsdam, Germany, 2007.

SHEVTSOV, S. et al. *Optimization of the composite cure process based on the thermos-kinetic model*. Advanced Materials Research. Vol. 569, 2012. p. 185-192.

SINGH, A. K.; HARSHA, S. P.; PARASHAR, A. *Finite Element Analysis of CNT reinforced epoxy composite due to Thermo-mechanical loading*. Procedia Technology, Vol 23, 2016. p. 138-143.

SMAALI, M. A. *Contribution à l'étude expérimentale du phénomène d'ondulation d'une fibre de carbone noyée dans une résine thermodurcissable tout au long de la cuisson*. 2005. 216 p. Thesis (Doctorate in Mécanique des Solides, des Matériaux, des Structures et des Surfaces) - Sciences pour l'Ingénieur, École Nationale Supérieure de Mécanique et d'Aérotechnique & Faculté des Sciences Fondamentales et Appliquées, France, 2005.

SOUSA, M. F. et al. *Mechanically relevant chemical shrinkage of epoxy molding compounds*. 14th International Conference on Thermal, Mechanical and Multi-Physics Simulation and Experiments in Microelectronics and Microsystems (EuroSimE). Wroclaw, Poland, 2013.

USUI, S.; WADELL, J.; MARUSICH, T. *Finite Element Modeling of Carbon Fiber Composite Orthogonal Cutting and Drilling*. Procedia CIRP, Vol. 14, 2014. p. 211-216.

WANG, R-M.; ZHENG, S-R.; ZHENG, Y-P. *Polymer matrix composites and technology*. Beijing: Woodhead Publishing, 2011. 555 p.

WISNOM, M. R. et al. *Curing stresses in thick polymer composite components - Part I: Analysis*. The 12th International Conference on Composite Materials. Paris, France, 1999.

WRIGHT, R. E. Thermosets, reinforced plastics and composites. In: HARPER, C. A. *Handbook of plastics, elastomers & composites*. 4th Ed. New York: McGraw-Hill, 2002. p. 109-188.

ZHANG, J.; XU, Y. C.; HUANG, P. *Effect of cure cycle on curing process and hardness for epoxy resin*. eXPRESS Polymer Letters, Vol. 3, 2009. p. 534-541.

APPENDICES

APPENDIX A – Heat Flux Boundary Condition on COMSOL® [Abaqus Verification]

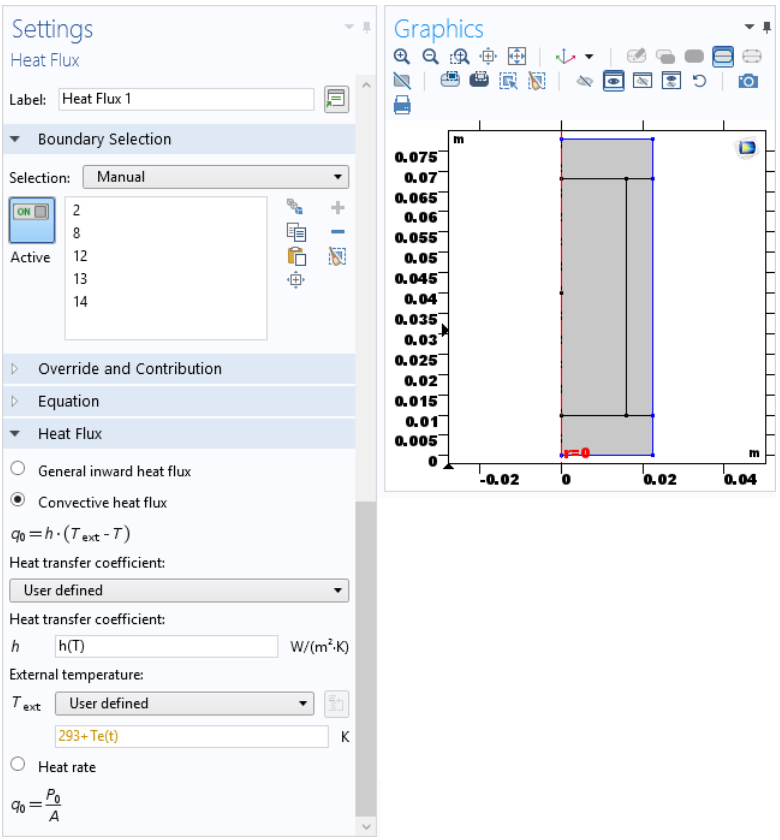

APPENDIX B – Heat Source Boundary Condition on COMSOL® [Abaqus Verification]

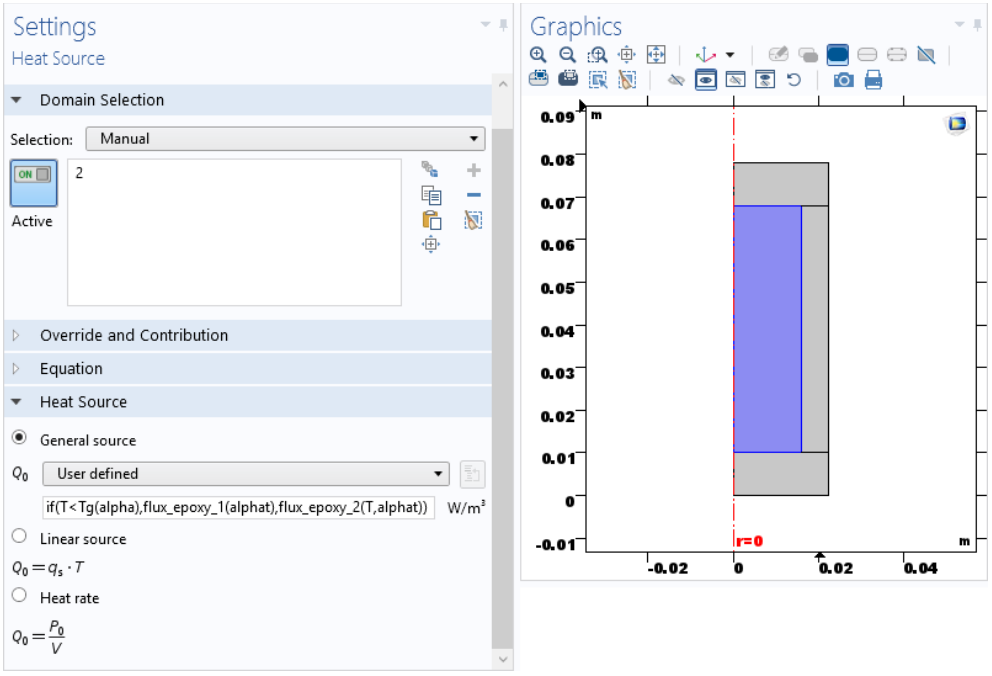

APPENDIX C – External Temperature on COMSOL® [Abaqus Verification]

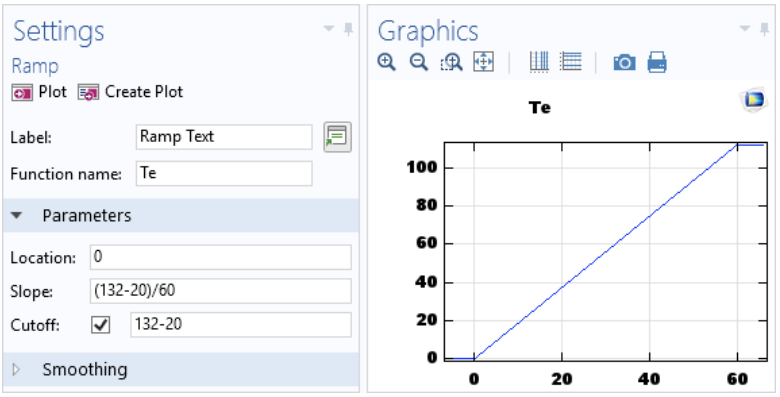

APPENDIX D – Epoxy Resin's Thermal Expansion [Thermo-chemical-mechanical model]

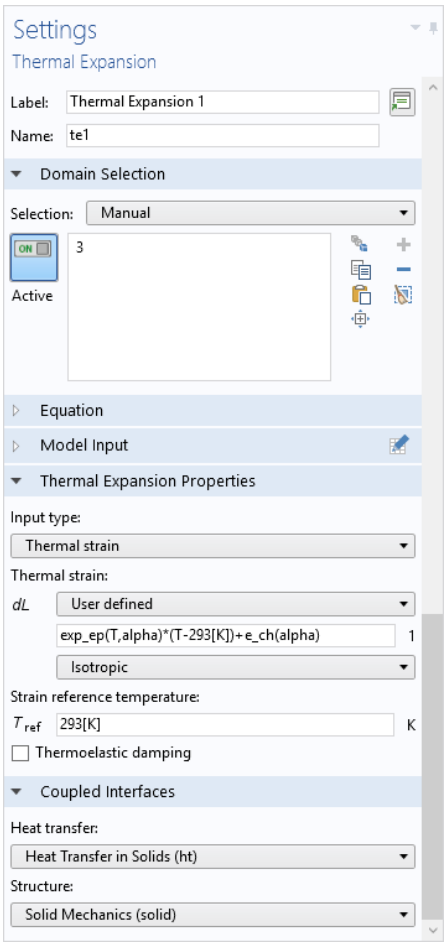

APPENDIX E – Mesh Convergence Test [Glycerine; Thermo-chemical model; Thermo-chemical-mechanical model]

As the Abaqus Verification involved a shorter time duration and the thermo-chemical phenomena alone, the following progression of models had to consider reductions in computational time and memory. It was decided to maintain a quadrilateral mesh to represent the epoxy (or glycerine) elements, which is the region of interest, while a triangular mesh inserted into the mould allowed a decline in the total number of elements. The quadrilateral mesh was created by fixing the number of divisons on the vertical and horizontal edges of the epoxy geometry. As for the triangular mesh, it was applied as a free mesh, according to the software's default option, only considering a *finer* mesh size.

Firstly, the bottom edge was set to have 8 divisions, while the epoxy's right edge had 20 divisions. This proportion (2x5) resulted in a relatively uniform mesh distribution throughout the epoxy resin (Figure 68), giving a total of 349 elements for the full geometry. Simulations, however, led to disturbance in the degree of cure rate, $d\alpha/dt$, as observed in Figure 69.

Figure 68: Mesh convergence test [8x20 mesh].

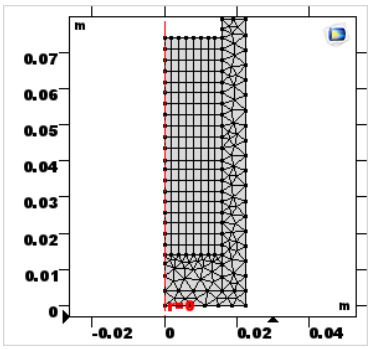

Source: Author.

Figure 69: Degree of cure rate evolution for point 1 (centre of the epoxy): (a) in total time and (b) zoomed in the disturbance area [8x20 mesh].

(a)

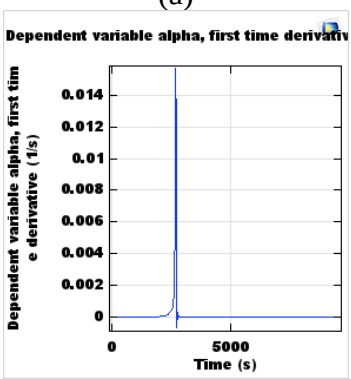

Source: Author.

(b)

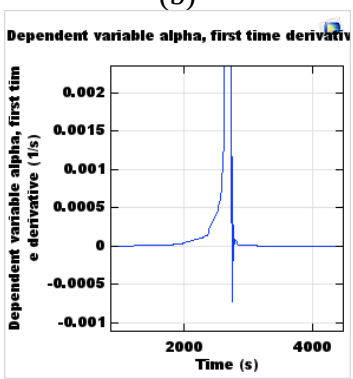

Source: Author.

Hence, a finer mesh was applied to the geometry. Horizontal divisions were increased to 10 while vertical ones became 25 (2x5 proportion). The resulting mesh, with 501 elements, can be seen in Figure 70. Results still showed disturbance for $d\alpha/dt$ evolution in point 1, which is the centre of the mould-filling material (Figure 71).

Figure 70: Mesh convergence test [10x25 mesh].

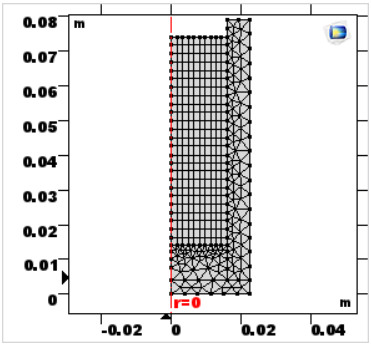

Source: Author.

Figure 71: Degree of cure rate evolution for point 1 (centre of the epoxy): (a) in total time and (b) zoomed in the disturbance area [10x25 mesh].

(a)

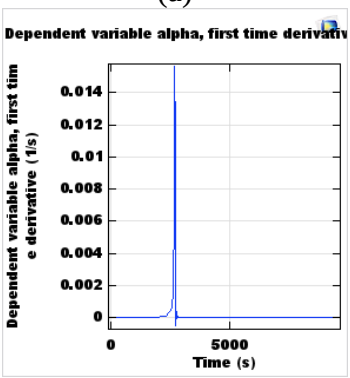

Source: Author.

(b)

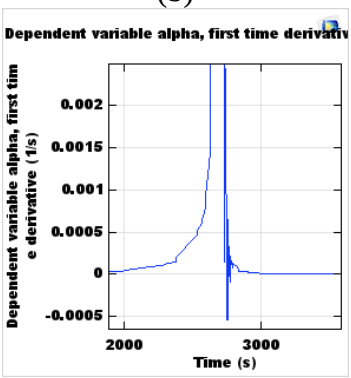

Source: Author.

Consequently, a third mesh refinement was carried out, applying 12 horizontal and 30 vertical divisions to the epoxy geometry containing quadrilateral elements. This provided a mesh with 645 elements (Figure 72), also resulting in a degree of cure rate evolution without the disturbance previously registered (Figure 73).

Figure 72: Mesh convergence test [12x30 mesh].

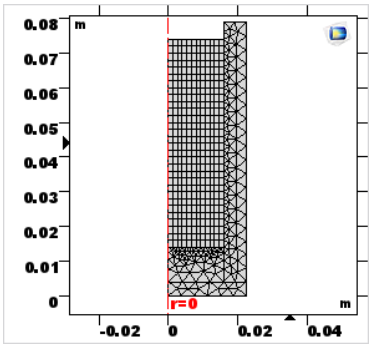

Source: Author.

Figure 73: Degree of cure rate evolution for point 1 (centre of the epoxy): (a) in total time and (b) zoomed in the disturbance area [12x30 mesh].

(a)

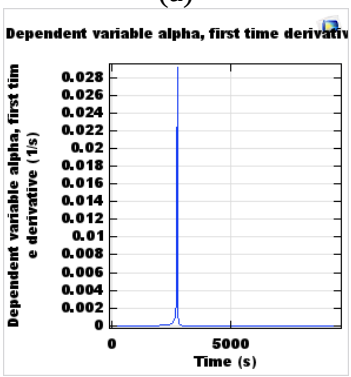

Source: Author.

(b)

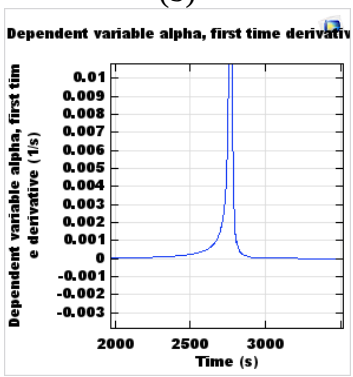

Source: Author.

Besides the absence of disturbance from the last adopted type of mesh, it was especially verified a delay on the peak temperature within the geometry, represented by point 1 at the centre of the resin, as well as an increase in its value in more than 14 K. Maximum values for degree of cure at the centre on the internal (point 1) and external (point 4) surfaces, though, didn't show significant changes – up to 0.2% for alpha1 and 0.3% for alpha4.

A following mesh refinement was performed do verify the changes in results. A 14x35 element division was applied (Figure 74), generating a mesh with 885 elements. As well as for the 12x30 mesh, it did not show disturbance in degree of cure rate evolution (Figure 75). As results weren't too much improved by this mesh refinement – the variable with previous higher differences, temperature at the centre T1, presented an error of 0.17%, taking the 14x35 mesh as reference (Table 19) –, the 12x30 mesh has shown to be appropriate for future simulations (thermo-chemical, thermo-chemical-mechanical and glycerine simulations), finalising, hence, the mesh convergence test.

Figure 74: Mesh convergence test [14x35 mesh].

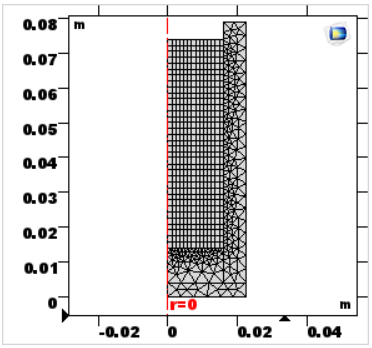

Source: Author.

Figure 75: Degree of cure rate evolution for point 1 (centre of the epoxy): (a) in total time and (b) zoomed in the disturbance area [14x35 mesh].

(a)

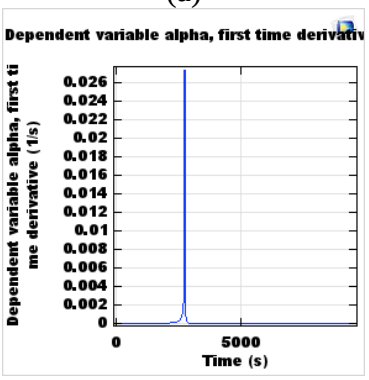

Source: Author.

(b)

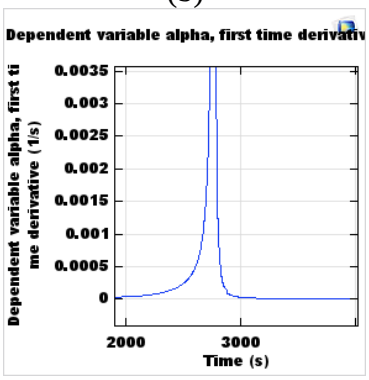

Source: Author.

Table 19: Maximum degree of cure and temperature for the mesh convergence test.

Epoxy mesh	Number of elements	Final alpha1 [%]	Final alpha4 [%]	T1 peak [K]	T1 error** [K]	Time at T1 peak [s]
8x20	349	97.5965	86.8955	497.4538	2.6280	2745
10x25	501	97.2981	86.8992	497.3148	2.6554	2746
12x30	645	97.3727	87.2011	511.7317	0.1672	2791
14x35	885	97.2941	87.0797	510.8757	-	2788

*Point 1: centre of the epoxy; point 4: centre on the external radius of the epoxy (see Figure 49);
** Reference: T1 for 14x35 mesh.

ANNEXES

ANNEX A – Epoxy Resin's Specific Heat Capacity (RABEARISON, 2009).

$\boldsymbol{\alpha}$	$\boldsymbol{T}$ $[K]$	$\boldsymbol{c_p}$ $[J/(kg.K)$	$\boldsymbol{\alpha}$	$\boldsymbol{T}$ $[K]$	$\boldsymbol{c_p}$ $[J/(kg.K)$
0	293	1902.5	0	413	2217.5
1	293	1401.25	1	413	2217.5
0	303	1928.75	0	423	2243.75
1	303	1445.625	1	423	2243.75
0	313	1955	0	433	2270
1	313	1490	1	433	2270
0	323	1981.25	0	443	2296.25
1	323	1534.375	1	443	2296.25
0	333	2007.5	0	453	2322.5
1	333	1578.75	1	453	2322.5
0	343	2033.75	0	463	2348.75
1	343	1623.125	1	463	2348.75
0	353	2060	0	473	2375
1	353	1667.5	1	473	2375
0	363	2086.25	0	483	2401.25
1	363	1711.875	1	483	2401.25
0	373	2112.5	0	493	2427.5
1	373	1756.25	1	493	2427.5
0	383	2138.75	0	503	2453.75
1	383	1800.625	1	503	2453.75
0	393	2165	0	513	2480
1	393	1845	1	513	2480
0	403	2191.25	0	523	2506.25
1	403	1889.375	1	523	2506.25

ANNEX B – Epoxy Resin's Thermal Conductivity (RABEARISON, 2009).

$\boldsymbol{\alpha}$	$\boldsymbol{T}$ $[K]$	$\boldsymbol{k}$ $[W/(m.K)$
0	293	0.188
1	293	0.350099
0	303	0.188
1	303	0.347372
0	313	0.188
1	313	0.344645
0	323	0.188
1	323	0.341918
0	333	0.188
1	333	0.339191
0	343	0.188
1	343	0.336464
0	353	0.188
1	353	0.333737
0	363	0.188
1	363	0.33101
0	373	0.188
1	373	0.328283
0	383	0.188
1	383	0.325556
0	393	0.188
1	393	0.322829
0	403	0.188
1	403	0.320102

$\boldsymbol{\alpha}$	$\boldsymbol{T}$ $[K]$	$\boldsymbol{k}$ $[W/(m.K)$
0	413	0.188
1	413	0.317375
0	423	0.188
1	423	0.314648
0	433	0.188
1	433	0.311921
0	443	0.188
1	443	0.309194
0	453	0.188
1	453	0.306467
0	463	0.188
1	463	0.30374
0	473	0.188
1	473	0.301013
0	483	0.188
1	483	0.298286
0	493	0.188
1	493	0.295559
0	503	0.188
1	503	0.292832
0	513	0.188
1	513	0.290105
0	523	0.188
1	523	0.287378

ANNEX C – Epoxy Resin's Elastic Shear Modulus (JOCHUM & GRANDIDIER, 2004).

α	G [MPa]
0	0.00001
0.05	0.00001
0.12	0.00001
0.22137	0.00001
0.33105	0.11605
0.44134	0.882
0.53055	2.46
0.60569	3.75
0.65624	4.94
0.70114	5.89
0.74061	6.65
0.77456	7.3525
0.80379	7.85
0.82901	8.4
0.85055	9.09667

α	G [MPa]
0.86922	9.92
0.88527	11.1
0.89908	12.8667
0.91099	14.975
0.92128	18.2
0.93019	21.3667
0.93793	24.3
0.94465	27.2333
0.95048	29.6333
0.95551	31.4
0.95984	32.9
0.96394	34.1333
0.96733	35
0.9705	35.6333
0.97319	36.3333

α	G [MPa]
0.97566	36.7667
0.9778	37.1333
0.98148	37.7333
0.98302	37.9333
0.98443	38.2
0.98567	38.3333
0.98682	38.6
0.98783	38.5667
0.98878	38.7667
0.98962	38.9333
0.99043	39
0.99052	39.0333
0.99052	39.2
0.99052	39.3667
0.99052	39.4